SPSE

Photographic
SCIENCE AND ENGINEERING

Interference Comparators for Coordinate Measurement of Ballistic Plates • *A. Chitayat* 249

Reciprocity Characteristics of AgBr and AgCl Emulsions • *A. Hautot* 254

The Influence of Some Addition Agents on the Rate of Development of Liquid Photographic Emulsion • *K. Futaki and Y. Ohyama* 257

Contribution to the Theory of the Characteristic Curve • *H. Frieser and E. Klein* 264

Kinetics of Development by the Ferro-EDTA Complex Ion • *T. H. James* 271

Experiments on the Formation and Crystallographic Stability of AgBr Grains in Saturated Bromide- and Ammonia-Complex Solutions • *R. Matejec* 281

Measurement of Changes in pH in Photographic Coatings during Development • *J. Eggers* 284

Analysis of Printer Integrating Circuits • *Robert K. Rickard* 288

The Effect of Gamma-Ray Exposure on Camera Films • *G. M. Corney* 291

Short Communications: Cloud Undercast Presentation for Flight Simulator Operation • *W. B. Klemperer and J. E. Ekstromer* 296

Processing with Saturated Paper • *Seymour Schreck* 298

Color Photography at 400,000 Frames per Second • *Winston O. S. Johnson* 300

Discussion and Evaluation: Reappraisal of Additive Color Photography • *L. H. Wheeler* 302

Book and Journal Reviews 305

New Products and Developments • *Frank Smith* 310

Coming Technical and Scientific Meetings 287

RAPID PROCESSING SYMPOSIUM ANNOUNCEMENT 253

Volume 4 · Number 5

SEPTEMBER-OCTOBER · 1960

Editorial Policy

Photographic Science and Engineering is dedicated to the advancement of the knowledge and application of photography and other directly related sciences. Its pages are open to all who wish to report on new studies dealing with the theory of photosensitive systems, the design of photographic instruments and apparatus useful in the treatment of photographic materials, photographic optics and illuminants, the use of photography for scientific or engineering measurement or recording, and photographic instrumentation and data recording. Only original papers should be submitted except on special invitation.

Manuscripts should be typed double-spaced on white bond paper with 1¼-in. margins all around. Literature references should be exact, and should include titles of journals, names of authors, numbers of volumes and pages, and year of publication. Book references should include title of volume, names of authors, publisher, number of edition, year of publication, and chapter and pages cited.

Graphs, charts, and other line illustrations should conform to good usage such as given in the American Standards Association Document Y-15, "A Guide for Preparing Technical Illustrations for Publication and Projection." Continuous-tone photographs should be made on 8- by 10-inch glossy paper and should show pertinent image detail sufficiently clearly to permit reduction to fit a 3-in. column in this journal. All illustrations should be numbered in soft blue pencil on the back to correspond with captions typed on a separate page. Tables should also be submitted on separate pages appropriately identified. An abstract should accompany each manuscript.

Papers intended for publication (two copies) and books for review should be submitted to the editor, T. H. James, Research Laboratories, Eastman Kodak Co., Rochester 4, N.Y. Correspondence regarding proofs and reprints should be directed to Jennie H. Allen, 94 Hastings Ave., Croton-on-Hudson, N.Y. All papers submitted for publication will be reviewed by members of the Editorial Review Board and if not accepted will be returned to the author. Published papers become the property of the Society and are protected by appropriate copyrights. Each author receives one copy of the issue in which his contribution appears. Authors may order reprints of their papers at the time they return the galley proofs. The Society does not assume responsibility for material in transit, nor guarantee publication of unsolicited material.

Photographic
SCIENCE AND ENGINEERING

official publication of the
Society of Photographic Scientists and Engineers

September-October 1960
Volume 4, Number 5

EDITORIAL STAFF

T. H. James, *Editor*
Jennie H. Allen, *Managing Editor*
H. F. Nitka, *Associate Editor*
Norman A. Exley, *Assistant Editor*
S. C. Goddard, *Feature Editor*
Frank Smith, *Feature Editor*

EDITORIAL REVIEW BOARD

J. H. Altman	Marilyn Levy
R. S. Barrows	C. S. McCamy
Richard L. Bent	J. A. Maurer
B. R. Harriman	F. W. H. Mueller
John H. Jacobs	H. F. Nitka
R. Clark Jones	W. S. Shoemaker
Peter Krause	Thos. D. Smith
John H. Ladd	William West
K. G. Leistner	Deane R. White

Photographic Science and Engineering is published six times a year by the Society of Photographic Scientists and Engineers.

• Address remittances, orders for subscriptions and for single copies, claims for missing numbers, and notices of change of address to the Society at Box 1609, Main Post Office, Washington, D.C. Subscription to nonmembers of the Society, $12.00 per year; subscription cost to members included in $8.00 annual dues; single copies, $2.00 each.

• The publication office is at 20th and Northampton Streets, Easton, Pa. Second-class mail privileges authorized at Easton, Pa. This publication is authorized to be mailed at the special rates of postage prescribed by Section 132.122.

• The Society is not responsible for the accuracy of statements made by authors and does not necessarily subscribe to their views.

© Copyright 1960 by the Society of Photographic Scientists and Engineers, Inc. Permission to reprint any part of the contents, except in reviews and abstracts, must be obtained in writing from the Editorial Vice President.

PHOTOGRAPHIC SCIENCE AND ENGINEERING
Volume 4, Number 5, September-October 1960

Interference Comparators for Coordinate Measurement of Ballistic Plates

A. CHITAYAT, *OPTOmechanisms Inc., Mineola, L.I., N.Y.*

The requirements, design criteria, and limitations of interference comparators for coordinate measurement of ballistic plates are discussed. Topics treated include monochromatic light sources, signal-to-noise and maximum travel considerations, rates of read-out attainable, direction sensing methods, and means for automatic read-out. The device used by OPTOmechanisms for semiautomatic read-out is described.

The need for extremely accurate coordinate measurement of photographic images on film has increased appreciably with the advent of satellites, and the fields of geodesy and navigation require accuracy in photographic measurements beyond the capabilities of present-day mechanical techniques. With the use of the Michelson-type interferometer, discussed in this paper, light fringes are electronically counted to determine the exact X and Y coordinates of satellites and stars, recorded photographically.

There follows a description of the requirements, design criteria, and limitations of interference comparators. In particular, details are given of the method of approach used by OPTOmechanisms Inc. in the development and manufacture of an interferometric system (Fig. 1) for the measurement of 8 by 8-in. ballistic plates. The capabilities for very fast read-out (1 in./sec), as well as precise measurements in two axes up to 12 in., make the system usable for the accurate measurement of a large number of plates in a short period of time.

The Optical System

The design problems of an interferometric system are multifold. Of major importance is the choice of the optical system that can achieve sufficient percentage of modulation for relatively long path lengths. In addition, the brightness of the light source, the efficiency of the optics, and the photodetection scheme place stringent limitations on the photoelectric fringe detection. These factors influence the signal-to-noise ratio, and therefore determine the maximum read-out speed achievable. The two-axes mechanical ways for extremely accurate movement of the ballistic plate and microscope place another limitation on the over-all accuracy.

In the OPTO Comparator, the electronic reversible counting of fringes from zero up to 100 kc, as well as automatic read-out, have determined the practicability of using the system to measure a large number of points, of the order of 6,000 daily. This feature is highly important, since the number of points measured, in order to determine an accurate statistical average, is rather large for each ballistic plate.

Presented at the 1960 Annual Conference, Santa Monica, California, 9 May 1960. Received 14 April 1960. The equipment described was developed under Air Force Contract No. AF 08(606)-1732.

Automatic vs Manual Control

The quality of the images recorded by the photographic plate automatically places a limitation on the use of the interferometer. The state of the art of lenses and film emulsion at this date is such that the minimum size of the image is not smaller than 2 μ in diameter, and in most cases much larger than that. Furthermore, the center of average emulsion density (equivalent center of gravity) of the image does not correspond to the desired point to be measured. Thus, automatic methods using a scanner may prove to be inaccurate unless the image is symmetrical about its center. However, if the shape of the image relative to its center can be predicted, then a constant correction can be introduced in the scanning system to compensate for slight errors.

The OPTO Interferometer utilizes a semiautomatic means for read-out, namely a "pre-positioner." This device (Fig. 2) allows the operator to position the micrometer to within 0.01 in. of the point of interest. In operation, a rough layout on paper or on the photograph is made, indicating the approximate points to be measured. With the ballistic plates placed within the comparator and the layout positioned on the pre-positioner, the operator moves the cross hairs a and b of the pre-positioner at will to the points to be measured. Then, by depressing a key on the control panel, the X and Y servo drives are energized to bring the microscope field over a preselected position of the ballistic plate. The operator then uses joy-stick controls for the final alignment of cross hairs.

Recent research on the improvement of film emulsion and lenses has indicated that point images of extremely fine size are possible. The images formed are predictable, thus allowing for the possi-

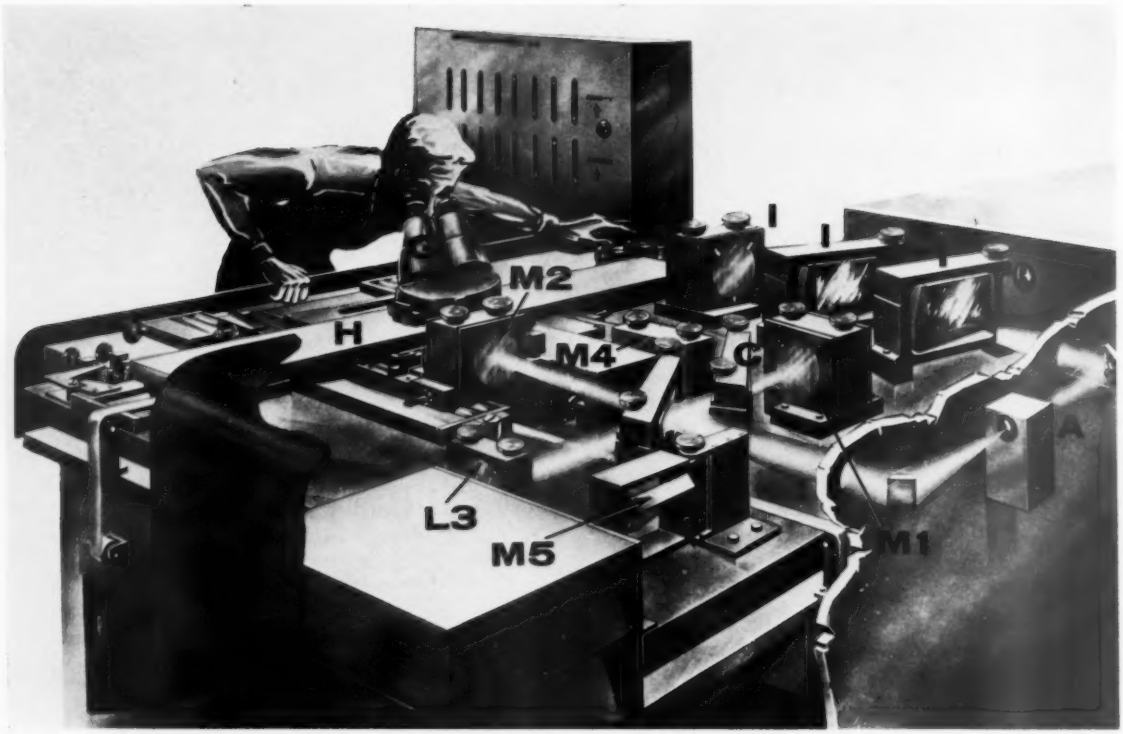

Fig. 1. Interferometer for the measurement of 8 by 8-in. ballistic plates.

A. Light source
C. Compensator
D. Beam splitter
G. Binocular microscope
H. Microscope casting
I. Optics for X-axis
L3. Focusing lens
M1. Y-axis fixed mirror
M2. Y-axis movable mirror
M4. X-axis movable mirror
M5. Mirror for visual observation of fringes

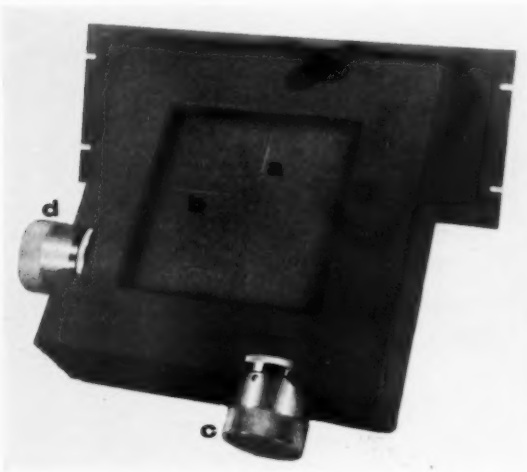

Fig. 2. Pre-positioner. a. X-axis cross hair
b. Y-axis cross hair
c. X-axis adjusting knob
d. Y-axis adjusting knob

bility of incorporating a tracking system in one optical path of the binocular microscope, which centers the cross hairs on the center of lumination of the point of interest. The pre-positioner may then be used in conjunction with a rotating disc sensor that scans and tracks the point of interest. Thus approximate position is determined by programming the pre-positioner, while final reading is achieved by the automatic scanner.

The Interferometer

A Michelson-type interferometer[1] is most suitable for 8 by 8-in. measurements. In order to achieve read-out in two axes two interferometers with a single light source are required. Figures 1 and 3 show the optics used, while Fig. 4 illustrates the optical schematic in the Y axis only.

A movable mirror, M2, is mounted on the ballistic plate holder for the measurement of fringes in the Y-axis. The viewing binocular microscope, G, containing a reticle, is mounted on a casting that is moved in the X-axis. Supported by this casting, mirror M4, for fringe measurement, is placed in the

1. R. D. Huntoon, *J. Opt. Soc. Am.*, **44**: 264 (1954).

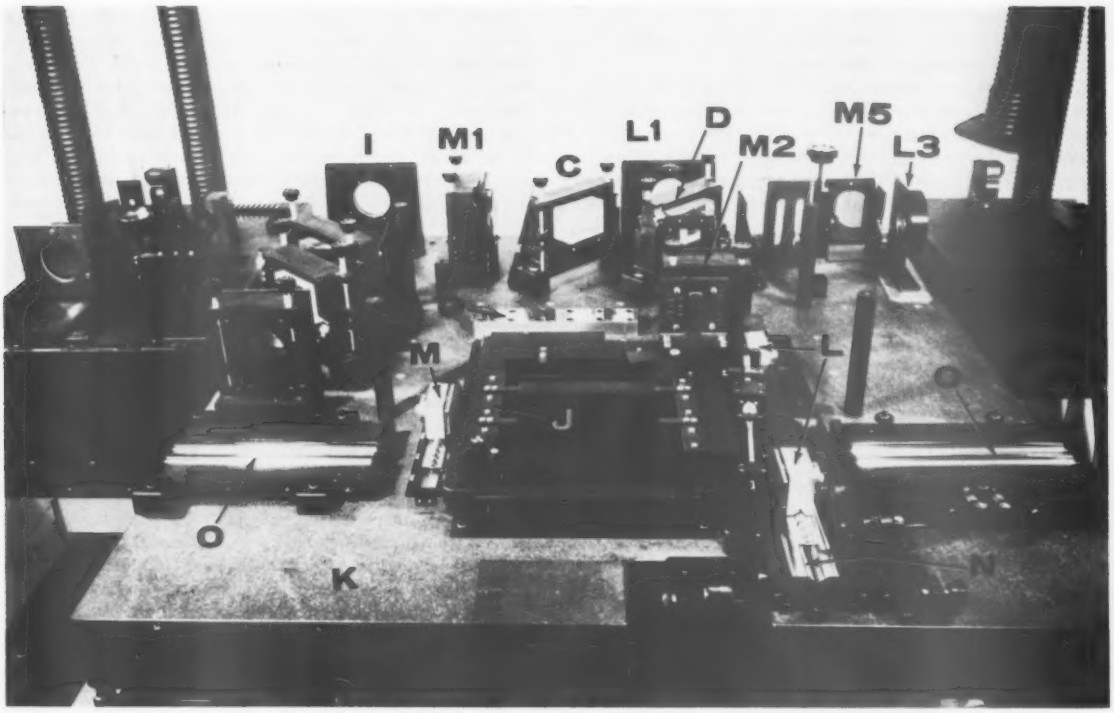

Fig. 3. Partial view of optics, ways, and ballistic plate holder for the interferometer.

C. Compensator
D. Beam splitter
I. Optics for X-axis
J. Ballistic plate holder
K. Granite plate
L. V-ways
M. Flat way
N. Steel bars
O. X-axis ways
L1. Collimating lens
L3. Focusing lens
M1. Y-axis fixed mirror
M2. Y-axis movable mirror
M5. Mirror for visual observation of fringes

second interferometer. The formation of fringes is caused by the interference of the light waves reflected from the fixed mirror, M1, and the movable mirror, M2. Thus, as the light path length through M1 is different from the path length through M2 by an integral number of whole wavelengths, the rays of light reflected will be in phase. On the other hand, if the path difference is an integral number plus one half of a wavelength, then cancellation of light rays occurs in the central portion of the viewed illumination. Therefore, as M2 is moved, cancellation and transmission of illumination occur consecutively, and the number of fringes can be detected by the photomultiplier tubes. When a mercury light source is used, a fringe count is produced for each 10 μin. movement (approximately) of M2.

Reversible Counting

A fringe-counting circuit must distinguish the direction of motion of the fringes in order to automatically correct for vibration or retraced motion. Therefore, when sinusoidal vibrations exist, the average counter reading corresponds to the actual measurement; furthermore, any overshoots by the operator do not contribute to deterioration in accuracy.

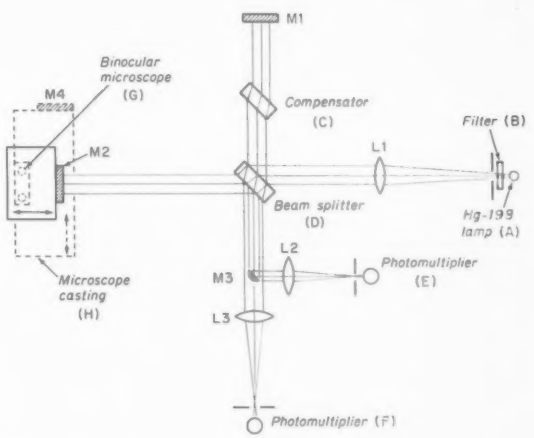

Fig. 4. Optical schematic diagram of the interferometer.

A. Light source
B. Filter
C. Compensator
D. Beam splitter
E and F. Y-axis photomultiplier tubes
G. Binocular microscope
H. Microscope casting
L1. Collimating lens
L2 and L3. Focusing lenses
M1. Y-axis fixed mirror
M2. Y-axis movable mirror
M3. Phase separating mirror
M4. X-axis movable mirror

Certain interferometers utilize the vibration of the fixed mirror and detect the phase relation between a tuning fork drive and the output of a phototube. Others utilize the same effect obtained by cycling the pressure of the atmosphere in which the interferometer is enclosed.

The OPTO Interferometer utilizes a thin film in the central portion of the compensator, C, to effectively decrease the light path by one-eighth of a wave. This portion is detected by one photomultiplier, E, which is 90° out of phase, relative to the outer portion detected by photomultiplier F. Therefore, by determining whether the signal of E leads or lags that of F, the direction of motion of M2 is provided. This is achieved electronically by a gating circuit which produces positive or negative signals to trigger the reversible counter.

The Light Source

The most important factor in determining the maximum distance measurable by an interferometer is the spread of wavelengths emitted from the monochromatic light source. The interference fringe contrast or modulation obtainable with a monochromatic single isotope source is a function of the line half-width which is inversely proportional to the square root of the atomic weight. For this reason, Hg^{198}, produced by nuclear bombardment of gold,[2] is superior to krypton, helium, and cadmium sources. In order to achieve better contrast at the high orders of displacement, cooling of the source is maintained at 15°F by continuously blowing cold air.

The OPTO Interferometer has shown its measuring ability for maximum lengths of 12 in. Further increase in length may be achieved by reducing the existent bandwidth of the green line by further cooling. An appreciable increase of signal-to-noise levels may possibly be achieved by passing the light through a beam of atoms used as a light absorber, or by using a Fabry-Perot spherical interferometer as a monochromator.[3]

Corner Cube vs Mirrors

The observation of fringes in a Michelson Interferometer necessitates that the mirror M2 remain parallel throughout its full travel; the maximum angular deviation allowable is of the order of 0.1 sec of arc. The "ways" made for the OPTO Interferometer have been able to meet these requirements during a short testing period. However, no assurance is possible that the highly accurate adjustments of the ways can be maintained after prolonged periods of testing. Consequently, two cube corners are used interchangeably with M1 and M2, allowing larger deviations in the ways without influencing fringe detection.[4] Tests with cube corners have shown that a decrease in intensity and contrast is observed when compared to the results with mirrors. However, their advantages may outweigh this slight signal-to-noise decrease.[5] Another possible configuration is to use a corner cube and a mirror to replace M1, keeping M2 as a front surface mirror. This possibility may be an optimum method of approach, used as a compromise between mechanical and optical considerations.

The Structure

One of the important design considerations in an interference comparator is the mechanical and thermal stability of the optical mounts in order to assure that all adjustments are maintained over extended periods of measurements. Since the interferometer is a laboratory instrument, components of large size are allowable. The working base is a granite plate 4 ft square and 8 in. thick, ground and lapped to a flatness of one-half of a wave. It is supported through vibration isolators by annealed steel pipes. Two covers surround the instrument for thermal stability. All heat-emitting components such as amplifiers and servo drives are located at large distances from the granite plate to reduce temperature gradients.

Mechanical Movement

In order to achieve a total system accuracy of 1 μ, it is necessary that the ways be aligned to within 1 sec of arc. Furthermore, the moving mirrors must remain parallel within 0.1 sec. Figure 3 shows the configuration of the ways in the Y axis. The movement contains two V-ways, L, and one flat way, M, in accordance with kinematic design principles. The V-blocks ride on balls which in turn roll on two hardened steel bars, N. To illustrate the degree of precision, the balls, blocks, and bar are manufactured to a tolerance closer than 1 μ. The V-blocks rotate around the axis of precision ball bearings, so that the height of the ballistic plate is determined by the average diameter of the balls instead of by that of the largest one.

The ways for the X axis, O, guide the motion of the microscope casting; they are located on the outer area of the ballistic plate holder. The large separation of the ways allows a high degree of angular accuracy. Since all the X and Y ways are located on the same granite plate, stability is maintained between the two axes.

A servo system drives the ballistic plate and microscope in accordance with the setting of the prepositioner, in order to locate the point of interest within the field of view. Joy-stick manual control determines the final setting throughout a variable speed motor drive. The variation of d-c and a-c voltages on a servo motor allow for the control of the setting speed between 1 in./sec to 1 μ/sec.

2. William F. Meggers, *J. Opt. Soc. Am.*, **38:** 7 (1948).
3. G. W. Stroke, *Quarterly Progress Report, Research Lab. Electronics Mass. Inst. Technol.*, July 1956, p. 27.
4. E. R. Peck, *J. Opt. Soc. Am.*, **38:** 1015 (1948).
5. M. V. Murty, *J. Opt. Soc. Am.*, **50:** 7 (1960).

Signal-to-Noise Considerations

The two main contributors to noise are the dark noise of the photomultiplier tube and the noise caused by the shot effect of the detected light from the mercury light source. In the interferometer discussed here, shot noise is the most prevalent. Consequently, the signal-to-noise ratio is proportional to the square root of the illumination arriving at the photodetector and the photosensitivity of the photocathode. In order to gather the maximum amount of light flux, 3-in. diameter optics of high efficiency are used; in addition, the collimating lens, L1, is made with an effective focal length of 1.5 m in order to increase signal strength. The photomultipliers, Type C7246, are chosen for their high sensitivities in the green portion of the spectrum.

If the error of measurement is not to exceed one count in 8 in., a signal-to-noise ratio of 70 : 1 is necessary. Under these conditions, the maximum signal bandwidth should not exceed 100 kc (or 1 in./sec) at the minimum separation of the mirrors. However, as the mirrors approach their maximum separation, the signal's percentage of modulation is only 10%, causing an appreciable decrease in signal-to-noise ratio for the same bandwidth. Then, in order to maintain the same signal-to-noise ratio, the system's bandwidth must be decreased to compensate for the decrease of signal. This is readily achieved by potentiometers linked to the ballistic plate drives, reducing maximum speed and bandwidth as the edges of the plate are approached. Consequently, maximum rates of travel are maintained without any sacrifice in accuracy.

Acknowledgments

In the preparation of this paper, the author had the advice and assistance of A. R. Brault, the originator of the OPTO Interferometer. In addition, the author wishes to acknowledge the assistance of his colleagues at OPTOmechanisms and Tropel Incorporated who supplied some of the information in this paper.

Rapid Processing Symposium 14–15 October 1960

Shoreham Hotel, Washington, D.C.

The Society will hold a Rapid Processing Symposium at the Shoreham Hotel, Washington, D.C., on October 14 and 15, in cooperation with the Fifth International Congress on High-Speed Photography, to be held in Washington October 16–22. A Preliminary Program has been mailed to SPSE members, listing 26 papers relative to: compact, simplified photo-processing equipment with short access time; special techniques associated with the development and design, the photographic chemistry involved, and the manner of utilization; and new features in the design and construction of larger processing machines, and advances in processing methods and control techniques. Related equipment will be exhibited. Symposium and hotel registrations cards are available from the Registration Chairman, Joe Mangiaracina.

Symposium Committees are being headed up as follows: *Papers Chairman:* Fordyce M. Brown, Photomechanisms, Inc., Box 67, Huntington Station, L.I., N.Y.

Conference Coordinator: Ira R. Kohlman, Colorfax Laboratories, Inc., 1160 Bonifant St., Silver Spring, Md.

Registration Chairman: Joseph Mangiaracina, 30 Brook Ave., Little Silver, N.J.

Program Chairman: Dwin R. Craig, LogEtronics, Inc., 500 E. Monroe Ave., Alexandria, Va.

Publicity Chairman: E. F. Richner, Eastman Kodak Co., 343 State St., Rochester 4, N.Y.

PHOTOGRAPHIC SCIENCE AND ENGINEERING
Volume 4, Number 5, September-October 1960

Reciprocity Characteristics of Silver Bromide and Silver Chloride Emulsions

A. HAUTOT, *University of Liège, Liège, Belgium*

A simple approach to the study of reciprocity characteristics of silver halide emulsions is obtained by using primitive emulsions. This method reveals that different sensitizer types have quite different actions on reciprocity. Some differences and analogies appear when silver bromide and silver chloride emulsions are compared. In both cases, sulfur sensitization seems to be the main cause of the high-intensity reciprocity failure.

Silver Bromide Emulsions

The reciprocity behavior of primitive silver bromide emulsions (without iodide) is characterized by Curve 1, Fig. 1, showing: (1) a very large low-intensity (L.I.) reciprocity failure, the L.I. curve starting with intensities such that a density of 1.0 is obtained for an exposure of about 10^{-2} sec; and (2) no appreciable high-intensity (H.I.) reciprocity failure for exposures between 10^{-2} and 10^{-5} sec. The latter (10^{-5} sec) is the shortest exposure that has been tested for these emulsions, which have low sensitivity.

Gold-, reduction-, and sulfur-sensitizing agents acting on these primitive emulsions exert a similar effect in the low intensity range, i.e., they strongly reduce the L.I. failure. In other words, the effective sensitization increases when the intensity decreases (Fig. 1, Curves 2, 3, and 4). On the other hand, the effect of sensitization for high intensities is specific to the type of sensitizer; gold salts (Fig. 1, Curve 2) and reducing agents (Fig. 1, Curve 3) induce no reciprocity failure between 10^{-2} and 10^{-6} sec, whereas sulfur-sensitizers (used alone or in combination with other sensitizers) produce a H.I. failure, the extent of which is shown by Curve 4. Curve 4 is the customary reciprocity curve, as previously drawn by Webb; it is representative of many commercial emulsions which are generally more or less sensitized by sulfur-containing gelatins.

The meaning of these curves calls for a short discussion.

Low-Intensity Exposures

According to Webb,[1] the L.I. failure is due to a lack of stability of latent subimage specks (or preimage specks) below a certain size; the intensity being low, it may be assumed that the preimage specks have faded before they have received the small additional quantity of silver necessary to form a stable speck. But what is the nature of this fading?

According to J. W. Mitchell,[2] positive holes are able to react with latent subimage specks. Therefore, subimage specks may easily disappear by rebromination, and the favorable effect of chemical sensitizers is to provide good traps for positive holes, thus avoiding the rebromination of subimage specks. The most favorable effect, however, would be expected when the bromine is liberated rapidly, that is, at high intensities. At low intensities, a long interval of time elapses between the absorption of each quantum to form a silver atom and a positive hole in a grain. Since a grain possesses at least a few internal traps for positive holes and is surrounded by a fair bromide acceptor (gelatin), chemical sensitization should be less effective at low intensities. Experimental data do not agree with this inference.

Now let us assume that the fading of preimage specks is due to the thermal dissociation $Ag \rightarrow Ag^+ + e^-$, which restores the crystal to its former state. The favorable action of chemical sensitizers on the L.I. curve then seems fairly obvious: the chemical ripening creates, at the grain surface, stable particles which act as condensation centers for the photolytic silver; in this way, the state of instability is avoided even for a slow increase in silver at low intensity. The remaining L.I. reciprocity failure in sensitized emulsions is due to the fact that not all the grains are sensitized.

High-Intensity Exposures

What is the meaning of the absence of H.I. reciprocity failure in unsensitized emulsions? A silver atom is formed by the reaction $Ag^+ + e^- \rightarrow Ag$ at a sensitivity speck (Ag^+ being an interstitial ion). The absence of reciprocity failure from 10^{-2} to 10^{-5} sec suggests that interstitial silver ions are permanently present at the periphery of the sensitivity centers; this distance does not exceed 2 or 3 lattice

Presented at the Annual Conference, Santa Monica, California, 31 May 1960. Received 9 May 1960.

1. Cf. J. H. Webb and C. H. Evans, *J. Opt. Soc. Am.*, **28:** 431 (1938); J. H. Webb, *J. Applied Phys.*, **11:** 18 (1940).

2. Cf. J. W. Mitchell, "Die Photographische Empfindlichkeit," *Phot. Korr., Sonderheft* **1,** Verlag Othmar Helwich, Darmstadt, 1957; *J. Phot. Sci.*, **5:** 49 (1957); *ibid.*, **6:** 57 (1958).

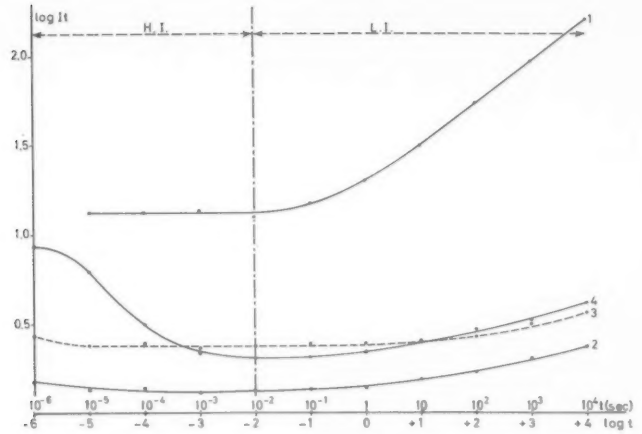

Figure 1. Reciprocity curves for silver bromide. Curve 1, primitive emulsion; Curve 2, gold sensitized; Curve 3, reduction sensitized; Curve 4, sulfur sensitized.

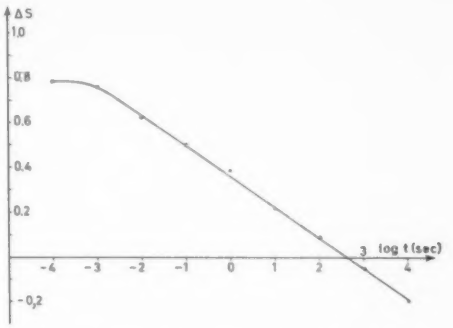

Fig. 3. Difference of speed (measured at $D = 0.5$, on a logarithmic scale) between fine-grain AgBr and AgCl emulsions for exposures between 10^{-4} and 10^{4} sec. $\Delta S = S_{AgBr} - S_{AgCl}$.

units, as suggested by measurements of the mobility of silver ions in silver bromide crystals. In the regular silver bromide lattice, the concentration of interstitial silver ions is very low (1 Ag^+ ion for 10^9 AgBr molecules at room temperature); thus, sensitivity centers are probably highly disturbed parts of the grains, and the interstitial silver ion concentration in such centers is much greater than in the normal lattice. The high photographic sensitivity of silver bromide emulsions, as well as the absence of H.I. reciprocity failure, must be related to this localized high concentration.

Gold and reduction sensitizers increase the sensitivity but do not change the concentration of interstitial ions at the sensitivity specks. However, sulfur sensitization produces a H.I. failure, the sensitivity at 10^{-6} sec being 4 to 5 times less than at 10^{-2} sec, for example. Stasiw[3] and colleagues, working with AgBr–Ag_2S crystals (0.01–0.02% Ag_2S), have proved the formation of $S^{=}Ag^{+}$ complexes (Ag^+ = interstitial ion). Probably a similar reaction occurs at the sensitivity specks of sulfur-sensitized grains, with two possible effects:

1. The formation of stable $S^{=}Ag^{+}$ complexes, which decreases the *concentration* of free Ag^+ ions at the periphery of the sensitivity centers (naturally, a few adjacent $S^{=}Ag^{+}$ complexes may produce stable compounds, such as Ag_2S); and
2. The decrease of the *mobility* of Ag^+ ions. The latter occurs if the complexes $S^{=}Ag^{+}$ are unstable with a short lifetime; in this case, Ag^+ ions are alternately captured and released by $S^{=}$ ions and their mobility is reduced.

Both effects (1) and (2) would tend to produce H.I. reciprocity failure. Taking the preceding assumptions into account, the mechanism of H.I. reciprocity failure in (pure) silver bromide emulsions seems to be reasonably clear.

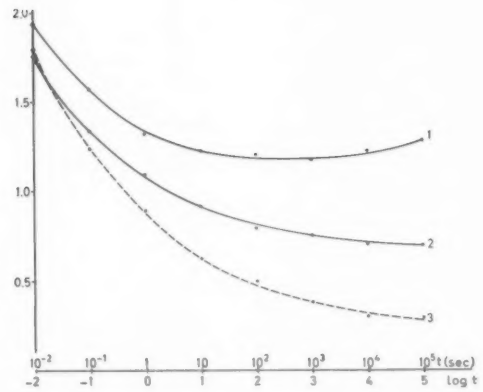

Fig. 2. Reciprocity curves for silver chloride. Curve 1, emulsion prepared without deliberate sensitizing; Curve 2, emulsion after-ripened 3 hr at 45°C; Curve 3, sulfur sensitized by allylthiourea.

Silver Chloride Emulsions

Very few reciprocity curves of silver chloride emulsions have been published. Studies carried out here have revealed that most gelatins which are inert towards silver bromide materials produce a certain sensitization (or fog) with silver chloride materials.[4]

Because of this marked reactivity of silver chloride towards traces of sulfiding compounds at a concentration of less than 10^{-6} grams/gram AgCl, we have not yet succeeded in preparing fully primitive silver chloride emulsions. However, the less sensitized ones were prepared with a gelatin which was practically inactive with silver bromide. In this case, the curve log *It* vs. log *t* possesses a marked H.I. failure (Fig. 2, Curve 1); this H.I. curve extends to

3. Cf. O. Stasiw, *Z. Elektrochem.*, **56**: 749 (1952).
4. A. Hautot and H. Sauvenier, *Sci. et inds. phot.*, **31**: 89, 137 (1960).

relatively low intensities, corresponding to a time of exposure of 10^2–10^3 sec (to be compared with 10^{-2} sec for silver bromide). The low intensity curve starts at $t > 10^3$ sec.

When this emulsion is simply after-ripened for 3 hr at 45°C (Fig. 2, Curve 2), or ripened after the addition of a sulfur sensitizing agent (allylthiourea, Curve 3), its sensitivity is somewhat increased and the low-intensity end of the H.I. curve is displaced towards much lower intensities: for $t = 10^5$ sec, this point is not yet present on Curve 3. The emulsion does not show L.I. reciprocity failure, except perhaps for extremely low intensities.

The main difference between silver bromide and silver chloride emulsions lies in the value of I for which the sensitivity reaches its maximum. Another difference concerns the density of reference D; for silver bromide, the optimum value of I is about the same for several values of D, but for silver chloride a change in reference density may be significant. The H.I. reciprocity failure also is much larger for silver chloride emulsions than for sulfur-sensitized silver bromide emulsions (and, even more so, than for the primitive silver bromide emulsion, or for silver bromide with any except sulfur sensitization).

The reciprocity failure of silver chloride emulsions for exposures shorter than 10^3 sec is responsible, in large measure, for the lower sensitivity of silver chloride materials. If silver bromide and silver chloride emulsions with similar grains (not ripened, not sensitized) are exposed to violet radiation of low intensity ($t = 10^3$ sec to obtain $D = 1$), their sensitivities are comparable, but, as shown in Fig. 3, the difference in speed increases with increasing intensity.

The large H.I. failure of silver chloride emulsions, which extends to exposures at relatively low intensities, can be understood if it is supposed that the cause of the H.I. failure is the same as in sulfur-sensitized silver bromide emulsions. It may be assumed:

1. That the specific reactivity of silver ions toward $S^=$ ions is the larger in silver chloride; this agrees with our previous observation on the fogging action of traces of sulfiding agents on silver chloride emulsions;
2. That the formation of $S^=Ag^+$ (interstitial Ag^+) is more probable in silver chloride, or that the stability of the complex is higher, or that the complex more easily forms stable sulfur compounds such as Ag_2S; thus the concentration or, alternatively, the mobility of free Ag^+ in the vicinity of the sensitivity specks is lower in silver chloride, producing a H.I. failure even for relatively low intensities.

Note*

More recent experiments on the high-intensity reciprocity failure of fine-grain silver chloride emulsions show that the slope of the reciprocity curves decreases in the time range from 10^{-2} to 10^{-7} sec, and the portion of the curves corresponding to times of 10^{-3} to 10^{-5} sec approaches a horizontal line. This observation applied to silver chloride emulsions prepared with an inactive gelatin, with or without after-ripening or with sulfur sensitization by after-ripening, and developed in a surface latent image developer. The effect of sensitization on the silver chloride materials, except for fog formation, is relatively small.

Experimental Details

The fine grain silver bromide emulsions used in this investigation (0.1–0.2 μ) were prepared by precipitation in the presence of an inert gelatin. The concentration of labile sulfur in this gelatin was less than 1 μg/gram AgBr, and after-ripening for 5 hr at 45–50°C did not increase speed by more than 0.15. The precipitation was carried out in the presence of a moderate but variable excess of potassium bromide at 45–55°C, and the finished emulsion contained 40% silver bromide and 60% gelatin. Other emulsions were physically ripened to attain grain size of 0.8–1.0 μ, but the gelatin cannot be considered to be inert for emulsions of this grain size, and the results obtained more or less approached those obtained with partially sensitized fine-grain emulsions; hence the results with the coarse-grain emulsions are of less theoretical significance and are not reported here.

Some fine-grain AgBr emulsions were prepared with active gelatins; their reciprocity curves were similar to those obtained with emulsions prepared with inert gelatin and sulfur-sensitized by after-ripening. Other silver bromide materials were prepared from an aqueous sol (0.1–0.2 μ) by adding inactive gelatin at 35°C and cooling. Their reciprocity response did not differ essentially from that of normal fine-grain emulsions prepared in the presence of inert gelatin, but their sensitivity was lower. After-ripening of these unusual materials did not change their speed or reciprocity curves, provided the gelatin used was inactive towards an ordinary silver bromide emulsion. Hence, insofar as reciprocity characteristics are concerned, the general character of fine-grain silver bromide materials reported here seems to be typical of the silver bromide—gelatin system and roughly independent of the process of preparation.

Sulfur sensitization was obtained with sodium thiosulfate or allylthiourea. The concentration of sensitizer and the time of ripening were chosen to reach full sensitization. The two sensitizers seem to have the same qualitative effect on the reciprocity characteristics although some quantitative differences were noted.

Reduction sensitization was obtained with α-amino-α-imino-methanesulfinic acid and gold sensitization with potassium aurodithiocyanate or sometimes with gold chloride. Reciprocity curves of sensitized materials were studied with silver bromide emulsions only, since sensitization of silver chloride materials is still in the experimental stage.

The silver chloride emulsions have the same grain size as the silver bromide (0.1–0.2 μ). An unavoidable increase in grain size occurs, however, upon after-ripening the silver chloride emulsions.

Development was of the surface latent-image type and was carried out in a p-hydroxyphenylglycine–potassium carbonate solution without sulfite. Variation in the developer concentration, time of development, and temperature changed the speed but had no significant effect on reciprocity.

* Added 10 June 1960.

PHOTOGRAPHIC SCIENCE AND ENGINEERING
Volume 4, Number 5, September-October 1960

The Influence of Some Addition Agents on the Rate of Development of Liquid Photographic Emulsion

K. FUTAKI AND Y. OHYAMA, *Photographic Division, Mitsubishi Paper Mills Co., Ltd., Kyoto, Japan*

The effect of some heterocyclic thiones and other addition agents on the rate of development of a silver chloride liquid emulsion by a dilute Phenidone–hydroquinone developer has been examined. A correlation was observed between the blue-black toning effect of the heterocyclic thiones and the acceleration of development by these agents. N-dodecylpyridinium salt, however, accelerates development but does not have a blue-black toning effect, and some derivatives of benzimidazole and 5-methyl-7-hydroxy-1,3,4-triazaindolizine have a blue-black toning effect but retard or have little effect on the rate of development.

In a previous paper,[1] we described the influences of some active compounds on the color of the developed silver as related to the chain length of their alkyl substituents and demonstrated the usefulness of the "liquid emulsion technique"[2] for testing the effects of additions to an emulsion. The color becomes more blue-black with an increasing number of carbon atoms in the alkyl groups among homologues of 6-alkyl-7-hydroxy-5-methyl-1,3,4-triazaindolizines (**VI**, see below). On the other hand, among the alkyl homologues of 2-alkyl-1,3,4-oxadiazoline-5-thione (**I**), the methyl derivative shows the strongest blue-black toning effect, and the color of developed silver shifts toward warm black with an increasing number of carbon atoms in the alkyl groups.

The present paper deals with the application of the same technique to a study of the influence of these and other addition agents on the rate of development. One of the authors has already reported[3] the effect of additions on the rate of development of coated paper, using an ordinary concentrated developer; the effect was found to be difficult to determine, especially in the case of acceleration.

The "liquid emulsion technique," as already indicated by L. J. Fortmiller and T. H. James,[4] avoids the complications caused by diffusion effects in coated layers and, when used along with a very dilute developer, it is particularly useful for testing the accelerating effect on development. Dilution of the developer (Phenidone–hydroquinone[1]) causes a profound retardation of development, as shown in Fig. 1, so that it becomes easier to determine an accelerating effect of additions upon development. The color of the developed silver, however, is also affected by the dilution, as shown in Table I; these effects will be discussed later.

Twenty-three compounds were tested. The majority of them showed both remarkable accelerating effects on the rate of development and blue-black toning effects on the color of developed silver. Acceleration, however, is not a general feature of additions, and another type of blue-black toner which shows a retarding effect on development will be described.

The names and structural formulae of the compounds tested are as follows:

I. 2-Alkyl-1,3,4-oxadiazoline-5-thiones

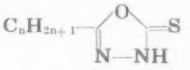

Alkyl = methyl-, *n*-propyl-, *n*-amyl-, *n*-heptyl-, and *n*-nonyl-

(n = 1, 3, 5, 7, and 9)

II. 3-Alkylbenzoxazoline-2-thiones

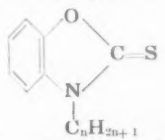

Alkyl = methyl-, ethyl-, *n*-propyl-, *n*-butyl-, and *n*-amyl-

(n = 1, 2, 3, 4, and 5)

III. Azolidine-2-thiones

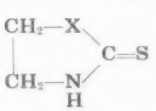

a. X = NH imidazolidine-2-thione

b. X = O oxazolidine-2-thione

c. X = S thiazolidine-2-thione

Presented at the 1960 Annual Conference, Santa Monica, California, 12 May 1960. Received 27 April 1960.

1. K. Futaki, Y. Ohyama, and T. Iwasaki, *Phot. Sci. & Eng.*, **4**: 97 (1960).
2. T. Iwasaki, Y. Ohyama, and K. Futaki, *Bull. Soc. Sci. Phot. Japan*, No. 9 (Dec. 1959), p. 16.
3. Y. Ohyama, *Bull. Chem. Soc. Japan*, **25**: 18 (1952).
4. L. J. Fortmiller and T. H. James, *Phot. Sci. & Tech.*, **17B**: 102 (1951).

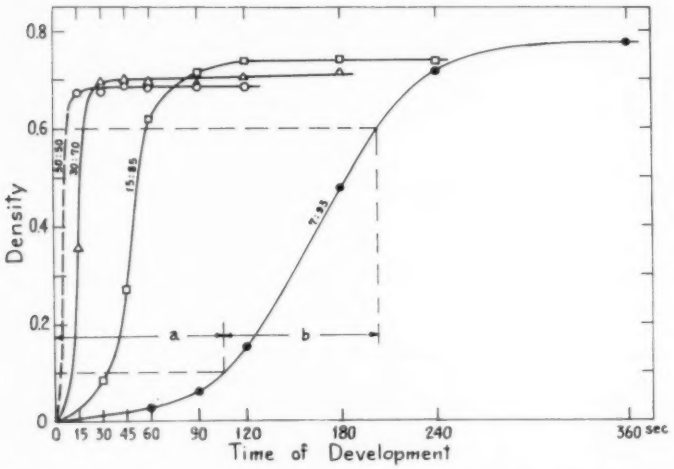

Fig. 1. Effect of dilution of the developer on the rate of development. Dilution ratios (stock soln. : gelation soln.) are specified on curves.

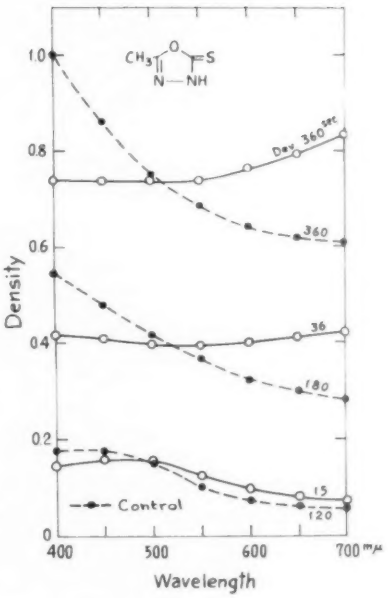

Fig. 2. Some examples of spectrophotometric densities for the silver dispersions developed for various periods. Solid curves—with added 2-methyl-1,3,4-oxadiazole-5-thione (0.01 mole/mole AgCl); broken curves—without it.

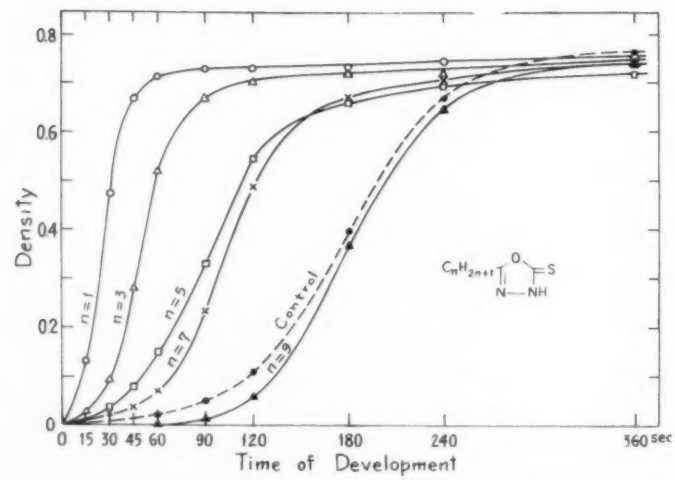

Fig. 3. Time-density curves for development in the presence of various alkyl homologues of 2-alkyl-1,3,4-oxadiazoline-5-thione (0.01 mole/mole AgCl).

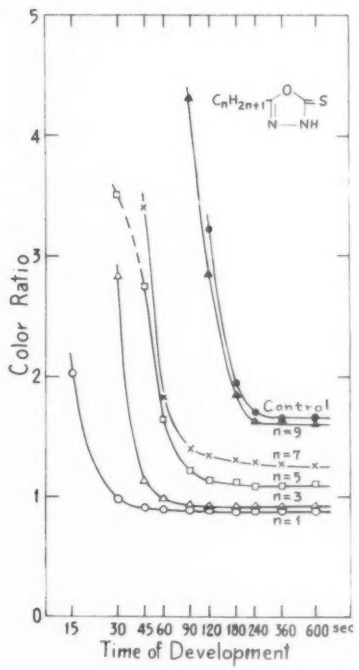

Fig. 4. Effect of duration of development on the color ratio of silver dispersions developed in the presence of various alkyl homologues of 2-alkyl-1,3,4-oxadiazoline-5-thione (0.01 mole/mole AgCl). The top curve is the control.

TABLE I. Effect of Dilution of Developer without Addition Agent on Rate of Development and Color Ratio of Developed Silver

Dilution ratio Stock soln.: gelatin soln.*	Acetic acid stop soln.	Time in sec to reach $D = 0.1$ (a)	Time in sec to reach $D = 0.6$ from 0.1 (b)	Color ratio
50:50	9 N	4(?)	4(?)	1.15
30:70	5 N	10	10	1.30
15:85	3.5N	33	25	1.49
7:93	2.5N	106	97	1.66

* The concentration of the gelatin solution was adjusted so that the final concentration was kept constant for each case.

TABLE III. Effects of 2-Alkyl-1,3,4-oxadiazoline-5-thione on Rate of Development and on Color Ratio of Developed Silver

Number of alkyl carbon atoms	Amount added, mole/mole AgCl	Time in sec to reach $D = 0.1$ (a)	Time in sec to reach $D = 0.6$ from 0.1 (b)	Color ratio
1	0.01	13	23	0.88
3	0.01	32	40	0.93
5	0.01	51	86	1.11
7	0.01	69	75	1.26
9	0.01	134	85	1.61
Control	0	117	109	1.66

IV. N-Dodecylpyridinium *p*-toluenesulfonate

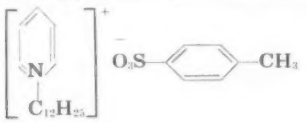

V. Benzimidazoles and benzotriazole

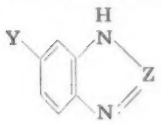

	Y	Z	
a.	H	CH	benzimidazole
b.	Cl	CH	5-chlorobenzimidazole
c.	CN	CH	5-cyanobenzimidazole
d.	NO_2	CH	5-nitrobenzimidazole
e.	H	N	benzotriazole

VI. 6-Alkyl-5-methyl-7-hydroxy-1,3,4-triazaindolizines

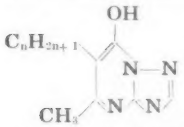

Alkyl = ethyl-, *n*-butyl-, *n*-hexyl-, and *n*-octyl-

(n = 2, 4, 6, and 8)

Experimental Procedure

The experimental procedure used in this investigation was essentially identical with that reported in previous papers,[1,2] i.e., a photographic silver chloride emulsion was developed in the liquid state by a dilute Phenidone–hydroquinone developer,[1] after the addition of small amounts of several organic substances. Additions, however, were made after exposure, instead of before exposure as in previous experiments.[1,2]

Development was stopped and the emulsion was fixed after various periods of development by adding, in succession, a small portion of a stop solution and a fixer. Finally, the spectrophotometric density of the silver dispersion was measured. The compositions of the photographic emulsion and the processing solutions used in the work were also identical with those used in the previous experiments.[1,2]

The rates of development can be expressed by the time–density curves at any level of dosing and can be compared with the one obtained without addition (control). Since the characteristics of a curve can be evaluated from two points on the curve, namely at the toe and near the shoulder, we chose the points at the densities of 0.1 and 0.6 respectively. The time required to reach the density of 0.1 from the start of development (denoted as a in Fig. 1, for example) corresponds to the induction period; the reciprocal of the time required to reach the density of 0.6 from 0.1 (denoted as b in Fig. 1) is

TABLE II. Spectrophotometric Densities and Color Ratios for Silver Dispersion

Time of dev, sec	Density (D), mμ							Representative density*	Color ratio, $D(400)/D(700)$
	400	450	500	550	600	650	700		
Developed with 2-methyl-1,3,4-oxadiazole-5-thione (0.01 mole/mole AgCl)									
15	0.145	0.157	0.153	0.125	0.098	0.082	0.072	0.114	2.02
30	0.417	0.410	0.397	0.396	0.402	0.412	0.423	0.412	0.986
360	0.740	0.740	0.740	0.740	0.765	0.795	0.835	0.772	0.887
Developed without addition agent (control)									
120	0.177	0.178	0.151	0.101	0.075	0.064	0.055	0.111	3.22
180	0.549	0.478	0.416	0.367	0.325	0.299	0.283	0.400	1.94
360	1.010	0.860	0.750	0.684	0.643	0.620	0.610	0.768	1.66

* Representative density is an arithmetic mean of the densities at 400, 550, and 700 mμ, i.e. = 1/3 [$D(400) + D(550) + D(700)$].

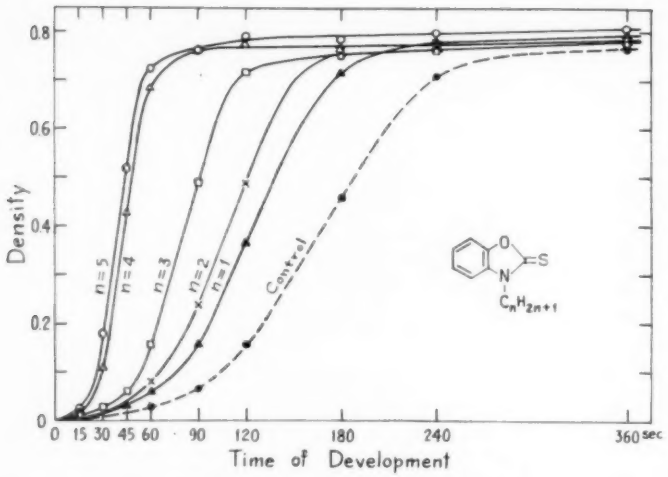

Fig. 5. Time-density curves for development in the presence of various alkyl homologues of 3-alkylbenzoxazoline-2-thione (0.05 mole/mole AgCl).

proportional to the rate of density-increase beyond the induction period and corresponds to the slope of the straight line part of a curve. We determined these two important time values (a and b) from the curves and tabulated them for comparison.

Because the developed silver images usually have a distinct color (as shown in Fig. 2, for example), an arithmetic mean of densities at three main wavelengths, namely 400, 550 and 700 mμ was taken as a representative density of the developed silver. As an indication of the "color" of the developed silver, the "color ratio"[5] was calculated from the ratio of the density measured at 400 mμ to that at 700 mμ as described in our previous paper.[1] The values are listed also in the present tables together with the rate-indicating time values a and b.

5. T. H. James and W. Vanselow, *Phot. Sci. & Eng.*, **1**: 104 (1958).

TABLE IV. Effects of 3-Alkylbenzoxazoline-2-thione on Rate of Development and on Color Ratio for Developed Silver

Number of alkyl carbon atoms	Amt added, mole/mole AgCl	Time in sec to reach $D=0.1$ (a)	Time in sec to reach $D=0.6$ from 0.1 (b)	Color ratio
1	0.05	76	77	1.69
2	0.05	66	68	1.64
3	0.05	54	46	1.62
4	0.05	28	24	1.38
5	0.05	26	22	1.28
Control	0	104	104	1.65

Results and Discussion

1. *2-Alkyl-1,3,4-oxadiazoline-5-thione* (**I**). As a typical example of results obtained with these homologues, the spectrophotometric densities of the silver developed for various periods after adding the 2-methyl derivative are shown in Table II and Fig. 2. The curves show a remarkable accelerating effect on the rate of development and a blue-black toning effect on the color of developed silver.

Figure 3 shows time-density curves of development at a concentration of 0.01 mole/mole AgCl of the

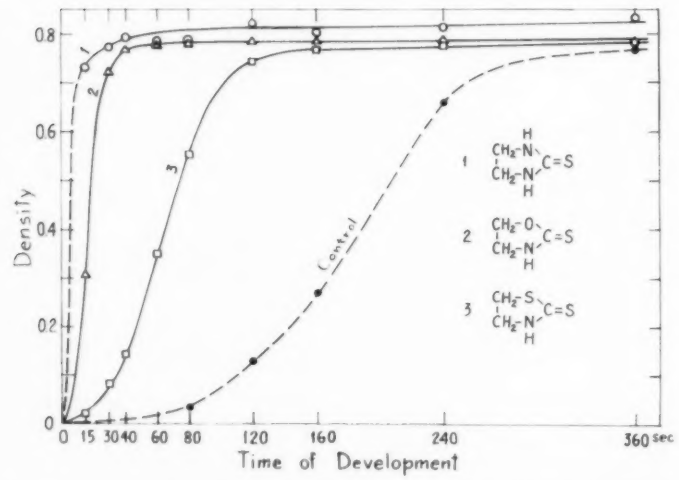

Fig. 6. Time-density curves for development in the presence of various alkyl homologues of azolidine-2-thiones (0.025 mole/mole AgCl).

TABLE V. Effects of Azolidine-2-thiones on Rate of Development and on Color Ratio for Developed Silver

Compound	Amt added mole/mole AgCl	Time in sec to reach $D=0.1$ (a)	Time in sec to reach $D=0.6$ from 0.1 (b)	Color ratio
Imidazolidine-2-thione	0.025	3(?)	4(?)	0.84
Oxazolidine-2-thione	0.025	9	13	0.98
Thiazolidine-2-thione	0.025	34	52	1.30
Control	0	110	116	1.70

TABLE VI. Effects of N-Dodecylpyridinium *p*-toluenesulfonate on Rate of Development and on Color Ratio of Developed Silver

Amt added, mole/mole AgCl	Time in sec to reach $D = 0.1$ (*a*)	Time in sec to reach $D = 0.6$ from 0.1 (*b*)	Color ratio
0.05	32	19	1.68
0.01	68	69	1.75
0 (Control)	93	103	1.64

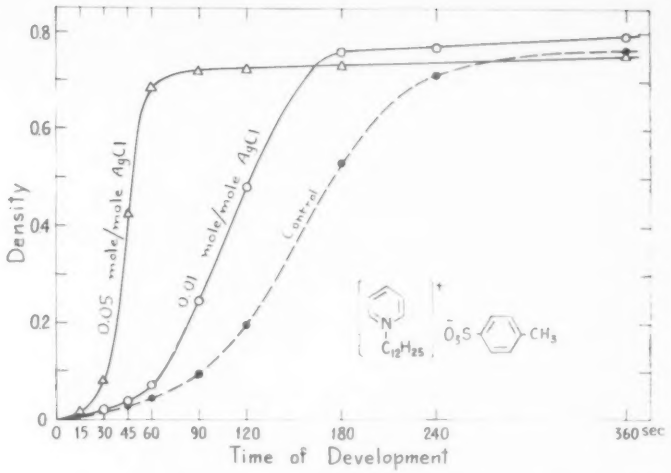

Fig. 7. Time-density curves for development in the presence of 0.01 and 0.05 mole N-dodecylpyridinium-*p*-toluenesulfonate/mole AgCl.

substances in this series of homologues; the rate-indicating time values (*a* and *b*) and color ratios are also summarized in Table III. The methyl derivative shows the strongest accelerating effect on the rate of development, and with increasing number of carbon atoms in the alkyl groups, the accelerating property decreases regularly in this series of homologues.

The effect of duration of development on the color ratio of developed silver is shown in Fig. 4. In each case, the color ratio is very large (yellow to red-brown color) at an early stage of development, but decreases rapidly with the continuation of development and reaches a limiting value (warm black to blue black). These limiting values (usually at 10-min development) are used for the evaluation of the toning effect of the addition agents. It is clear that, in this case, the methyl derivative is also the strongest blue-black toner and the color of developed silver shifts toward warm black (the color ratio increases) with an increasing number of carbon atoms in the alkyl groups, as already reported in the previous paper.[1]

We conclude that, for this series of homologues, there is an apparent correlation between the accelerating effect on the rate of development and the blue-black toning effect.

2. *3-Alkylbenzoxazoline-2-thiones* (**II**). In contrast to the case mentioned above, both the accelerating effect of the 3-alkylbenzoxazoline-2-thiones on the rate of development and the blue-black toning effect on the color of developed silver became stronger with an increasing number of carbon atoms in the alkyl groups, as shown in Fig. 5 and Table IV. An apparent correlation between the two effects is also found in this case.

3. *Azolidine-2-thiones* (**III**). The effects of imidazolidine-2-thione (**IIIa**), oxazolidine-2-thione (**IIIb**), and thiazolidine-2-thione (**IIIc**) are shown in Fig. 6 and Table V. A striking accelerating effect on the rate of development was found for both **IIIa** and **IIIb**. Both were more active than N-dodecylpyridinium *p*-toluenesulfonate (**IV**), a well-known development accelerator of the quaternary base type (Fig. 7), while **IIIc** is almost equal in activity to the quaternary base. All the azolidine-2-thiones also have a blue-black toning effect, and both effects decrease in an order of **a, b, c.**

4. *Apparent Correlation between Blue-Black Toning Effect and Acceleration of Development.* The three types of compounds (**I, II,** and **III**) mentioned above are heterocyclic thiones, and there seems to be a correlation between the accelerating effect and the blue-black toning effect on development.

Also, there is an apparent correlation between the two effects when the concentration of the developer (without additions) is varied as shown in Fig. 1 and Table I. However, in the case of N-dodecylpyridinium *p*-toluenesulfonate (**IV**), acceleration of development is not accompanied by a blue-black toning effect, as shown in Table VI, and it is well known that there are many blue-black toners which retard development. Some examples of this type of blue-black toner are found in the derivatives of benzimidazoles or hydroxytriazaindolizines, as shown in Secs. 5 and 6, below.

It must be concluded, therefore, that an apparent correlation between the two effects found in the heterocyclic thiones is not a general feature of additions, but is peculiar to this class of compound. A correlation is also apparent between the fogging tendency of these compounds and the acceleration of development, and of course such a relationship is not restricted to this type of compound alone.

5. *Benzimidazoles and Benzotriazole* (**V**). As shown in Fig. 8 and Table VII, benzimidazoles rather retard development in spite of their blue-black

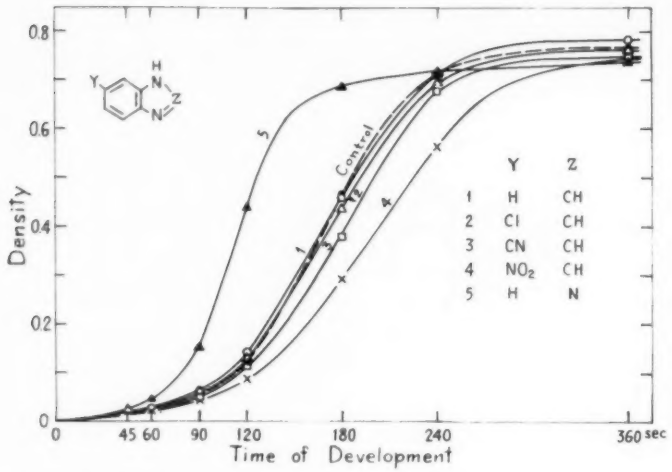

Fig. 8. Time-density curves for development in the presence of benzimidazoles and benzotriazole (0.05 mole/mole AgCl).

TABLE VII. Effects of Benzimidazoles and Benzotriazole on Rate of Development and Color Ratio for Developed Silver

Compound	Amt added, mole/mole AgCl	Time in sec to reach $D=0.1$ (*a*)	Time in sec to reach $D=0.6$ from 0.1 (*b*)	Color ratio
Benzimidazole	0.05	107	101	1.65
5-Chlorobenzimidazole	0.05	111	102	1.57
5-Cyanobenzimidazole	0.05	116	104	1.36
5-Nitrobenzimidazole	0.05	126	124	1.15
Benzotriazole	0.05	79	62	1.05
Control	0	116	89	1.65

toning tendency, and both effects become stronger if the substitution is made at the 5-position with the more electronegative groups, i.e. in the order of chloro-, cyano- and nitro-groups. (Note that the 5 and 6 positions in the benzimidazoles are equivalent. *Ed.*) On the other hand, benzotriazole accelerates development in spite of its strong blue-black toning effect (stronger than 5-nitrobenzimidazole) and its antifogging tendency.

6. 6-Alkyl-5-methyl-7-hydroxy-1,3,4-triazaindolizines (**VI**). Figure 9 and Table VIII show the effect of the triazaindolizines. The accelerating effect on development found in some of these derivatives is not so manifest as in the case of the heterocyclic thiones, and the triazaindolizines rather resemble in their properties benzotriazole and the benzimidazoles mentioned above.

The effect on the rate of development shifts from acceleration to retardation with an increasing number of carbon atoms in the alkyl substitution group of the triazaindolizines. This shift is accompanied by the strong blue-black toning effect on the color of developed silver, as was reported in detail in our previous paper.[1] (Among the homologues, the octyl derivative showed the strongest effect on tone.)

The type of blue-black toner described in Secs. 5 and 6 has a strong antifogging property, in contrast to the fairly strong fogging tendency of the heterocyclic thiones mentioned in Secs. 1, 2, and 3.

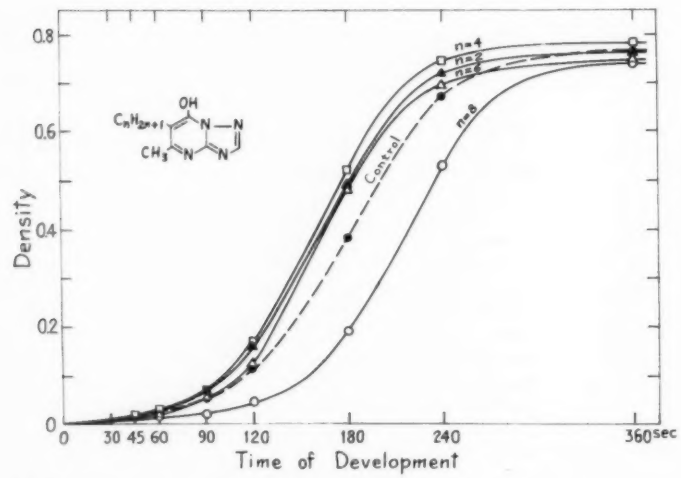

Fig. 9. Time-density curves for development in the presence of 6-alkyl-7-hydroxy-5-methyl-1,3,4-triazaindolizines (0.05 mole/mole AgCl).

TABLE VIII. Effects of 6-Alkyl-7-hydroxy-5-methyl-1,3,4-triazaindolizines on Rate of Development and on Color Ratio of Developed Silver

Number of alkyl carbon atoms	Amt added, mole/mole AgCl	Time in sec to reach $D=0.1$ (*a*)	Time in sec to reach $D=0.6$ from 0.1 (*b*)	Color ratio
2	0.05	104	97	1.54
4	0.05	100	94	1.45
6	0.05	112	94	1.18
8	0.05	154	101	0.96
Control	0	114	108	1.63

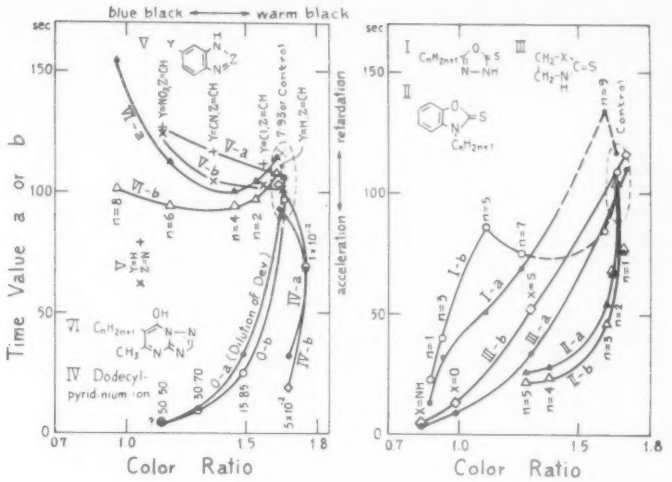

Fig. 10. Relation between the rate of development and the color shift of the developed silver. *Left:* Effect of benzimidazoles, benzotriazole, and triazaindolizines compared with dodecylpyridinium ion and the effect of dilution of the developer. *Right:* Effect of the heterocyclic thiones (alkyloxadiazolinethiones, alkylbenzoxazolinethiones, and thiazolidinethiones).

The relation between the rate of development expressed in time values a or b and the color ratio is quite different for these two types of blue-black toner, as illustrated in Fig. 10. The relation is also different among the heterocyclic thiones themselves (**I**, **II**, and **III**), and the relation for **II** closely resembles that observed when the concentration of developer is changed.

The authors wish to express their thanks to Katsuo Hohjoh for his assistance in carrying out the tedious laboratory experiments.

Back Issues Available

Photographic Engineering—1950–1956

Volumes 1 through 6 (4 issues each volume)..... $5.00 per volume..... $1.50 per issue
Volume 7 (2 single issues, Nos. 1 and 2, plus two issues, Nos. 3 and 4, combined under one cover)..... 5.00 per volume..... 1.50 per single issue
3.00 for combined issue

Photographic Science and Engineering—since 1957

Volumes 1 and 2 (4 issues each volume)
Volume 3 (6 issues)
Members—$6.00 per volume..... $1.75 per issue
Nonmembers—8.00 per volume..... 2.00 per issue

Subscription to current volume (6 issues)
Nonmembers.....$12.00
Members.....Included in $8.00 annual dues

An index appears in the final issue of each volume except Volume 6 of *Photographic Engineering*. This index was published separately and is included with the issues when Volume 6 is ordered.

Order from:

Edward S. Cobb, *Managing Secretary*
Society of Photographic Scientists and Engineers
Box 1609, Main Post Office
Washington, D.C.

PHOTOGRAPHIC SCIENCE AND ENGINEERING
Volume 4, Number 5, September-October 1960

Contribution to the Theory of the Characteristic Curve

H. FRIESER* AND E. KLEIN, *Agfa Scientific Photographic Laboratory, Agfa AG, Leverkusen, West Germany*

A general theory of the characteristic curve is derived which agrees in principle with results previously obtained by other authors. Application of the theory permits a comparison with experimental results and allows an appraisal of the effects of grain size distribution, statistical quanta effects, and sensitivity distribution on the location and shape of the characteristic curve.

The spread of the grain size distribution exclusively determines the shape of flat characteristic curves; random quanta effects and sensitivity distribution can be expected to influence results only when the grain size distribution is very narrow. The sensitivity distribution can be determined by comparison of the experimentally and theoretically computed characteristic curves. It is shown that in a very highly sensitive negative emulsion a grain must absorb on the average 10–15 quanta to become developable. On this basis, an estimate can be made of the theoretically possible increase in sensitivity. The absorption of the elementary layer may be derived from transmission and reflection measurements of the thick layer. This elementary layer differs from one which is not an integral part of a composite layer.

I. Factors Determining the Characteristic Curve

The fact that a given exposure of a photographic layer renders only a certain number of its grains developable shows that a grain must absorb a certain minimum number of quanta, r^*, in order to become developable. Here, r^* is an individual characteristic of each grain for given conditions of development and can depend on the size of the grain as well as on properties acquired by chance during grain growth and chemical ripening (see below). In the computation of the characteristic curve $S(\log Q_0)$, it is necessary to know, therefore, the number of grains rendered developable as a function of the exposure Q_0 (in quanta per square centimeter). In addition we must know how much these grains contribute to density. The location and shape of the characteristic curve, as has been shown by many other workers,[1] depend on the following four factors:

1. The size of the silver halide grains (diameter d) varies, and this results in a certain size distribution function $\eta(d)$ which gives information about the frequency of different grain size classes. In each class i there are

$$N\eta_i = N_i \text{ grains} \tag{1}$$

$$\text{with} \qquad \sum_0^\infty \eta_i = 1 \quad \text{and} \quad \sum_0^\infty N_i = N \tag{2}$$

N being the total number of grains under consideration. The grain size distribution governs the shape of the characteristic curve partly because light absorption is dependent upon grain size and partly because grains of different size contribute differently to density.

2. Within any size class i there is a statistical absorption of quanta. When each grain of class i absorbs q_i quanta on the average, then some grains will absorb r^* *and more* quanta, whereas others will not reach the number r^*. However, only grains that absorb at least r^* quanta can contribute to the total density. The probability that a grain will absorb r^* quanta is given by the Poisson function:

$$w(q_i, r^*) = e^{-q_i}(q_i^{r^*}/r^*!) \tag{3}$$

The fraction of the grains of class i that absorb at least r^* quanta then becomes

$$p(q_i, r^*) = 1 - e^{-q_i} \sum_0^{r^*-1} \frac{q_i^{r^*}}{r^*!} \tag{4}$$

3. The value of r^* depends on the size class i but can vary also *within* a given size class. Hence a function $\beta(i, r^*)$ can exist which gives the frequency of occurrence of different r^* values. It follows that $N_i\beta(i, r^*)$ is the fraction of grains of class i which are developable after absorption of

Presented at the Annual Conference, Santa Monica, California, 13 May 1960. Received 9 May 1960.

* Present address: Institut f. wiss. Photographie, Technische Hochschule, Munich 2, West Germany.

1. P. C. Burton in *Fundamental Mechanisms of Photographic Sensitivity*, J. W. Mitchell, Ed., Butterworth Sci. Pubs., London, 1951, p. 188; also, P. C. Burton in Mees, *The Theory of the Photographic Process*, rev. ed., Macmillan, New York, 1954, Chap. 5; also J. H. Webb, *J. Opt. Soc. Am.*, **38**: 27 (1948).

r^* quanta $\left[\sum_0^\infty \beta(i, r^*) = 1\right]$. The function $\beta(i, r^*)$ is known as the sensitivity distribution.

4. The shape of the characteristic curve is also influenced by the thickness of the photographic layer, since the absorption of individual elementary layers, and hence their contribution to the total density, varies with layer depth. The influence of layer thickness can be expressed by the following equation (see also Part III, Sec. 2a):

$$S(\log Q_0) = \frac{1}{D}\int_{\log Q_0 - D}^{\log Q_0} s(\log Q_0)\ \partial \log Q_0 \qquad (5)$$

where $S(\log Q_0)$ and $s(\log Q_0)$ are the characteristic curves of the thick and the elementary layers, respectively, Q_0 is the exposure, and D is the optical density of the layer. The value of D is computed from the transmission and reflection coefficients τ and ρ by the equation

$$D = \log (1 + \rho)/\tau \qquad (6)$$

II. Computing the Elementary Characteristic Curve

On the basis of the factors considered in Part I, it is now possible to derive the expression for the characteristic curve, it being sufficient to treat the elementary layer only, since it is simple[2] to compute the characteristic curve of the thick layer by means of Eq. (5).

Assume that 1 sq cm of an elementary layer with N grains is hit by Q_0 quanta, of which Q are absorbed. Assume further that one grain of the size class i absorbs $\alpha_i Q_0$ quanta; then all grains of the class i will absorb $Q_i = N_i \alpha_i Q_0$ quanta. Given $Q = Q_0 \sum_0^\infty N_i \alpha_i$, it follows that

$$Q_i = Q\frac{N_i\alpha_i}{\sum_0^\infty N_i\alpha_i} = Q\frac{\eta_i\alpha_i}{\sum_0^\infty \eta_i\alpha_i} \qquad (7)$$

Hence *each* grain of class i *on the average* absorbs q_i quanta, where

$$q_i = \frac{Q_i}{N_i} = \frac{Q_i}{N\eta_i} = \frac{Q\cdot\alpha_i}{N\sum_0^\infty \eta_i\alpha_i} \qquad (8)$$

The fraction of grains of class i that absorb at least r^* quanta is $p(q_i, r^*)$ according to Eq. (4), but since r^* can vary from grain to grain (sensitivity distribution $\beta(i, r^*)$), the fraction of the grains of any size class that becomes developable is given by:

$$\sum_{r^*} p(q_i, r^*)\ \beta(i, r^*)$$

Thus the number N_i' of *developable* grains of class i equals

$$N_i' = N\eta_i \sum_{r^*} p(q_i, r^*)\ \beta(i, r^*) \qquad (9)$$

The total number N' of grains of all size classes which contribute density then equals:

$$N' = \sum_0^\infty \eta_i N \sum_{r^*} p(q_i, r^*)\ \beta(i, r^*) \qquad (10)$$

However, grains of different size contribute different amounts to the total density. The relative density contribution of N_i' developable grains of class i (Eq. (9)) is:

$$s_i = \frac{N_i'\mu_i}{\sum_0^\infty N_i\mu_i} \qquad (11)$$

where $\sum_0^\infty N_i\mu_i$ represents the maximum density of the layer.

Altogether, N' grains are made developable by absorption of Q quanta (Eq. (10)) with a corresponding density of:

$$s = \frac{\sum_0^\infty N_i'\mu_i}{\sum_0^\infty N_i\mu_i} = \frac{\sum_0^\infty \eta_i\mu_i \sum_{r^*} p(q_i, r^*)\ \beta(i, r^*)}{\sum_0^\infty \eta_i\mu_i} \qquad (12)$$

The values for μ_i (Eq. (11)) and α_i (Eq. (8)) can be obtained from previously published data. The relation between the density S and the number N of developed grains per square centimeter which have a mean projective area $\bar{j}e$ has been derived by Nutting and by Arens, Eggert, and Heisenberg[3,4,5]:

$$S = \frac{1}{2\,3} N\,\bar{j}e. \qquad (13)$$

In this equation, allowance must be made for the varying relation between the size of the developed and the undeveloped grains which is affected by development conditions.[5] An appropriate proportionality factor is not included in the equation when relative densities only are being considered. Thus, $\bar{j}e$ in Eq. (13) is proportional to the square of the grain diameter with the result that

$$\mu_i = \varphi d_i^2 \qquad (14)$$

A value for α_i in Eq. (8) is obtained from the fact that the probability of a grain absorbing a certain number of quanta increases with grain size, and more specifically with grain volume for exposure to light in the region of silver halide absorption. It follows that:

$$\alpha_i = \psi d_i^3 \qquad (15)$$

2. E. Zeitler, *Phot. Korr.*, **95:** 99 (1959).

3. P. G. Nutting, *Phil. Mag.*, **26:** 423 (1913).

4. H. Arens, J. Eggert, and E. Heisenberg, *Z. wiss. Phot.*, **28:** 356 (1931).

5. E. Klein, *Z. Elektrochem.*, **62:** 993 (1958).

Substituting Eq. (14) in Eq. (12), we obtain:

$$s = \frac{\sum_0^\infty \eta_i d_i^2 \sum_{r^*} p(q_i, r^*)\, \beta(i, r^*)}{\sum_0^\infty \eta_i d_i^2} \qquad (16)$$

in which q_i may be computed from Eqs. (8) and (15):

$$q_i = \frac{Q}{N} \frac{d_i^3}{\sum_0^\infty \eta_i d_i^3} \qquad (17)$$

It will be noted that the proportionality factors φ and ψ of Eqs. (14) and (15) cancel out in (16) and (17). It should also be noted that Eq. (16) changes into (16a) for roentgen and electron exposures (particle exposure) where $r^* = 1$, i.e.

$$s = \frac{\sum_0^\infty \eta_i d_i^2 (1 - e^{-q_i})}{\sum_0^\infty \eta_i d_i^2} \qquad (16a)$$

This equation will be discussed more fully in another paper.

III. Application of the Theory

1. *Computation of Characteristic Curves from Given Parameters*

In the application of Eq. (16), q_i values are computed according to Eq. (17) for a continuous series of given values of Q/N. In this manner, initial densities of the elementary layer are obtained as a function of the mean number of quanta absorbed by each grain.

To permit a theoretical analysis of the influence of different distributions in Eq. (16) upon the shape of the characteristic curve, three different grain distributions, η_1, η_2, η_3, are postulated first. These result analytically from log normal Gaussian functions of the form:

$$\frac{\partial H}{\partial \log d} = \frac{1}{\sigma \cdot \sqrt{2\pi}} e^{-\frac{[\log (d/d_0)]^2}{2\sigma^2}} \qquad (18)$$

where H is the frequency, d the grain diameter, and σ the standard deviation (log = logarithm to the base ten). The grain diameter in this analysis is defined as the diameter of a sphere which has the same volume as the grain. Then,

$$\eta = \frac{\partial H}{\partial d} = \frac{0.43}{d \cdot \sigma \sqrt{2\pi}} e^{-\frac{[\log (d/d_0)]^2}{2\sigma^2}} \qquad (19)$$

and the individual distributions which have been chosen become:

$$\eta_1 \ (\sigma_1 = 0.235)$$

$$\eta_2 \ (\sigma_2 = 0.118)$$

$$\eta_3 \ (\sigma_3 = 0.059)$$

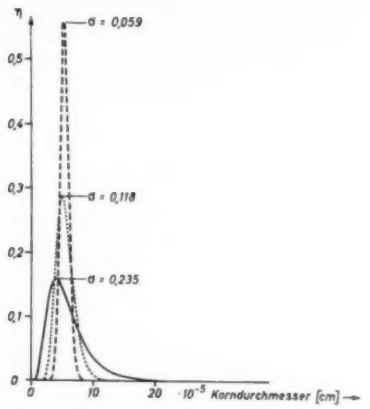

Fig. 1. The grain size distribution η (Eq. (19)), used as a basis for the theoretical computations.

with d_0 having the same value, 5.3×10^{-5} cm, for all three distributions. η_1 is the grain distribution of a commercial negative emulsion.

The values of η as a function of diameter are plotted in Fig. 1.

The most frequent diameter values d_{max} can be computed from d_0 as follows:

$$d_{max} = d_0 e^{-5.3\sigma^2} \qquad (20)$$

In Fig. 2, values of $p(q, r^*)$ are shown for various values of r^* as determined by Eq. (4); these were computed earlier by Webb.[1] Values of q_i, computed by Eq. (17), have to be substituted here for q.

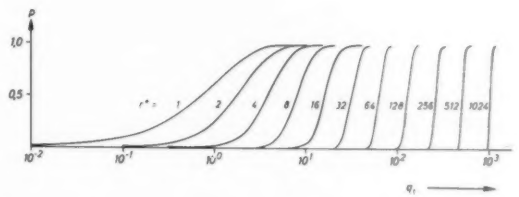

Fig. 2. The quantities $p(q,r^*)$ for various values of r^*, plotted as a function of the mean absorbed quanta per grain.

The various special cases which were computed by means of Eq. (16) are listed in Table I and are shown graphically in Figs. 3 A-C, and 5.

When all grains of a layer are of equal size (i.e. there is no grain size distribution, and $\sigma = 0$ in Eq. (19)), and when in addition $\beta(i, r^*) = 1$ (i.e. all grains have equal sensitivity), Eq. (16) becomes

$$s = p(q_i, r^*) \qquad (21)$$

In this special case the curves of Fig. 2 are equivalent to the desired characteristic curves. It is to be noted that relatively flat characteristic curves are obtained even in the total absence of grain size distribution

TABLE I

η	p	β	Figure
η_1	1	1	3A
η_1	$p\ (q_i, r^*)$	1	
η_2	1	1	3B
η_2	$p\ (q_i, r^*)$	1	
η_3	1	1	3C
η_3	$p\ (q_i, r^*)$	1	
η_1	$p\ (q_i, r^*)$	$\beta\ (i, r^*)$, $r_0^* = 16$	5
η_3	$p\ (q_i, r^*)$	$\beta\ (i, r^*)$, $r_0^* = 16$	

when the r^* values are small (great sensitivity of the grains); the gradation increases with increasing r^*.

When grain size distribution ($p = 1, \beta = 1$) is the only parameter being considered, then:

$$s = \frac{\sum_{d_i}^{\infty} \eta_i d_i^2}{\sum_{0}^{\infty} \eta_i d_i^2} \tag{21a}$$

The appropriate values of mean absorption of quanta per grain $(Q/N)_i$, which effects developability of all grain classes greater than d_i, can then be computed from:

$$\left(\frac{Q}{N}\right)_i = \frac{r^*\, d_i^3}{\sum_{0}^{\infty} \eta_i d_i^3} \tag{21b}$$

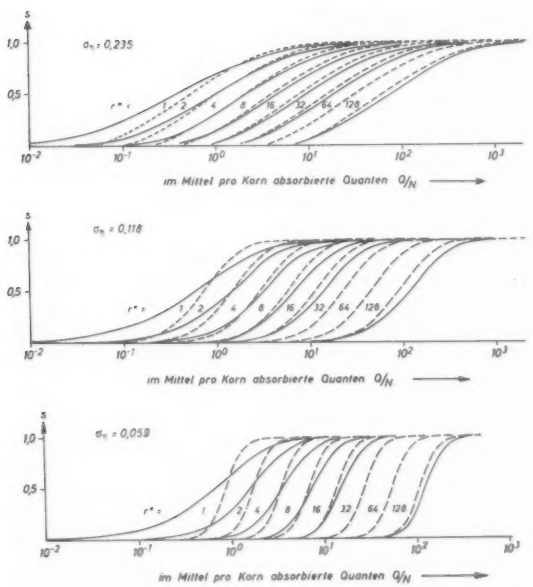

Figs. 3A, B, C. The theoretically computed characteristic curves, s, (Eq. (16)) that correspond to the special data listed in Table I. Q/N is the mean absorbed quanta per grain. The solid line curves apply when grain distribution and quanta statistics are considered. The broken line curves were computed by means of Eqs. (21a) and (21b).

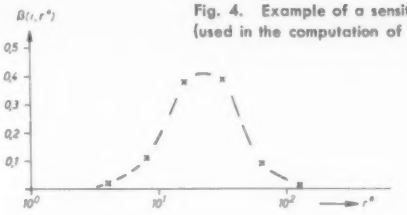

Fig. 4. Example of a sensitivity distribution (used in the computation of curves shown in Fig. 5)

When the curves of Figs. 3 A-C, which were computed solely on the basis of grain size distribution, are compared with those which also include quanta-statistical data (p values), it is evident that the grain distribution primarily governs the shape of the characteristic curve and that quanta fluctuations are significant only when the r^* values are small. However, the influence of quanta fluctuations becomes noticeable for large r^* values when the spread of the grain size distribution decreases.

Since few experimental data are available on the sensitivity distribution $\beta(i, r^*)$, an arbitrary distribution has been adopted such as shown in Fig. 4. It corresponds analytically to the equation

$$\beta = \frac{\partial H}{\partial r^*} = \frac{0.43}{r^*\sigma\sqrt{2\pi}}\, e^{-\frac{[\log (r^*/r^*_0)]^2}{2\sigma^2}} \tag{22}$$

where $r^*_0 = 16$ and $\sigma = 0.25$.

In this way, one can examine at least theoretically the effect of such a distribution on various characteristic curves. It will be apparent from Fig. 5 that even the wide distribution of sensitivity assumed in this example is totally masked by the effects of grain distribution when this distribution is wide (η_1). The sensitivity distribution becomes noticeable only with narrow grain size distribution (η_3). The same distribution $\beta(i, r^*)$ was used as a basis for each grain class i in the computations for Fig. 5; furthermore, the value $r^*_0 = 16$ was employed for all curves. An appraisal of the influence of the individual distribution is given subsequently.

2. *Comparison of Experimental and Theoretical Characteristic Curves*

(a) *The Relation between Q/N and Q_0*

When we deal with experimentally determined characteristic curves, we obtain densities as a func-

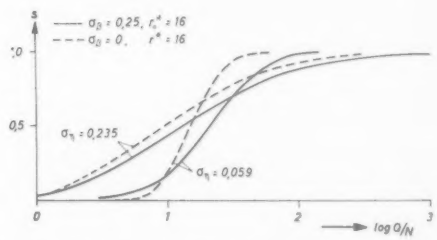

Fig. 5. The effect of the sensitivity distribution on the shape of the characteristic curve for a variety of grain size distributions.

tion of Q_0, the number of incident quanta per square centimeter. Since this always involves "thick" layers, it is necessary first of all to compute the curve of the elementary layer by means of the integral Eq. (5); this can be done graphically when D is known (Eq. (6)). Now, in order to permit comparison of such a characteristic curve with one of an elementary layer that has been computed theoretically (Eq. (16)), we must assign appropriate values of Q_0 to the abscissa values Q/N of the theoretical curve (mean number of quanta *absorbed per grain*). The absorption of quanta in elementary layers of different thickness was computed previously[6] on the basis of available experimental values. This yielded the following equation for a layer thickness of zero ($z = 0$), i.e., the topmost elementary layer:

$$q' = \left(\frac{Q}{NQ_0}\right)_{z=0} = \frac{4.47\,\bar{d}^3(1+\rho)(1-\rho-\tau)}{A\,(1+\rho-\tau)} \log\frac{1+\rho}{\tau} \qquad (23)$$

where $\bar{d}$ is the arithmetic mean grain diameter in cm (computed from d_0 by $\bar{d} = d_0 e^{2.65\sigma^2}$), ρ and τ are the reflection and transmission coefficients, respectively, and A is the silver content of the layer in grams per square centimeter. This work[6] yielded the significant result that the $q'_{(z=0)}$ value of an emulsion is nearly independent of the silver content when this content is not too low (small τ values). This means that the values of ρ, τ, and A vary with layer thickness in such a fashion that $q'_{(z=0)}$ is practically independent of them. This result will become more understandable from the following discussion of Eq. (23).

Even when A has relatively small values, ρ becomes constant and τ small with respect to 1. Moreover, $\log(1+\rho)/\tau$ becomes nearly proportional to the silver content. Equation (23) yields a constant value under these conditions which depends only on $\bar{d}^3$. It is this constancy of $q'_{(z=0)}$ with respect to practically significant values of A and τ that makes it possible by means of Eq. (5) to compute the density of a "thick" layer from an elementary layer. "Elementary layer" in this context refers to the uppermost layer of a "thick" layer and not to a thin layer outside and separate from the total layer composite. Such a separate, elementary layer would be exposed only by incident quanta, whereas the elementary layer of a composite emulsion is exposed also by quanta reflected from lower strata. We obtain then from Eq. (23):

$$Q_0 = Q/q'N \qquad (24)$$

With the aid of this expression, we can now relate the Q/N values of the theoretical curves to the Q_0 values of some given layer. Of course, the values η_i, $p(q_i, r^*)$, and $\beta(i, r^*)$ of the appropriate experimental layer and its characteristic curve must be used in the computation of the theoretical curves.

6. H. Frieser and E. Klein, *Z. Elektrochem.*, **62:** 874 (1958).

(b) Determination of the Sensitivity Distribution and of the r^* Values

The elementary characteristic curve and the corresponding grain size distribution η are determined for a photographic layer. Next, the theoretical elementary curves are computed by means of Eq. (16) for various values of r^*, but with constant $\beta(i, r^*) = 1$. Using Eqs. (23) and (24), appropriate Q_0 values are obtained for the Q/N abscissa values of the theoretical curves. Therefore, it is possible to include the experimental curves in the plot of the theoretical curves. In the event that a theoretical and an experimental curve coincide, the correct value of r^* is immediately evident, i.e., the number of quanta that must be absorbed by a grain to become developable is known. Such a coincidence of curves indicates also that the assumption that $\beta(i, r^*) = 1$ is correct within the limits of measurement; in other words, sensitivity distribution does not affect the results in this instance. However, when it is impossible to match the experimental curve with any theoretical curve, an empirical β-distribution must be introduced in the form of Eq. (22), wherein values for r^* can be estimated (see Part III, Sec. 3) from a comparison of the experimental curve with the curves computed for $\beta = 1$. One of these empirically derived β-distributions will yield agreement with the experimental data, and by this indirect method a good approximation will be obtained to the sensitivity distribution.

Of course, when β does depend on grain class i, it is necessary in principle to introduce several distributions of $\beta(i, r^*)$. However, in practice it is usually sufficient to use a constant value $\beta(r^*)$ for all grain size classes. In any event, it does not seem possible to compute the functions $\beta(i, r^*)$ from the experimental curves. As for the value of r^*, which is so important in the elementary process because it is the *minimum* quantity that renders a grain developable, it suffices to seek an agreement between experiment and theory in the region of low densities.

Experimentally determined characteristic curves of two high-speed negative emulsions, A and B, are shown in comparison with theoretically computed curves in Fig. 6A, B. The two experimental curves have very different gradients. The data for these emulsions are shown in Table II.

TABLE II

	Emulsion A	Emulsion B
Grain size distribution, Eq. (19)	$\eta(\sigma = 0.27;\ d_0 = 0.63\ \mu)$	$\eta(\sigma = 0.098;\ d_0 = 1.34\ \mu)$
τ	0.23	0.40
ρ } Eq. (23)	0.23	0.19
A	$4.2 \cdot 10^{-4}$ grams Ag/cm²	$4.3 \cdot 10^{-4}$ grams Ag/cm²
Sensitivity distribution, Eq. (22)	$\beta \approx 1$	$\beta = \beta(\sigma = 0.60;\ r_0^* = 14)$

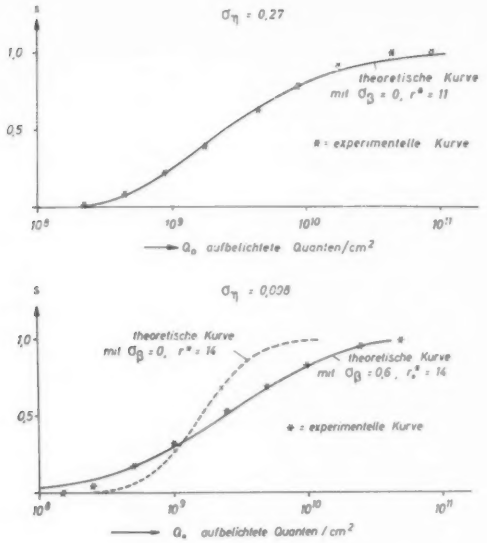

Figs. 6A, B. Comparison of theoretically computed and experimental characteristic curves of high-speed emulsions of different gradation (see data in Table II).

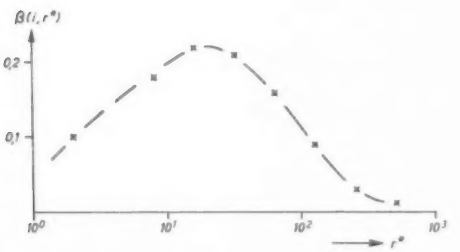

Fig. 6C. Sensitivity distribution used in the computation of the theoretical characteristic curve of Fig. 6B.

The experimental characteristic curve of layer A can be matched with a theoretical curve using a value of $r^* = 11$ without the need of a sensitivity distribution, but, in order to match the curve of layer B, a sensitivity distribution β (Eq. (22)) must be included (valid for each grain class). Refer to Part III, Sec. 3, for a discussion on the estimation of β from the experimental values. The sensitivity distribution used is shown in Fig. 6C. It is noteworthy that this distribution agrees well with the data published by Meidinger.[7] Of course, one expects in principle that layer A should also have a sensitivity distribution, but due to uncertainties in evaluation it would not become apparent until its standard deviation approached $\sigma_\beta \approx 0.2$. Therefore, the results can be interpreted only as evidence for a sensitivity distribution having σ_β values smaller than 0.2.

7. W. Meidinger, *Z. Phys. Chem.*, **114**: 89 (1925).

From a comparison of Figs. 6A and 6B, we conclude: With layers of flat gradation, the dispersion of the sensitivity distribution is so small that it hardly affects the shape of the characteristic curve. However, the sensitivity distribution is quite apparent when the gradation is steep. The grains were rendered developable after absorption of $r^* = 14$ quanta on the average. It can be calculated that, in the region of very small densities (toe of the characteristic curve), grains are also rendered developable after absorption of $r^* = 4$ quanta. Thus, e.g. in case B, when $s = 0.07$, the fraction of these grains ($r^* = 4$) is approximately 60%. Accordingly, the upper limit of the values cited by Silberstein and Trivelli, $r^* = 1$ to 4 (Mees, Ref. 1; cf. also Ref. 7) is reached for certain grains.

The size of the latent image speck (number of silver atoms per speck) can be estimated only if the dispersion of the latent image is known. It is certain that not all of the 14 quanta result in the formation of silver atoms (instability of the very small specks); moreover, absorption will occur at different crystal sites. This makes the formation of stable specks more difficult.

3. *The Influence of Different Distributions on the Shape of the Characteristic Curve*

It is evident from Part III, Secs. 1 and 2, that the dispersion of the individual distributions controls the effect of the various other distributions that depend on the values η, $p(q_i, r^*)$ and $\beta(i, r^*)$. Among these, the grain size distribution usually is the dominant factor.

A log normal Gaussian distribution can be assumed with assurance for η and with good approximation for $p(q_i, r^*)$; the latter approximation becomes increasingly better for large values of r^*. β-functions are not known, but even these can be expressed by Gaussian distributions. Since the individual distributions are independent of each other, it follows that the standard deviation σ is given by the following relation:

$$\sigma = \sqrt{(3\sigma_\eta)^2 + \sigma_p{}^2 + \sigma_\beta{}^2}. \qquad (25)$$

This relation was first applied by Burton[1] in his analysis of the characteristic curve. Of course, the σ_p values must be derived from distributions which are based on the same argument, in this instance preferably log Q/N (absorbed quanta). Furthermore, the spread of the grain size distribution σ_η must be converted to a volume spread ($3\sigma_\eta$), since the absorption increases with the volume of the grain.

Burton used the spread of the grain *area* distribution ($2\sigma_\eta$) which makes a difference of 9/4 in Eq. (25).

A detailed computation is required to show that a characteristic curve is characterized by the standard deviation $\sigma = 3\sigma_\eta$ when only the grain size distribution is taken into account.

Let $p = 1$ and $\beta = 1$, then Eq. (16) becomes Eq. (21a) and, with due consideration of Eq. (18), this may be written in the integral form:

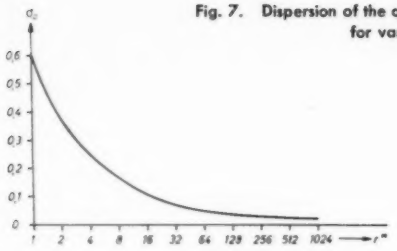

Fig. 7. Dispersion of the quanta distribution for various values of r^*.

$$s = \frac{\int_{d_i}^{+\infty} d^2\,(\partial H/\partial \log d)\,\partial \log d}{\int_{0}^{\infty} d^2\,(\partial H/\partial \log d)\,\partial \log d} \qquad (26)$$

Now, it can be proven that the function $d^2 \dfrac{\partial H}{\partial \log d}$ also has a Gaussian distribution, where

$$d^2 \frac{\partial H}{\partial \log d} = \frac{1}{\sigma_\eta \sqrt{2\pi}}\, d_0{}^2 \cdot e^{2\cdot 2.3^2 \sigma_\eta{}^2}\, e^{-\frac{[\log (d/d_0')]^2}{2\sigma_\eta{}^2}} \qquad (27)$$

with $$d_0' = d_0 \cdot 10^{2.3\cdot 2\cdot \sigma_\eta{}^2}$$

i.e., the new distribution has the same deviation σ_η but is displaced to another mean value d_0'.

Thus, the standard deviation, $\sigma_\eta = 3\sigma_\eta$, of the characteristic curve is not computed by means of Eq. (27) but is obtained by correlating the exposure and the grain diameter:

$$3 \log d = \log Q_0 \qquad (28)$$

In other words, the function $\partial H/\partial \log Q_0$ is a Gaussian function having a standard deviation $3\sigma_\eta$.

The σ_p values are obtained by approximating the function by a Gaussian integral:

$$p(q_i, r^*) \approx \frac{1}{\sigma_p \sqrt{2\pi}} \int_{-\infty}^{\log q_i} e^{-\frac{[\log (q_i/r^*)]^2}{2\sigma_p{}^2}}\, \partial \log (q_i / r^*) \qquad (29)$$

The σ_p value is obtained as a function of r^* as shown in Fig. 7.

The influence of the spread of the quanta distribution σ_p on the characteristic curve may be estimated from σ_η and σ_p by computing $[(3\sigma_\eta)^2 + \sigma_p{}^2]^{1/2}$ as a function of σ_p (see Fig. 8). It is evident that the quanta distribution can be disregarded with increasing accuracy as the sensitivity of the grains becomes smaller (higher values of r^*), provided only that the grain size distribution is broad.

The σ_η range encompasses all values that are common in practice.

As mentioned previously, the effect of the sensitivity distribution $\beta(i, r^*)$, and thus of σ_β, increases with decreasing values of σ_η (Eq. (25)). The effect of different β-functions is illustrated in Fig. 9 for the r^* value of 16.

Recalling that the σ_η of a normal negative emulsion is only about 0.27, one realizes that a very broad sensitivity distribution is required to affect the total dispersion and hence the shape of the characteristic curve. Burton[1] has demonstrated that it is possible to express the experimental characteristic curves by Gaussian integrals. The total spread σ, therefore, can be determined experimentally (from the elementary curve). An estimation of r^*, on the other hand, can be made from the curve computed with $\beta = 1$ (Eq. (22)). Approximations of σ_β may be obtained from Eq. (25) by rearranging it to the form

$$\sigma_\beta = \sqrt{\sigma^2 - (3\sigma_\eta)^2 - \sigma_p{}^2} \qquad (30)$$

where $\sigma_p \approx \sigma_p(r^*)$. This procedure was used to derive the sensitivity distribution shown in Fig. 6C. Burton's[1] estimate of σ_β (sensitivity distribution), therefore, appears to be too high in relation to his other spread values, and this explains the apparently great influence of sensitivity distribution on the characteristic curve.

Attention should also be called to some work by Webb[8] in which he cites a minimum r^* value of the order of 10. In his work, exposure latitude of the characteristic curve is related to statistical concepts of quanta effects. From his curves of grain size distribution, one can compute an approximate value of 0.14. By reference to Fig. 8, it is then found that the quanta dispersion for $r^* = 10$ has no influence on the characteristic curve. This curve is determined solely by the grain size distribution. The spread of the characteristic curve is about 0.4, which is in good agreement with $\sigma = 3\sigma_\eta$.

Acknowledgments

Acknowledgment is made of the kind assistance rendered in this work by Miss Hanna Dreher and Hans-Jorg Metz.

8. J. H. Webb, *J. Opt. Soc. Am.*, **38**: 312 (1948).

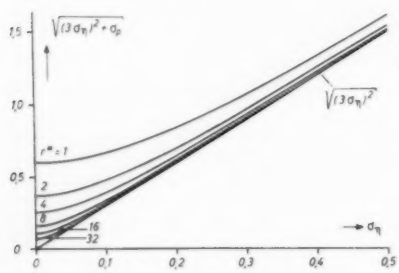

Fig. 8. The effect of quanta fluctuations on total dispersion for various values of r^*.

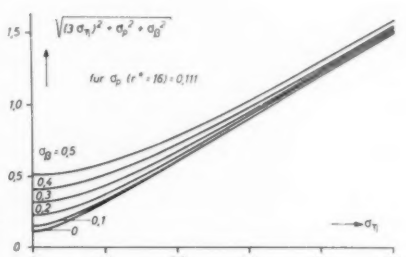

Fig. 9. The effect of sensitivity distribution on total dispersion when $r^* = 16$.

PHOTOGRAPHIC SCIENCE AND ENGINEERING
Volume 4, Number 5, September-October 1960

Kinetics of Development by the Ferrous Ethylenediaminetetraacetate Complex Ion

T. H. JAMES, *Research Laboratories, Eastman Kodak Company, Rochester, N.Y.*

A detailed study was made of the effect of pH, concentration, temperature, neutral salts, silver halide solvents, and quaternary ammonium salts on the rate of development by the ferro-EDTA complex. The complex rather than the unassociated ferrous ion is the active agent for both direct and solution physical development. The rate of development by a dilute solution decreased markedly with increasing pH, but in the presence of a quaternary ammonium salt and sufficient potassium nitrate, the rate at high exposure levels varied by less than 2-fold over the pH range 2.7–12.0. Ferro–EDTA solutions of high concentration showed only a small dependence of rate on pH even in the absence of the addenda. The development rates for the high exposure levels do not correlate with the oxidation-reduction potential of the solution, and ferric iron was without significant effect on the rate. Fog formation by the acid solutions was negligible. Increases in pH in the alkaline solutions caused increases in the rates of fog formation and of image development at low exposure levels which correlated qualitatively with changes in oxidation-reduction potential. The color of the developed silver and its distribution in depth in the emulsion layer varied with the temperature of development and with the gelatin-to-silver ratios. The temperature-dependence of the rate of development was unusually low in the low-temperature region (5°–20°C) under some conditions and the character of the developed silver changed markedly in this region. This is explained on the basis of a temperature-dependence of the retarding action of gelatin on development beyond the induction period. Addition of sufficient thiocyanate to a ferro–EDTA solution resulted in a shift from direct to solution physical development; contrary to results obtained with organic developing agents, this shift caused an increase in the total rate of development.

Ferrous ion acts as a photographic developer[1] when metallic iron or zinc is present to reduce the ferric ion formed in the development reaction. The rate of development, however, is very low. Much faster development is obtained with certain ferrous-ion complexes, such as the classical ferro-oxalate complex[2] first reported as a developer by Carey-Lea in 1877. The complex formed by ferrous ion and ethylenediaminetetraacetate ion (EDTA) is an even more active developer, and can be used over a wide range of pH values. Developers based on this complex can be prepared which show relatively little change in activity over a pH range of 3 to above 10, a property which makes them attractive for use in studies where it is desired to cover a wide range of pH with comparatively little change in the properties of the developer.

Relatively little attention has been paid the ferro–EDTA developers in the literature. Rzymkowski[3] published the first information on them, and Rasch[4] compared their photographic behavior with that of several conventional developers. Rasch prepared a ferro–EDTA developer which gave characteristic curves with motion-picture positive film which closely conformed to those obtained with the conventional M-Q developers. James and Vanselow[5] showed that development by a ferro–EDTA solution of pH 4.8 is accelerated both by quaternary ammonium salts and by thiourea. De Carvalho and Da Silva[6] have found ferro–EDTA developers useful for processing nuclear-track emulsions at a pH near the isoelectric point of the gelatin. No detailed study of the kinetics of development by the ferro–EDTA solutions has been published.

The basic oxidation-reduction system involved in development by this agent is:

$$Fe(EDTA)^{=} + Ag^{+} \rightleftharpoons Fe(EDTA)^{-} + Ag.$$

The concentration of ferrous ion in equilibrium with excess EDTA is very small, and the concentration of

Communication No. 2095 from the Kodak Research Laboratories, presented at the Annual Conference, Santa Monica, California, 12 May 1960. Received 6 May 1960.

1. H. Ammann-Brass, *Phot. Ind.*, **35**: 827 (1937).
2. C. E. K. Mees, *Theory of the Photographic Process*, rev. ed., Macmillan, New York, 1954, p. 538.
3. J. Rzymkowski, *Pharmazie*, **6**: 155 (1951); Belgian Patent 507,572, Dec. 1951; *Sci. et inds. phot.*, (2) **23**: 23 (1952); **25**: 385 (1954).
4. A. A. Rasch, private communication; see also G. M. Haist, J. R. King, A. A. Rasch, and J. I. Crabtree, *Phot. Eng.*, **7**: 182 (1956).
5. T. H. James and W. Vanselow, *Phot. Sci. and Tech.*, **3**: 69 (1956).
6. H. G. de Carvalho and A. G. da Silva, *Photographie corpusculaire II, Colloq. intern.*, **2e**, *Montreal 1958*, Presses Univ., Montreal, p. 197.

ferric ion is even smaller, as indicated by the dissociation constants[7] for the two complexes (14.22 is the value of log K reported for $Fe(EDTA)^{=}$ at 25°C and 24.9 for $Fe(EDTA)^{-}$). It is unlikely, therefore, that the unassociated ferrous ion plays a significant part in development by solutions of the ferrous complex, and the kinetic data in this paper can be accounted for on the assumption that the complex is the active developing agent. The oxidation-reduction potential[7,8] of a solution of the ferrous complex becomes more negative with increasing pH until a plateau is reached which extends from about pH 4 to 6. At higher pH, the potential again becomes more negative with increase in pH. (The convention followed here for the sign is such that a more negative potential implies a stronger reducing agent.) The potential is substantially independent of ionic strength. The susceptibility of the ferrous complex to aerial oxidation increases with increasing pH over the range, 3 to 10, although the solutions are stable in the absence of oxygen.[7]

In the present investigation, the dependence of the rate of development of a positive-type emulsion on pH, concentration, temperature, and addenda has been examined for both direct development and solution physical development. The ferro–EDTA developers show several unusual properties of theoretical interest.

Experimental Materials and Procedure

The ferro–EDTA solutions were prepared from ferrous sulfate and tetrasodium ethylenediaminetetraacetate (Na_4EDTA). The ferrous sulfate was dissolved in 0.002 M sulfuric acid; the Na_4EDTA and other components of the developer were dissolved in water. The two solutions were deaerated with nitrogen, mixed, and used with nitrogen-burst agitation under exclusion of air.

The pH of the solutions was adjusted to the desired value by use of acetic acid, a sodium acetate–acetic acid buffer, sulfuric acid, or sodium hydroxide. It was not necessary to use a buffer for the more concentrated solutions over much of the pH range, since the EDTA supplied sufficient buffer action in view of the low pH-dependence of the photographic activity of the developer.

A commercial high-contrast, motion-picture-positive film was used in most of the work. Some experiments also were carried out with a similar emulsion, *A*, which had a much lower concentration of gelatin (43 mg of silver, 8 mg of gelatin per sq dm) and Emulsion *B*, which had a higher concentration of gelatin (42 mg of silver, 129 mg of gelatin per sq dm). Exposures were made on the Eastman IIb (time-scale) Sensitometer with the normal positive lamp and filter, or were made to uniform illumination from a 6-w tungsten lamp, operated at 115 v at a distance of 140 cm from the film, and shielded by a ground-glass plate. The latter exposures were generally for 15 min to each side of the film, and represented the exposure level for maximum rate of development of the film when exposed to light of this quality and intensity. For some of the experiments on solution physical development, emulsion coatings which contained 0.48 mg of colloidal silver in addition to the regular silver halide grains were used without exposure (Coatings *C* and *D*, essentially the same but made at different times).[9] The sensitometric strips were read on an automatic densitometer. Spectrophotometric curves were obtained for all uniformly exposed and for unexposed strips, and silver determinations were made on an x-ray spectrometer.

Development was at 20.0°C, except when otherwise noted. The rate of gross development is expressed either in terms of the density–time or silver–time curves (slope rates: density/minutes or silver mass/minutes) or in terms of the reciprocal of the time required to produce a density of 0.2 above fog or a silver mass of 2.15 mg/sq dm (induction-period rates). The term "gross development" is used here to specify the development which takes place when the exposed film is immersed in the developer, regardless of whether direct, solution physical, or both kinds of development are occurring. The rates of solution physical development, determined for Coatings *C* and *D*, are expressed in terms of the slope of the density–time curves between densities 1.0 and 2.0, or of the reciprocal of the time required to produce a density of 0.8. The densities for solution physical development were measured at the maximum of the spectrophotometric curves, and were corrected for "fog" density measured at 700 mμ.[9]

Experimental Results

Sensitometric Curves

Sensitometric strips were developed in a series of solutions prepared from 30 gram of $FeSO_4 \cdot 7H_2O$, 100 grams of Na_4EDTA, and 0.5 gram of KBr per liter. The pH level was adjusted with acetic acid for pH below 10, and with sodium hydroxide for pH above 10. Only 30 grams of Na_4EDTA was used for solutions of pH below 3.4, since free acid precipitated when the higher concentration was used.

Figure 1 shows the characteristic curves obtained for various times of development of the commercial film at pH 2.73 and Fig. 2 shows the curves for pH 9.55. Figure 3 shows the change in gamma with time of development in six solutions covering the pH range, 2.75 to 10.35, and includes a curve for fog growth at pH 10.35. Figure 4 gives a plot of photographic speed, measured as the reciprocal of the exposure needed to produce a density of 0.2 above fog, as a function of gamma. This figure also includes data for a M-AA surface developer consisting of 2.5 grams of N-methyl-*p*-aminophenol sulfate, 10.0 grams of ascorbic acid, 1 gram of potassium bromide per liter, and enough sodium carbonate to give pH 10.2.

In the acid developers, density and gamma increased rapidly with increasing time at first, but the

7. J. Bond and T. I. Jones, *Trans. Faraday Soc.*, **55**: 1310 (1959).

8. R. Belcher, D. Gibbons, and T. S. West, *Analytica Chim. Acta*, **12**: 107 (1955).

9. T. H. James and W. Vanselow, *Phot. Sci. and Tech.*, **2**: 135 (1955).

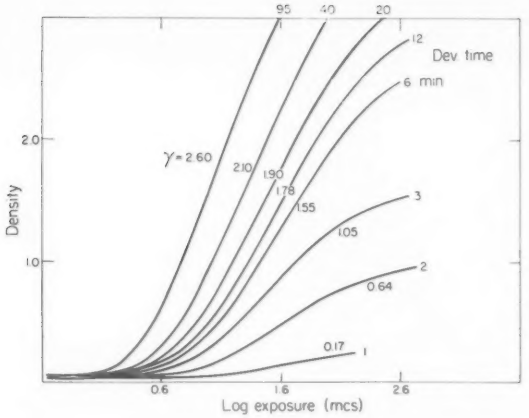

Fig. 1. Characteristic curves for commercial motion-picture positive film developed at pH 2.73 and 20°C.

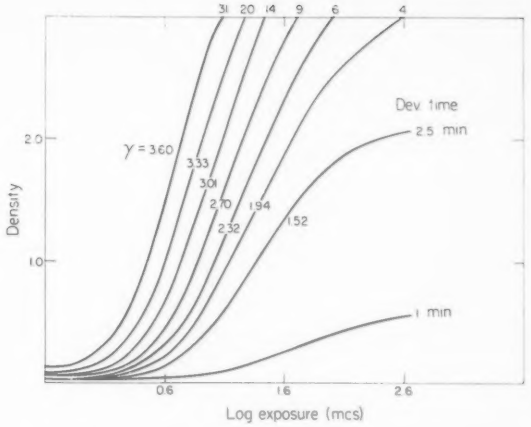

Fig. 2. Characteristic curves for commercial film developed at pH 9.55 and 20°C.

curves for both as a function of time show rather sharp breaks beyond which density and gamma increase much more slowly (see Fig. 3). These developers also are characterized by an almost negligible fog level, even for prolonged times of development. The density and gamma curves for the alkaline developers do not show the break, and the rate of increase changes more gradually. Fog formation became significant for the longer times of development in the alkaline solutions (Figs. 2 and 3), although, even at pH 10.35, the fog level was relatively low compared with image development. At pH 12, the developer was still active and showed discrimination between exposed and unexposed areas of the film, but the rate of fog formation was comparatively high.

The characteristic curves obtained with the ferro–EDTA developers resemble closely those obtained with conventional M-Q developers when motion-picture-positive film is used. No attempt was made to compare the properties of the two types in detail, but the ferro–EDTA developers generally gave lower speed for a given gamma when both types were compared at the same temperature (cf. Fig. 4). A close match between both curve shape and speed was obtained, however, when the ferro–EDTA developer of pH 5.3, containing 1 gram of KBr per liter, was used at 50°C and an M-Q developer was used at 20°C. The latter contained 1.0 gram of N-methyl-*p*-aminophenol sulfate, 5.0 grams of hydroquinone, 50.0 grams of sodium sulfite, and 1.0 gram of KBr per liter, with sodium metaborate to give pH 9.5.

Kinetics of Gross Development, Sensitometric Exposures

The pH-dependence of the rate of development by the ferro–EDTA complex varies with the salt content of the solution. The effect is largest for dilute solutions, and is illustrated in Fig. 5 for a series of developers which contained 1.55 grams (0.0056 *M*) of ferrous sulfate and 10.56 grams (0.028 *M*) of Na_4EDTA per liter. Both slope and induction-period rates decreased markedly with increasing pH

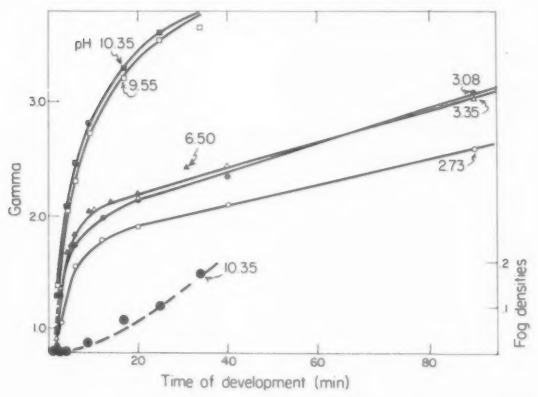

Fig. 3. Gamma–time of development curves for development at various pH levels as indicated on the curves, and at 20°C. The broken curve represents growth of fog density at pH 10.35.

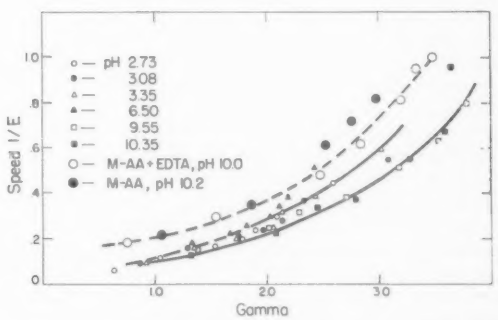

Fig. 4. Speed–gamma relation for development by ferro–EDTA (solid curves) and by M-AA (broken curve) solutions.

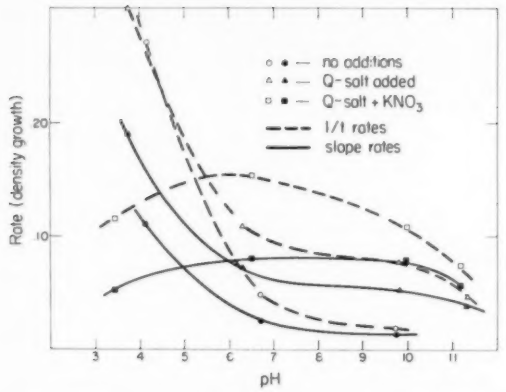

Fig. 5. Rate of development of commercial film at 20°C, log $E = 2.5$, as a function of pH. Circles, no addition; triangles, 0.5 gram α-picolinium-β-phenylethyl bromide added; squares, 0.5 gram α-picolinium-β-phenylethyl bromide and 100 grams potassium nitrate added.

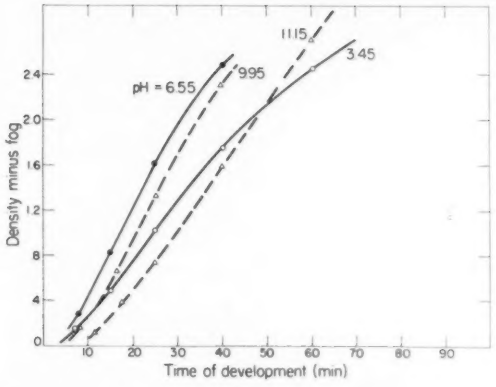

Fig. 6. Density–time of development curves for the ferro–EDTA developers containing α-picolinium-β-phenylethyl bromide and potassium nitrate, log $E = 2.5$, at 20°C; pH values are given on the curves.

for the solutions which contained no added neutral salt (solid and open circles in Fig. 5). The addition of 100 grams of potassium nitrate per liter increased the rates in the alkaline region and made the developer less pH-dependent (data not shown). The addition of a quaternary salt accelerated development in both the acid and the alkaline region and decreased the relative pH-dependence. The triangles in Fig. 5 show the rates obtained when the solutions contained 0.5 gram of α-picolinium-β-phenylethyl bromide per liter. The slope rates were increased by the quaternary salt at all pH values in spite of the added bromide ion which, by itself, would have decreased the rate. The $1/t$ rates, which are more sensitive than the slope rates to the bromide-ion content of the developer, were increased in the neutral and alkaline regions, but not in the low-pH region. The addition of 100 grams of potassium nitrate to the solutions containing the quaternary salt decreased the rate of development in the acid region but increased it in the neutral and alkaline regions, and produced a developer which showed a remarkably small dependence on pH at the higher exposure levels (Fig. 5, squares).

The form of the density–time of development curves (Fig. 6) does not depend markedly on pH, although the curve for pH 3.45 shows a relatively smaller induction period and a smaller slope beyond the induction period than the curves for the higher pH values. At a lower exposure level, log $E = 0.6$, the dependence of the form of the density–time of development curves on pH is greater (see Fig. 7).

The temperature-dependence of development over the range, 20.0° to 48.8°C, was greater at a low exposure level than at a high one, in agreement with results previously obtained with several conventional organic developing agents.[10] The data fit the Arrhenius equation reasonably well over this temperature range for the commercial film. However, marked departures from the Arrhenius equation were observed with Coating *A* (low gelatin) in the region, 5° to 30°C, and even for the commercial film when the alkaline developers were used. This departure will be illustrated in the next section for the uniformly exposed film.

Kinetics of Gross Development, Uniform Exposures

The rate of development of the uniformly exposed film, measured in terms of milligrams of Ag per minute, varied directly as the concentration of the ferro–EDTA complex. Figure 8 shows the dependence on concentration at pH 10.2 for 6.0° and 20.0°C. The Na_4EDTA concentration was kept constant at 41.7 grams per liter (0.11 *M*) and the KBr concentration at 1.0 gram per liter. The spectrophotometric curves for the samples developed at the highest concentration of ferro–EDTA were similar in form to those obtained in previous work with surface developers[11] and are thought to be

10. T. H. James, *Phot. Sci. and Tech.*, **2**: 81 (1955); T. H. James and W. Vanselow, *ibid.*, **1**: 77 (1954).

11. T. H. James and W. Vanselow, *Phot. Sci. and Eng.*, **1**: 104 (1958).

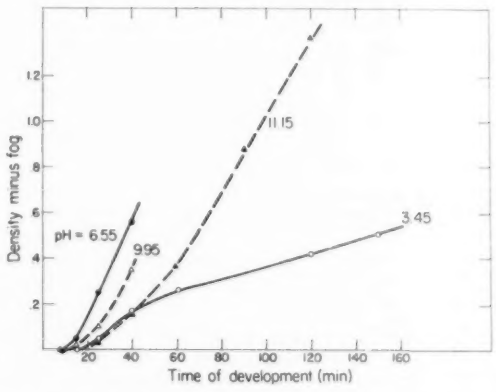

Fig. 7. Density–time of development curves for the same conditions as in Fig. 6, except log $E = 0.6$.

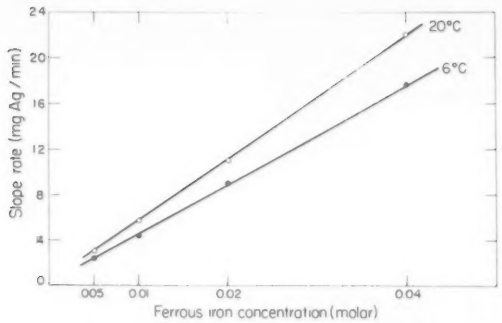

Fig. 8. Dependence of rate upon the ferrous-iron concentration. Commercial film developed at pH 10.2 at temperatures specified on the curves.

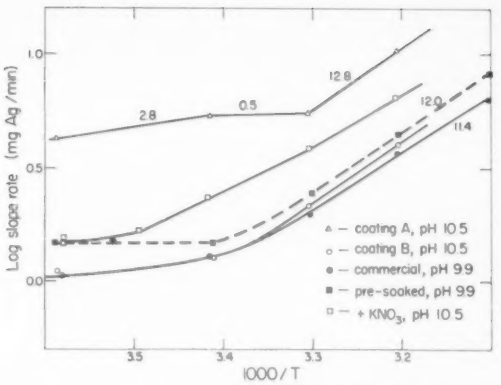

Fig. 9. Temperature-dependence plots for development at pH 9.9 and 10.5. The squares refer to the commercial film; presoak time (solid squares) 10–20 min; KNO_3 (open squares) 100 grams/liter.

representative of direct development. The curves for the samples developed at the lowest concentration (0.005 *M*) showed a slight maximum in density at 410–420 mμ, indicating that solution physical development was playing some part in the over-all process at this concentration.

Variation in the amount of excess EDTA had little effect upon the rate of development when the excess was sufficient to prevent precipitation of iron oxides or hydroxides and when 100 grams of potassium nitrate was used to minimize salt effects. Ferric iron also had little effect upon the rate. The addition, for example, of 0.002, 0.005, and even 0.01 *M* ferric chloride to a developer prepared from 0.02 *M* ferrous sulfate, 0.11 *M* Na_4EDTA, 1.0 *M* potassium nitrate, and 0.0084 *M* KBr (pH 10.3) caused no significant change in the rate of development, and had no effect on the shape of the spectrophotometric curves of the developed silver.

The temperature-dependence of development at pH 9.9 and 10.5 is shown in Fig. 9, where the log rate is plotted against the reciprocal of the absolute temperature. The developer contained 0.02 *M* ferrous sulfate, 0.11 *M* Na_4EDTA, and 0.0084 *M* KBr. The numbers given on the curves are over-all activation energies calculated from the slope of the curves at those points. Similar results were obtained for developers of lower pH, except that the temperature-dependence of the rate in the low-temperature region was somewhat larger.

In the high-temperature region, development by all of the ferro–EDTA solutions followed the Arrhenius equation reasonably well, as shown by the straight lines obtained in a log rate–reciprocal of absolute temperature plot. The departure from a straight-line relation in the region of lower temperature, which was particularly marked for the high-pH developers, was not prevented by presoaking the film in water at the temperature of the developer before immersion in the latter (see Fig. 9). Addition of 100 grams of potassium nitrate per liter to the developer increased the rate of development and appeared to shift to lower temperatures the region of departure from the straight-line relation. The precise significance of the activation energies calculated from the temperature-dependence is doubtful in view of the failure of the rates to follow the Arrhenius equation over an extended temperature range, but values have been calculated for each developer from the data in the higher-temperature range, and these values are listed in Table I. There

TABLE I. Activation Energies in Kcal/Mole for Development by Ferro-EDTA Solutions under Various Conditions

All solutions contain 0.02 *M* Fe and 0.0084 *M* KBr.

			Activation Energies for Coatings					
			Commercial		*A*		*B*	
pH	EDTA *M*	Treatment or addenda	Slope rates	1/*t* rates	Slope rates	1/*t* rates	Slope rates	1/*t* rates
5.3	0.11	———	10.7	12.8	10.3	13.0	10.3	13.0
6.0	0.015	———	11.9	12.5	———	———	———	———
9.9	0.11	———	11.4	11.9	———	———	———	———
9.9	0.11	Film presoaked	12.0	11.9	———	———	———	———
10.5	0.11	———	———	———	12.8	———	12.0	———
10.5	0.11	KNO_3 100 g/l	(11)	(10)	———	———	———	———

is no marked dependence of these values on the pH of the developer or on the silver halide concentration of the coating. For comparison, activation energies calculated for a ferro-oxalate developer of pH 5.3 used with the commercial coating are 8.7 kcal/mole for slope rates and 8.0 for induction period ($1/t$) rates.

The distribution of silver developed at the higher temperatures was nearly uniform throughout the thickness of the emulsion coating, and the increase in the amount of reduced silver with increasing development time was caused largely by an increase in the degree of reduction of the individual grains, as indicated by electron micrographs of the developed silver. At low temperatures, on the other hand, the grains near the top surface of the emulsion layer developed rather fully before a significant amount of development had taken place near the support side of the emulsion layer. This dependence of distribution upon temperature is the probable cause of the dependence of the color of the image upon temperature, as described in the next section.

Spectral Absorption and Covering Power of Developed Silver

The spectral absorption of the silver developed by the ferro–EDTA solutions varied with the degree of development and with the temperature of the developer. The general shape of the curves obtained by plotting total transmitted diffuse density against wavelength is the same as that previously described for the surface developers.[11] The ratio of the density measured at 400 mμ to that measured at 700 mμ decreased with increasing degree of development of the uniformly exposed film. For a given degree of development (equal amounts of silver), the ratio was smaller the lower the temperature. This is illustrated for the developer of pH 9.9 in Fig. 10, where $D(400\ \text{m}\mu)/D(700\ \text{m}\mu)$ is plotted against the mass of developed silver for the commercial coating. The dependence of the ratio on the temperature in the range, 5.6° to 20°C, was even more marked for film bathed in water before development at pH 9.9, but was less marked for film developed at pH 5.3.

As shown previously,[11] an increase in the relative amount of solution physical development produces an increase in the $D(400\ \text{m}\mu)/D(700\ \text{m}\mu)$ ratio. The observed increase in this ratio with increasing temperature of development in the ferro–EDTA solutions, however, appears to be much too large to be accounted for by an increase in solution physical development. Even at the highest concentration of Na_4EDTA, the rate of solution of silver halide in the ferro–EDTA developer at pH 10, measured as described previously,[9] is only about 50% greater than that in the M-AA surface developer, and the density ratio for the silver image produced by the M-AA solution is almost independent of temperature. The oxidation product of development, the ferri–EDTA complex, also can be eliminated as a possible source of color variation, since the addition of ferric chloride in amounts up to 0.01 *M* had no effect upon the spectral absorption of the silver developed by a 0.02 *M* ferro–EDTA solution of pH 9.9.

The covering power of the developed silver (density divided by mg Ag/sq dm) decreased with increasing time of development at first, then tended to level off. Except for silver deposits which are spectrally neutral, the precise values of the covering power depend upon the wavelength at which the density is measured. Figure 11 shows the covering power for densities measured at 700 mμ plotted against the mass of silver for Coating *B*. A corresponding plot for densities measured at 400 mμ would show a greater dependence upon temperature and a greater decrease with increasing mass of silver.

The covering power for densities measured at 700 mμ is nearly constant at a particular temperature over a silver mass range of 6 to 16 mg/sq dm. Averaged values over this range are given in Table II for the three emulsion coatings and several development conditions. The covering power of the commercial coating and of Coating *B* shows some decrease with increase in the temperature of development, but this trend is not clearly shown by the data for Coating *A*. The values for Coating *A* are consistently higher than those for the other two coatings.

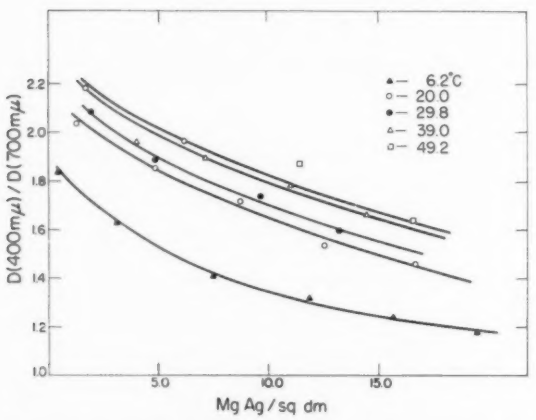

Fig. 10. Temperature dependence of the degree of departure from spectral neutrality of silver images developed at pH 9.9 on commercial film.

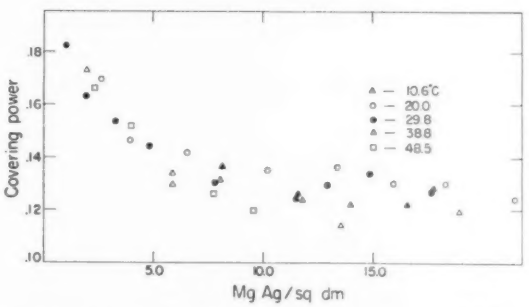

Fig. 11. Relation between covering power and mass of developed silver, Coating *B*, pH 5.3. Densities were measured at 700 mμ.

Solution Physical Development

The kinetics of solution physical development were investigated with the unexposed coatings, *C* and *D*. Thiocyanate ion, which markedly accelerates solution of silver halide, was used to raise the rate of solution to a point where the chemical reaction, rather than solution of the silver halide, was rate-controlling, i.e., the rate of solution was fast compared with that of the chemical reaction.

The rate of solution physical development by a low-salt solution consisting of 1.55 grams (0.0056 *M*) of ferrous sulfate, 10.56 grams (0.028 *M*) of Na_4-EDTA, and 2.0 grams (0.021 *M*) of KCNS per liter was dependent on pH, though not as strongly so as the rate of gross development of exposed film by the solution without the thiocyanate (cf. Fig. 12 with Fig. 5). Potassium nitrate increased the rate of solution physical development at pH 4 and above, and the rate in the presence of 100 grams of potassium nitrate per liter showed negligible dependence on pH over the range, 4 to about 9. T e rate decreased at both lower and higher pH.

The rate was independe t of the EDTA concentration over a wide range, so long as the amount of EDTA was sufficient to complex substantially all the ferrous ion. Figure 13 shows density–time of development curves for pH 4.45 and a constant amount of ferrous iron. With the exception of the data for the lowest amount of EDTA, which is only about half the amount necessary to complex all of the iron, all densities fall substantially on a common curve. Similar results were obtained at pH 10.3 with solutions containing 1.0 *M* potassium nitrate, 0.0056 *M* ferrous sulfate, and 0.021 *M* KCNS, the Na_4EDTA content varying from 0.028 to 0.11 *M* (Table III).

The rate of development in the initial stages varied directly as the concentration of the ferrous salt,

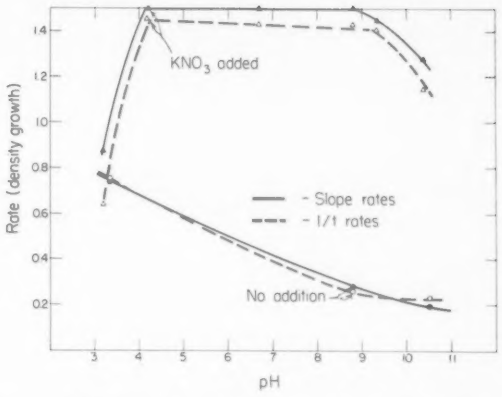

Fig. 12. Dependence of rate of solution physical development on pH, 20°C, Coating C. Circles, no additions; triangles, 1 M potassium nitrate added to developer; solid curves, slope rates; broken curves, 1/*t* rates.

TABLE II. Effect of Temperature of Development on Covering Power

Covering power calculated as density at 700 mμ divided by milligrams silver per square decimeter.

Developer pH	Treatment or addenda	Temperature, deg C	Covering Power for Coatings		
			Commercial	*A*	*B*
5.3	———	10.7	———	0.137	0.124
		20.0	0.134	0.151	0.131
		29.8	0.126	0.166	0.129
		38.8	0.119	0.153	0.120
		48.5	0.115	0.151	0.121
10.5	———	5.9	———	0.148	0.129
		19.9		0.157	0.129
		29.7		0.157	0.122
		38.9		0.148	0.112
9.9		6.2	0.127		
		20.0	0.126		
		29.8	0.123		
		39.0	0.117		
		49.2	0.104		
9.9	Water presoak	5.6	0.139		
		10.7	0.130		
		20.0	0.129		
		29.7	0.123		
		38.9	0.115		
		49.3	0.104		
10.5	KNO_3 100 grams/liter	6.2	0.140		
		13.1	0.132		
		20.1	0.137		
		29.7	0.130		
		39.0	0.120		

TABLE III. Rate of Solution Physical Development of Coating *D* at 20°C

All solutions contain 100 grams KNO_3 and 2.0 grams KCNS per liter.

$FeSO_4 \cdot 7H_2O$, grams/liter	Na_4EDTA, grams/liter	pH	Slope rate, D/min	$1/t$ ($D = 0.8$)
0.77	10.56	4.5	0.27	0.48
1.55	10.56	4.5	0.68	1.0
3.09	10.56	4.5	1.72	1.9
6.17	10.56	4.5	3.95	4.2
0.77	21.12	10.5	0.48	0.69
1.55	21.12	10.5	1.14	1.3
3.09	21.12	10.5	3.2	2.8
6.17	21.12	10.5	6.0	6.0
1.55	10.56	10.5	1.14	1.25
1.55	21.12	10.5	1.14	1.33
1.55	42.24	10.5	1.11	1.33

as shown by the variation in $1/t$ rates listed in Table III. As development progressed, the rate became more dependent on the concentration, as shown by the variation in the slope rates. This apparently greater than first-order dependence can be attributed to a loss of silver ions from the emulsion to the bulk solution, a loss which was greater the slower the development. A significant amount of silver plated out on the vessel walls in the experiments where the ferrous-salt content was low, and the amount increased with decreasing salt content. It is probable, therefore, that the true rate of development is proportional to the ferrous-iron content.

The marked dependence of rate upon ferrous-iron concentration shows that the measured rates were lower than the rate of solution of the silver halide. This was confirmed by measurement of the rate of solution in a high-activity N-methyl-*p*-aminophenol developer containing the same amount of Na_4EDTA. The effect of potassium nitrate on the rate of solution physical development by the ferro–EDTA developers suggests that diffusion of the complex through the gelatin is an important factor in determining the rate—a suggestion supported by the observation that development proceeds considerably faster in the top portions of the emulsion layer than in the portions near the film base, even though the distribution of silver halide grains and colloidal silver nuclei is uniform in depth throughout the emulsion layer.

The addition of sufficient thiocyanate to a conventional developer which acts primarily by the direct mechanism can convert the developer into one which acts primarily by the solution physical mechanism in the development of exposed, conventional emulsions.[12] This conversion can readily be accomplished with the ferro–EDTA solutions, and the solvent developer often develops faster than the one without the added solvent. This result is unusual, since past experience with N-methyl-*p*-aminophenol, hydroquinone, hydroxylamine, and *p*-phenylenediamine developers had always shown that the gross rate of development *decreased* when enough solvent was added to convert the developer to the solution physical type. The difference in behavior between a ferro–EDTA developer and a hydroquinone developer in this respect is illustrated in Fig. 14, where silver–time of development curves are given for two developers, one consisting of 4.4 grams of hydroquinone, 5 grams of sodium bisulfite, 1 gram of KBr, and enough borate buffer per liter to give pH 9.4, the other consisting of 1.4 grams of ferrous sulfate, 41.7 grams of Na_4-EDTA, and 1 gram of KBr per liter, pH 10.2. The two developers had roughly the same induction period, and the rate of development beyond the induction period was about twice as great for hydroquinone as for ferro–EDTA. The addition of 3 grams of KCNS per liter converted these developers to the solution physical type, with a marked decrease in the rate of development by hydroquinone and a significant increase in the rate of development by ferro–EDTA.

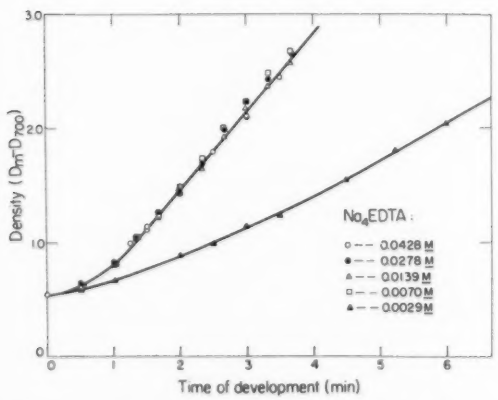

Fig. 13. Dependence of the rate of solution physical development on the EDTA concentration, pH 4.45, 20°C, Coating *D*. The ferrous-iron concentration was constant at 5.6 millimoles/liter.

12. E. Klein, *Z. Elektrochem.*, **62:** 505 (1958).

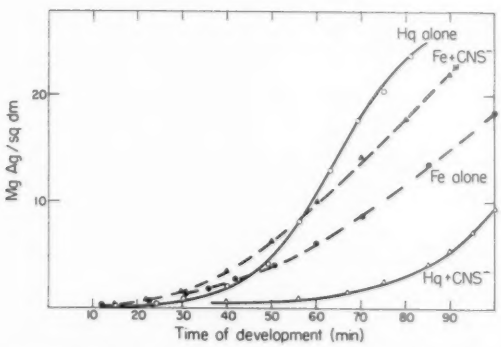

Fig. 14. Effect of KCNS (3 grams/liter) on the rate of development by a hydroquinone (Hq) and a ferro–EDTA (Fe) developer at 20°C.

Discussion

The solvent action of the ferro–EDTA developers for silver halide is very low *in the absence* of added solvent, and the more rapidly acting solutions develop primarily by the direct mechanism. Much of the data given for the rates of gross development can be interpreted as applying primarily to direct development. Solution physical development, however, is important in the more dilute solutions which react only slowly, such as those of low salt content and high pH, where the silver formed shows evidence of a considerable amount of physical development, both in its appearance under the electron microscope and in its spectral absorption. The specific rate of reduction of silver ions from solution is evidently relatively high in the presence of suitable silver nuclei, and only the low rate of solution of the silver halide prevents physical development from playing an important role, even in the more active solutions.

The ferro–EDTA complex, rather than ferrous ion, is the active agent in both direct and solution physical development, and the complex is active over a wide range of pH. When the EDTA is in excess in the dilute solutions without added potassium nitrate, the rates of development decrease with increasing pH. This change is in the opposite direction from that expected if a simple relation existed between the rate and the reduction potential of the solution. Further evidence that the reduction potential is not an important factor is provided by the observation that an increase in the ferric-iron content of the solution was substantially without effect upon the rate of development of the fully exposed emulsion. The decrease in rate with increase in pH appears to be largely associated with the charge effect.[13] At low pH, the singly charged ion, $Fe(EDTA)H^-$, is present and probably active as a developing agent. At higher pH (4 and above), the doubly charged ion, $Fe(EDTA)^=$, is the active developer. As the pH increases from the acid to the alkaline side of the isoelectric point of the gelatin, the net charge on the gelatin molecules changes from positive to negative. Both the increase in the negative charge of the active developer and the increase in the negative charge of the gelatin with increasing pH should act to decrease the rate of development. At very high pH, the formation of the ion, $Fe(EDTA)OH^=$, would act further to decrease the rate of development. Potassium nitrate minimizes the charge effect in the gelatin, and thus decreases the rate of development at pH below the isoelectric point and increases it at pH above the isoelectric point.

The positive ion of the quaternary ammonium salt is adsorbed by the negatively charged silver halide grains, depressing the negative charge, and generally increasing the rate of direct development. The quaternary ion may also increase the rate of solution physical development by increasing the rate of solution of the silver halide, as shown previously.[5] In the presence of both the quaternary salt and potassium nitrate, the rate of development, as shown in Fig. 5, does not change by more than 1.5-fold over the pH range, 3.45 to 11.15 (slope rate), at the exposure level log $E = 2.5$. The developers with high concentrations of developing agent and EDTA show relatively little dependence of rate on pH, even without the addition of quaternary salt and potassium nitrate. The high salt content of these developers should largely eliminate the charge effect of the gelatin.

Beyond the induction period, the acid ferro–EDTA developers produce an initial relatively rapid growth of gamma and density in the moderate to low exposure levels for direct development. Subsequently, a rather sharp break occurs in the rate of increase of gamma and density, and this is followed by a period of slow growth of these quantities. Fog formation is very low, and development can be continued for relatively long times without significant fog formation. The sharp break does not occur in development by the concentrated alkaline solutions, or by the dilute alkaline solutions containing quaternary salt and potassium nitrate, but the growth of fog becomes significant when development has proceeded to roughly the same region of gamma where the break occurs with the acid developers.

There may be a connection between the fog formation and the lack of a break in the gamma and density curves for the alkaline developers. The relatively low dependence of rate on pH for the high exposure levels and that in the early stages of density growth in the low exposure levels suggest that the rate of initiation of development and of continued development of the individual grains is roughly the same for the acid and alkaline developers so long as the grains contain relatively large latent-image nuclei. The grains with latent-image centers near the threshold size, however, appear to require much longer times for initiation of development by the acid solutions. The more rapid initiation by the alkaline solutions could be the result of a "latensification" which originates in the same reaction of the developer as that which produces fog. An explanation of how such fogging action could produce latensification has been given in an earlier paper.[14]

The increase in fogging action with increase in pH in the alkaline solutions may be associated with the change in the reduction potential. Support for this suggestion is found in the observation that ferric iron acts as an antifoggant in these solutions. A correlation between fog formation and reduction potential for developers of the hydroquinone series has been noted previously,[15] and the theoretical basis discussed.

The temperature-dependence of the ferro–EDTA developers shows an unusual behavior under some conditions. In the low-temperature region (5° to 30°C), the net rate of formation of silver often depends upon temperature to only a slight extent, but the character and distribution of the developed silver

13. T. H. James, *J. Phys. Chem.*, **43:** 701 (1939); *J. Chem. Phys.*, **12:** 453 (1944); *J. Franklin Inst.*, **240:** 15, 83 (1945).

14. T. H. James, *Phot. Sci. and Eng.*, **1:** 141 (1958).

15. T. H. James, *J. Franklin Inst.*, **234:** 371 (1942).

change with change in temperature. At the lowest temperatures, the grains near the surface develop largely to completion before much development occurs near the base. Evidently, once active development of the grains in the upper portions of the emulsion starts, reduction proceeds relatively rapidly and the net rate of development is controlled largely by the rate at which developer can diffuse to the sites of the actively developing grains. The regions near the film base remain "developer-poor" until the grains in the upper layers have developed to completion. The increase in density with increase in time of development is caused largely by an increase in the number of rather fully developed grains. This accounts for the comparative spectral neutrality of these images.[11]

As the temperature increases, the rate of development becomes less and less dependent on diffusion, and development in depth in the emulsion layer becomes more uniform. This behavior is just the opposite from that shown by moderate- to fast-acting organic developers.[16] The activation energy[16,17] for diffusion in gelatin of the agents previously investigated ranged from 6.5 to 8 kcal/mole, which is lower than the activation energies of the chemical reactions of development. The activation energy of diffusion of the ferro–EDTA complex should be no lower than 6.5 kcal/mole, and probably is considerably higher. The temperature coefficient of development by the ferro–EDTA solutions in the low-temperature region, however, is considerably smaller than that corresponding to an activation energy of 6.5. Hence, the relative rate of diffusion should increase more rapidly than the rate of development as the temperature increases, and diffusion should become less important in agreement with the observations on the distribution of silver in the developed layers.

In the high-temperature region, where diffusion does not appear to be a rate-determining factor, the over-all activation energy is 11–12 kcal/mole and probably represents that of the chemical reaction, uncorrected for heats of adsorption. There remains, then, the problem of explaining the very low temperature-dependence of the over-all reaction in the low-temperature region. We must either assume that the dominant mechanism of development is different at the low temperatures, or that some important temperature-dependent auxiliary process is operative at the low temperatures. The experimental results can be explained on the latter basis.

The rate of attack of the developing agent on the silver halide grain, either in fog formation or in development, is retarded by the adsorbed gelatin layer. As development proceeds, silver ions are converted to atoms which crystallize in the form of filaments, and a corresponding number of halide ions pass out into the solution. This process makes fresh silver halide surface available to the developer, and the fresh surface will be more reactive than the original one unless the adsorbed gelatin layer is reestablished. It is reasonable to expect that the rate of adsorption of gelatin on the fresh surface would increase with increase in temperature. In the low-temperature range, the rate of this adsorption may be too low effectively to restore the protective gelatin layer on the grain surface. Such a failure should be more marked in coatings with a very low gelatin content, and it is in these coatings that the largest departures from the temperature-dependence predicted by the Arrhenius equation are noted. The rate of development beyond the induction period is thus higher than it would be if the gelatin layer were restored as rapidly as new surface of silver halide was formed by the development reaction.

As the temperature increases, the rate of the chemical reaction would normally increase, but the rate of adsorption of gelatin on the fresh silver halide surface also would increase. These two factors oppose each other, and if the temperature-dependence of the adsorption of the gelatin is high enough, the rate of development of the individual grains *beyond the induction period* would actually decrease with increase in temperature. The rate of initiation of development, however, would continue to increase, and the net result would be an increase in the number of grains which had started to develop in a given time, but a decrease in the degree of development of those grains, in agreement with the observed distribution of silver in the layers developed in the low-temperature region. In the high-temperature region, the inhibiting effect of the formation of the adsorbed gelatin layer would be considerable, and might be approaching a maximum. The relative effect of a further increase in the rate of adsorption then would be small. An increase in temperature would result in an increase in the rate of development of the individual grains beyond the induction period, and the measured increase in the net rate would more closely represent the increase in the rate of the *inhibited* reaction.

If this explanation is correct, some manifestation of the temperature effects described should appear with other developers as well. Evidence of a similar phenomenon has been found with the ferro-oxalate developers and also with certain hydroquinone developers used with the coating in which the ratio of silver to gelatin is high. The temperature region in which the effect appears and the degree to which it occurs, however, should vary with the developer and the conditions of development. The effect may be particularly marked in the ferro–EDTA developers because of relatively weak adsorption of these developers by the silver halide surface. Gelatin would interfere to a smaller degree with adsorption of a more strongly adsorbed developing agent, hence the retarding influence would be less.

Acknowledgment

The writer is grateful to A. A. Rasch for helpful discussions during the course of this work.

16. T. H. James, *Phot. Sci. and Tech.*, **2**: 81 (1955).

17 J. E. LuValle, F. M. Dunnington, and C. Margnetti, *Phot. Eng.*, **6**: 42 (1955).

PHOTOGRAPHIC SCIENCE AND ENGINEERING
Volume 4, Number 5, September-October 1960

Experiments on the Formation and Crystallographic Stability of Silver Bromide Grains in Saturated Bromide- and Ammonia-Complex Solutions

R. MATEJEC, *Agfa Research Laboratory, Agfa AG, Leverkusen, West Germany*

Microscopic studies have been made on formation and crystallographic stability of flat silver bromide grains in bromide- and ammonia-complex solutions saturated with respect to silver bromide. While the usual triangular and hexagonal grains are formed at very low crystallization rates, rapid crystallization gives rise to special forms, strongly structurally defective, which frequently show preferred growth directions. The flat grains first produced are not stable in saturated complex solutions in the absence of a protective colloid. The rate of transformation from flat into compact grains (more or less well-defined octahedrons or cubes) increases with temperature and increasing complex concentration; it decreases when protective colloids are added (gelatin, polyvinyl alcohol).

From investigations with the light microscope[1] as well as with the electron microscope[2] the existence of predominantly flat-shaped, triangular or hexagonal grains bounded by (111)-faces in silver bromide emulsions is well known. Under certain conditions, it is possible to enable these AgBr grains to grow to a considerable size, which proved to be particularly advantageous for the performance of examinations with the light microscope: Frieser[3] has described a method whereby large-sized AgBr grains are formed by dilution and gradual evaporation of NH_3 from an NH_3-solution saturated with AgBr, and Ammann-Brass[4] has described the conditions under which such large-sized grains are formed by precipitation from KBr solutions containing gelatin when $AgNO_3$ solutions are added.

Form of Grains Obtained by Slow Crystal Growth

Slow crystal growth from NH_3 solutions,[3] as well as from KBr solutions,[4] always leads to large-sized flat-shaped regular and little-disturbed hexagonal or triangular AgBr grains.

When forming such regular grains by dilution or gradual evaporation of NH_3 solutions[3] saturated with AgBr, special care must be taken so that the solution is not locally cooled by evaporation of NH_3. In this case, $[Ag(NH_3)_n]^+$-complex salt is deposited, thus supplying nuclei of crystallization for the AgBr. This results in completely irregularly shaped AgBr grains. The formation of $[Ag(NH_3)_n]^+$-complex nuclei is suppressed by employing heated and slightly undersaturated AgBr solutions at the beginning of the precipitation. From KBr solutions containing gelatin, large-sized regular and flat-shaped AgBr grains are formed by precipitation with $AgNO_3$ solutions under the following conditions (see also Ref. 4): a limited number of nuclei at the beginning of precipitation, high temperature, slow precipitation, considerable excess of KBr, and intensive physical ripening. An exceptionally large excess of KBr ($> 5\ N$), however, causes a preferred formation of compact AgBr grains.

Figure 1 shows a schematic top view (A) and side view (B) of a flat hexagonal grain; the two parallel large-sized hexagonal top and bottom faces, as well as six narrow lateral faces, may be seen. Though all faces are (111)-faces, they differ in their behavior during crystal growth: the AgBr depositing from the solution prefers the six lateral faces,[2] thus forming flat-shaped grains.

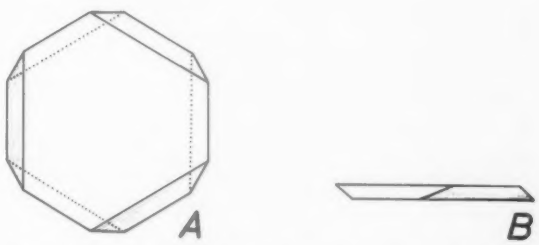

Fig. 1. Schematic diagram of flat hexagonal grain. *A*, top view; *B*, side view.

Presented at the Annual Conference, Santa Monica, California, 12 May 1960. Received 27 April 1960.

1. A. P. H. Trivelli and S. E. Sheppard, *The Silver Bromide Grain of Photographic Emulsions* (*Monograph No. 1 on the Theory of Photography*), Eastman Kodak Co., Rochester, N.Y., 1921. Cf. J. M. Eder, *Handbuch*, **I:** 1 (1932).
2. E. Klein, *Z. Elektrochem.*, **62:** 1000 (1958).
3. H. Frieser, *Z. wiss. Phot.*, **37:** 240 (1938); *ibid.*, **39:** 67 (1940).
4. H. Ammann-Brass, *Chimia*, **10:** 173 (1956).

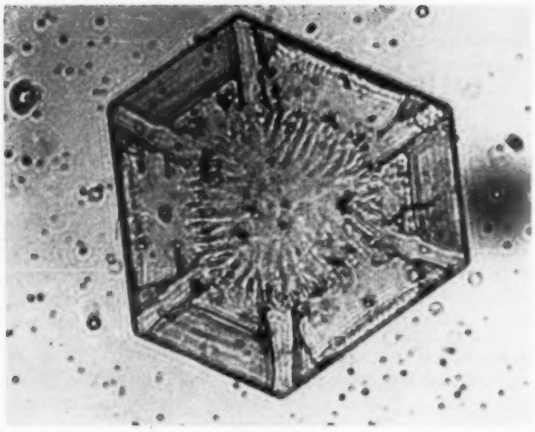

Fig. 2. Highly disturbed AgBr grain grown very rapidly from a solution with excess KBr by addition of $AgNO_3$ solution. 800×.

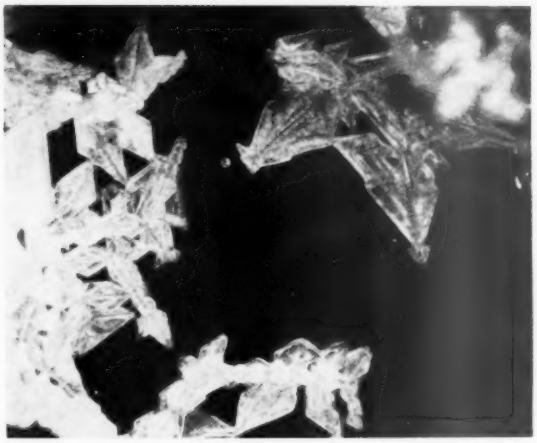

Fig. 3. Highly disturbed AgBr grain grown very rapidly from an NH_3 solution saturated with AgBr. Photomicrograph taken with reflected light; 400×.

Form of Grains from Rapid Crystal Growth

When AgBr grains grow quite rapidly from solutions containing an excess of KBr, their shape (triangular or hexagonal) is usually the same as that obtained by slow growth, but they usually show a quite pronounced pattern (see, e.g., Fig. 2). During rapid growth of AgBr from NH_3 solutions, however, certain directions of growth are preferred, spear-shaped crystals being formed regardless of whether the rapid crystallization is caused by sudden dilution or intensive evaporation of the NH_3 (Fig. 3).

Conversion of Grains in Concentrated $[Ag(NH_3)_n]^+$- or $[AgBr_n]^{-n+1}$-Complex Solutions

However, the regular flat-shaped grains obtained by the methods cited (see *Form of Grains Obtained by Slow Crystal Growth*, above; see also Refs. 3 and 4), are not in their state of minimum energy; i.e. these grains are not yet obeying the principle of Wulff, Gibbs, and Curie[5] ($\sum_i o_i \sigma_i$ = minimum for constant crystal volume, where o_i = magnitude of a special face F_i, and σ_i = capillary constant (specific surface energy) of the special face F_i).

When the grains are stored without any protective colloids in a concentrated aqueous KBr or NH_3 solution previously saturated with AgBr (with complex formation), the grains are again degraded on their narrow lateral faces (see Fig. 1), where the AgBr was deposited particularly rapidly during the primary crystal growth. The AgBr is redeposited either:

(a) On the large-sized triangular or hexagonal top and bottom faces of the same or of any adjacent

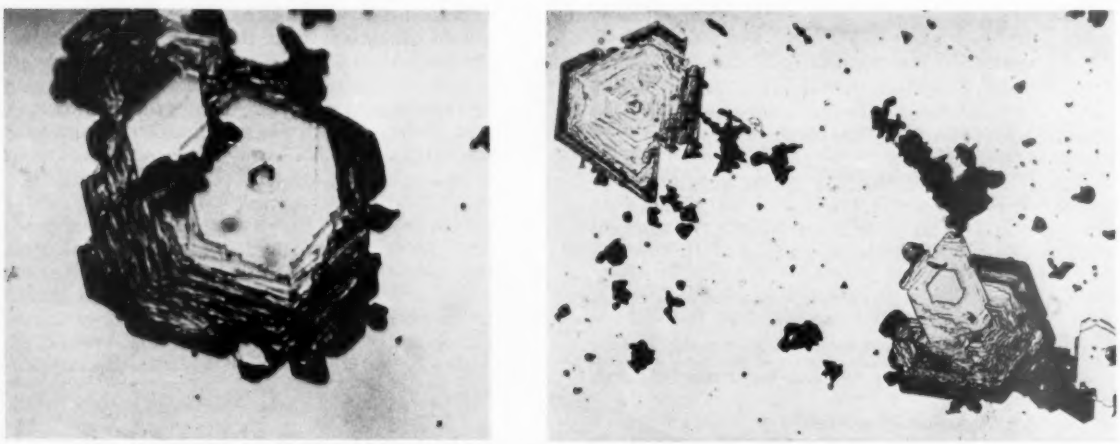

Fig. 4. Conversion of AgBr grains. The flat-shaped grains are transformed to compact grains. Photomicrographs taken with transmitted light; 800×.

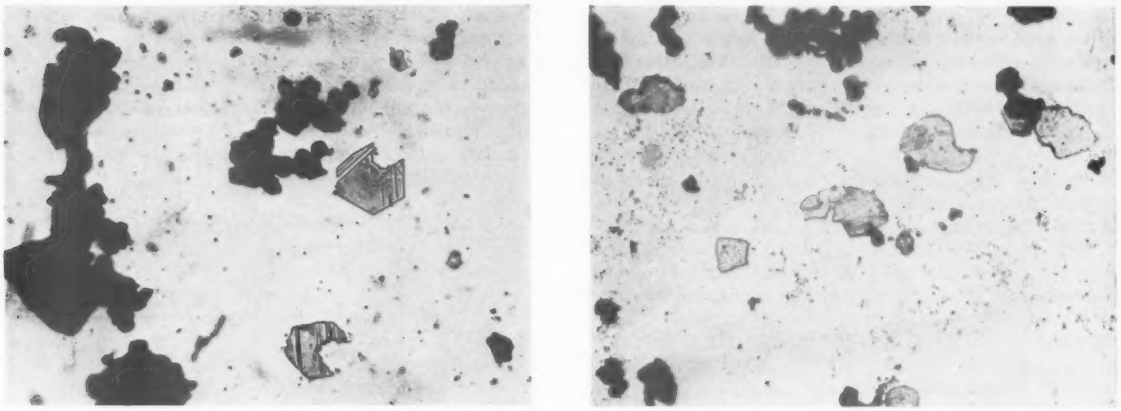

Fig. 5. Conversion of AgBr grains. Small-sized compact grains (the dark grains) grow at the expense of the large flat-shaped grains. Photomicrographs taken with transmitted light; 400×; *Left*, early stage; *right*, advanced stage.

grain (subsequently, clearly visible terraces (see Fig. 4) are formed on the originally level large-sized faces); or

(b) The AgBr is conveyed from large-sized flat grains through the solution phase to small and compact AgBr crystals (seen as dark grains in the photomicrographs taken with transmitted light), so that these small-sized compact grains are actually growing at the expense of the large ones (see Fig. 5).

The rate of grain conversion increases with rising temperature and increasing complex concentration, i.e. with increasing NH_3 or Br^- concentration. Protective colloids such as gelatin or polyvinyl alcohol, as well as stabilizers (1-phenyl-5-mercaptotetrazol) and optical sensitizing dyes (erythrosin) reduce the grain conversion or, under certain circumstances, suppress it entirely. At the end of this grain conversion, compact grains are always obtained. Regular octahedrons and cubes are more or less easily discerned (Fig. 6).

Discussion

Thus, according to the above statements (see also Ref. 2), two different types of (111)-faces occur on the flat-shaped, triangular or hexagonal AgBr grains:

1. The narrow lateral faces (see Fig. 1) which show both fastest growth and fastest degradation. A high supersaturation of the solution causes the AgBr to deposit predominantly on these narrow lateral faces, resulting in the formation of flat-shaped crystals.
2. The two large parallel triangular or hexagonal top and bottom faces, on which AgBr deposits only very slowly, and from which it dissolves only sparingly.

5. J. W. Gibbs, *Scientific papers, Thermodynamics I*, Longmans, Green, London, 1906, p. 320. P. Curie, *Bull. soc. franc. minéral*, **8**: 145 (1885). G. Wulff, *Z. Krist. Mineral. Petrog.*, **34**: 449(1901).

The solubility of AgBr is higher from the narrow lateral faces than from the large-sized top and bottom faces. When AgBr grains are brought into contact with saturated AgBr complex solutions, the result is an AgBr concentration in the solution, which ranges between the saturation concentrations of the two types of faces: A physical ripening of the faces occurs which conveys AgBr from the crystal faces of higher solubility (narrow lateral faces) to faces of lower solubility (large top and bottom faces). Thus the flat-shaped AgBr grains are converted to compact grains.

Photographic Significance of Grain Conversion

Lattice imperfections ("sensitivity centers"[6]),

6. J. W. Mitchell, *Z. Physik*, **138**: 381 (1954).

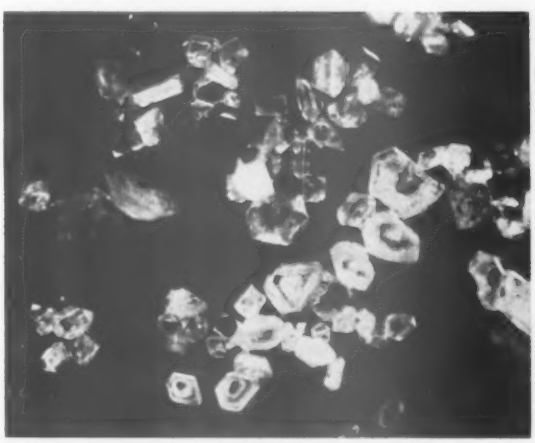

Fig. 6. Final stage of grain conversion. Compact grains are obtained that are clearly discernible cubes and octahedrons. Photomicrograph taken with reflected light; 400×.

produced by an initial state of grain conversion during physical ripening might be significant for the subsequent chemical ripening. Furthermore, it has been previously shown[7] that structural lattice imperfections exist which are able to initiate the development process just as are the latent-image nuclei formed by exposure. Because structural lattice imperfections may occur or may be set free by a subsequent conversion of the emulsion grains, this process may be partially responsible for the occurrence of a so-called "storage fog." Gelatin or other protective colloids, however, intensively restrain this "recrystallization."

7. E. Klein and R. Matejec, Lecture at the Intern. phot Conf., Liège, 1959, *Z. angew. Phys.*, **12**: 26 (1960).

PHOTOGRAPHIC SCIENCE AND ENGINEERING
Volume 4, Number 5, September-October 1960

Measurement of the Changes in pH in Photographic Coatings During Development

J. EGGERS, *Agfa Research Laboratories, Agfa AG, Leverkusen, West Germany*

Hydrogen ion is liberated during development by organic developing agents. Because of slow diffusion in the emulsion layer, it was thought possible that the decrease in pH in the developing emulsion might be much greater than in the bulk solution. Measurements of the pH at the bottom of a developing layer were made on a model consisting of a flat membrane glass electrode coated with a Lippmann emulsion. Development was initiated by a flash exposure of the coated electrode immersed in the developer. By simultaneous flash exposure of a glass plate similarly coated with emulsion and immersed in the developer, the growth of density parallel to the change in pH could be followed. Measurements were made with different emulsion thicknesses and in developers of different buffer capacity.

The development of photographic emulsions with organic developing agents — e.g., hydroquinone, Metol, *p*-aminophenol, *p*-phenylenediamine—causes hydrogen ions to be released or hydroxyl ions to be used up. This is indicated by the general equation for development (Eqs. (1a) and (1b)):

$$x\mathrm{AgBr} + \mathrm{E} + 2\mathrm{OH}^- \xrightarrow{k_1} x\mathrm{Ag} + x\mathrm{Br}^- + \mathrm{OX} + 2\mathrm{H_2O} \quad (1a)$$

$$x\mathrm{AgBr} + \mathrm{E} \xrightarrow{k_1} x\mathrm{Ag} + x\mathrm{Br}^- + \mathrm{OX} + 2\mathrm{H}^+ \quad (1b)$$

where E = the developing agent
OX = the developer oxidation product, e.g., benzoquinone or hydroquinone disulfonic acid
x = a value which generally ranges between 2 and 4, depending on the developer substance, pH value, and presence of sulfite
k_1 = the velocity constant of development

When sulfite is present, the electroneutrality is ensured by released Na^+ ions.

The large reduction of pH value in the developer solution, which is to be expected as a result of the low concentration of free H^+ and of free OH^- ions, fails to occur because of the considerable concentration of buffer agents (e.g., Na_2CO_3, borax). The buffer effect is expressed by Eq. (2):

$$\mathrm{HY} + \mathrm{OH}^- \underset{k_{-2}}{\overset{k_2}{\rightleftharpoons}} \mathrm{Y}^- + \mathrm{H_2O} \quad (2)$$

where HY = the undissociated buffer agent
Y^- = the anion of the buffer agent
k_{-2} and k_2 = the velocity constants of the reverse and forward reactions of the equilibrium

Also, Eqs. (3a) and (3b) apply.

$$k_2/k_{-2} = K_S/K_W \quad (3a)$$

$$[\mathrm{OH}^-] = 10^{-14}[\mathrm{Y}^-]/K_S[\mathrm{HY}] \quad (3b)$$

where K_S = the acid dissociation constant of the buffer substance

Presented at the Annual Conference, Santa Monica, California, 12 May 1960. Received 27 April 1960.

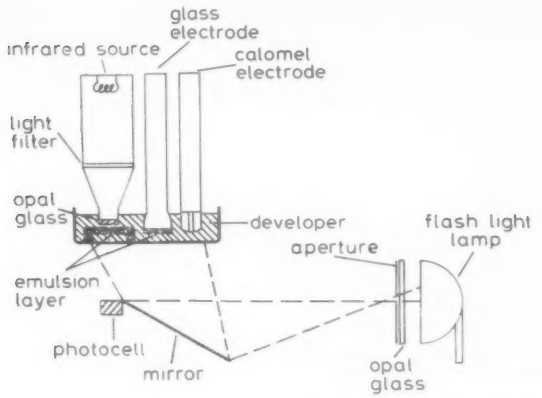

Fig. 1. Apparatus for exposure and development.

$K_W = 1.8 \cdot 10^{-16}$ is the constant of dissociation of water at 20°C.

The product $K_W[H_2O] = [H^+][OH^-]$ is called the ion product of water and equals $1.8 \cdot 10^{-16} \cdot 55 \approx 10^{-14}$ (one liter of water contains 55 moles).

The development reaction, however, does not take place in the solution but in the photographic emulsion. It has been assumed that, as a result of the slower diffusion in the emulsion layer in the immediate vicinity of the site of reaction, there occurs temporarily a larger decrease in pH, while the same level as in the developer solution is only restored after a new supply of buffer material has arrived.

The general Fick's differential equation for diffusion, together with the Nernst's solution for linear concentration decrease, has been applied to the OH^- concentration (Eq. (4)).

$$\frac{\partial[OH^-]}{\partial\tau} = \frac{D_{OH^-}}{\delta\Delta}([OH^-]_\infty - [OH^-]) \qquad (4)$$

where D_{OH^-} = the diffusion coefficient (μ^2/sec)
δ = the partial emulsion thickness of the measuring range of pH (μ)
Δ = the total emulsion thickness (μ)
$[OH^-]_\infty$ = the OH^--ion concentration with $\tau = \infty$
τ = the time after initiation of development

In an analagous manner, the change in concentration of the developing agent by diffusion was formulated.

Measuring Apparatus

The solution of this problem required the measurement of the change in pH in the emulsion, if possible, as a function of the time, and an observation of the simultaneously occurring increase of photographic density formation.

For that purpose, the surface of a flat membrane glass electrode was coated with definite quantities of a Lippmann emulsion and the layer dried in nonactinic light. When this electrode was immersed in a developer solution, practically no silver development occurred without exposure (the fog formation was negligible). Measurements of a pH-dependent potential can as well be carried out with the coated glass electrode against a saturated calomel electrode as with the uncoated electrode. A somewhat longer period of equilibration is necessary, however.

Figure 1 is a diagram of the experimental apparatus. The development is initiated by an electronic flash exposure of the coated glass electrode immersed in the developer. Silver formation is observed on a coated glass plate positioned next to the glass electrode in the developer, which is simultaneously exposed to the flash. The density of silver formed in this manner is measured by the absorption of infrared light behind an opal plate and then recorded.

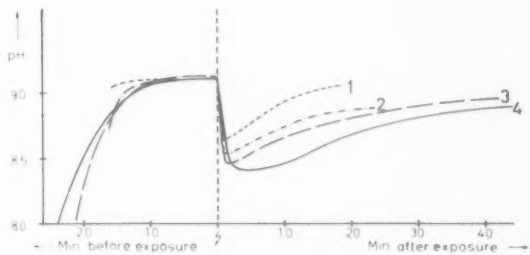

Fig. 2. Change in pH during development in a Metol-hydroquinone developer, showing the effect of variation in the thickness of the layer. Curve 1, 12 grams Ag/sq m, 5.7 mg emulsion/cc (sicc); Curve 2, 24 grams Ag/sq m, 11.4 mg emulsion/cc (sicc); Curve 3, 36 grams Ag/sq m, 17.1 mg emulsion/cc (sicc); Curve 4, 48 grams Ag/sq m, 22.8 mg emulsion/cc (sicc). Agfa Final Developer.

Experimental Results

After reproducibility is examined, the dependence of the pH-time curves on the layer thickness is determined in a Metol-hydroquinone developer containing sulfite, with borax and citric acid as buffer substances (Fig. 2). The glass electrode is immersed in the developer under nonactinic light. After its equilibration to the pH value of the developer, a flash exposure is made. A lowering of pH is observed, followed by a subsequent recovery of the pH, due to diffusion effects. The degree of both the drop and the recovery of the pH depends on the thickness of the layer.

The process of simultaneous reduction in pH and increase in density is shown in Fig. 3, in which three different exposure intensities have been used. A more intense exposure results in a greater reduction in pH and an increase in rate of development.

A less active developer causes a considerably slower increase in density formation and a smaller reduction in pH (Fig. 4). This pH reduction is much smaller because the rate of development is of the same magnitude as the rate of diffusion.

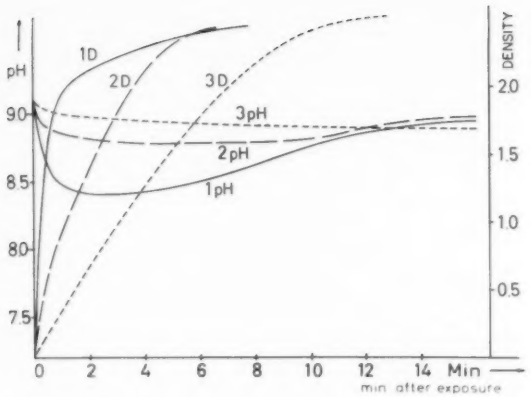

Fig. 3. Change in pH and increase in density during development in the same Metol-hydroquinone developer as in Fig. 2, showing the effect of variation in the intensity of exposure; coating, 3.8 grams Ag/sq m. Relative intensity of exposure; Curve 1, 1; Curve 2, $^1/_2$; Curve 3, $^1/_4$.

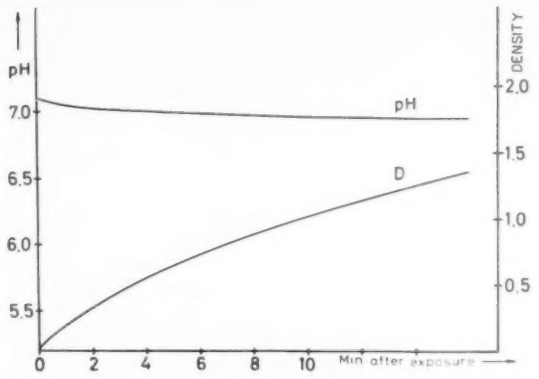

Fig. 4. Change in pH and increase in density during development in Agfa 47 (Amidol-sulfite) developer, coating, 3.8 grams Ag/sq m. Relative intensity of exposure, 1.

Mathematical Analysis of Results

Equations (1), (2), and (3), in combination with the equation of Hurter and Driffield and with the diffusion equations for [E] and [OH^-], were used to establish the following system of velocity differential equations.

The rate of change of density, S, with respect to time, τ, is:

$$\frac{dS}{d\tau} = -\frac{d(S_\infty - S)}{d\tau} = k_1[E][OH^-](S_\infty - S) \quad (5)$$

where S_∞ = density at infinite time of development
k_1 = rate constant of development

The value of $dS/d\tau$ has been assumed as an approximation to be proportional to the developing agent concentration [E] and to the hydroxyl-ion concentration [OH^-]. For an exact calculation, the concentration of the active form of the developing agent should be taken, which includes the dependence on pH.

The rate of change of the concentration of OH^- ion with respect to time, τ, is:

$$\frac{d[OH^-]}{d\tau} = \frac{2k_1}{x}[E][OH^-]p(S_\infty - S) - k_2[HY][OH^-] + k_{-2}[H_2O][Y^-] + \frac{D_{OH^-}}{\delta\Delta}([OH^-]_\infty - [OH^-]) \quad (6)$$

where p = a constant proportional to the photometric constant. The other symbols have been defined above.

The rate of change of the concentration of the developing agent, E, with respect to time, τ, is:

$$\frac{dE}{d\tau} = -k_1[E][OH^-]p(S_\infty - S) + \frac{D_E}{\delta\Delta}([E]_\infty - [E]) \quad (7)$$

where D_E = diffusion coefficient of the developing agent.

The equations representing the buffer system are:

$$\frac{d[Y^-]}{d\tau} = k_{-2}[HY][OH^-] - k_{-2}[H_2O][Y^-] + \frac{D_{Y^-}}{\delta\Delta}([Y^-]_\infty - [Y^-]) \quad (8)$$

$$\frac{d[HY]}{d\tau} = -k_2[HY][OH^-] + k_{-2}[H_2O][Y^-] + \frac{D_{HY}}{\delta\Delta}([HY]_\infty - [HY]) \quad (9)$$

where D_{Y^-} and D_{HY} are the diffusion coefficients of these substances. Index ∞ means a concentration or a value at the time $\tau = \infty$.

The simplifying assumption was made that the concentrations [OH^-], [E], [Y^-], and [HY] are only changed by reactions on the rear of the emulsion layer in the vicinity of the glass electrode membrane and that the recovery of concentration is by diffusion from the developer solution through the emulsion.

In order to obtain a mathematical solution of the equations the following simplification was assumed for the remaining part of the layer: The concentration of OH^--ion and developing agent [E] drops linearly from the surface to the partial layer, δ, in the vicinity of the glass electrode membrane, δ being small with respect to the total layer thickness, Δ. The difference in the concentrations between the two limits determines the velocity of diffusion.

For a mathematical evaluation, an approximate knowledge of all constants is necessary. This is somewhat difficult for the velocity constants k_2 and k_{-2} having an order of magnitude of 10^2 to 10^{11} liter/mole-sec. Assuming that the buffer equilibrium (2) or (3a) should be approximately steady, the following simplification of Eqs. (5)–(9) seems admissible:

$$\frac{dS}{d\tau} = -\frac{d(S_\infty - S)}{d\tau} \approx k_1[E][OH^-](S_\infty - S) \quad (10)$$

$$\frac{d[OH^-]}{d\tau} \approx -\frac{2k_1}{x}p\frac{10^{-14}}{K_{S^*}}[E][OH^-](S_\infty - S) + \frac{D^*_{OH^-}}{\delta\Delta}([OH^-]_\infty - [OH^-]) \quad (11)$$

$$\frac{d[E]}{d\tau} \approx -k_1p[E][OH^-](S_\infty - S) + \frac{D_E}{\delta\Delta}([E]_\infty - [E]) \quad (12)$$

The magnitude of K_{S^*} may be estimated from a derivation which does not consider the diffusion of [Y^-]:

$$K_{S^*} \approx K_S q^2([Y^-] + [HY]) \quad (13)$$

where K_S is the acid dissociation constant of the buffer substance and

$$q = \frac{[HY]}{[Y^-] + [HY]} \tag{14}$$

Furthermore, for q the following equation is valid:

$$[OH^-] = \frac{10^{-14}}{K_S}\left(\frac{1}{q} - 1\right) \tag{15}$$

If $[OH^-] \approx 10^{-5}$ mole/liter and $K_S \approx 10^{-9}$, we obtain $q \approx 0.5$.

If the buffer agent concentration $[Y^-] + [HY]$ equals 0.5, we obtain for $K_S{}^*$ the order of magnitude 10^{-10}.

The diffusion coefficient $D^*_{OH^-}$ in Eq. (11) is not necessarily an intrinsic constant of the OH^- ion. It is possible that the supply of OH^- ions comes from the anions of the buffer substance.

After entering the constants k_1, $K_S{}^*$, x, p, $D^*_{OH^-}$, D_E, δ, and Δ, estimated according to the experimental results, Eqs. (10)–(12) were numerically integrated with the aid of an electronic computer, and the time functions experimentally determined for the OH^- ions and the density formation process were compared with the values calculated. Figure 5 compares the calculated curves with the experimental results of pH change and density formation shown in Fig. 3. The influence on the course of the curves of a systematic variation of the individual constants k_1, p, and $D^*_{OH^-}$ by $\pm 20\%$ is demonstrated.

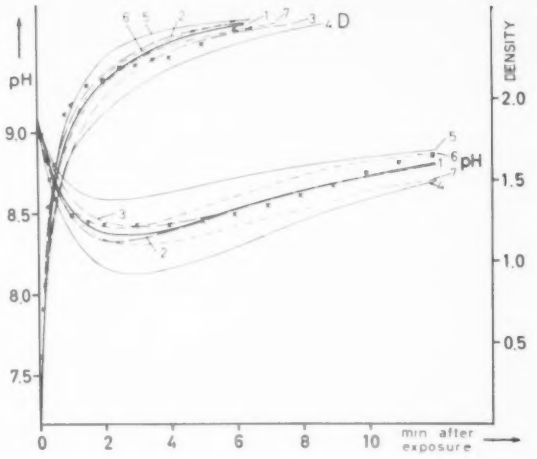

Fig. 5. Comparison of the calculated and the experimental time functions of pH value and density D. × = measured value of pH and density D. *Curve 1*, calculated curves for pH and density D; *Curve 2*, constant k_1 raised 20%; *Curve 3*, constant k_1 lowered 20%; *Curve 4*, constant p raised 20%; *Curve 5*, constant p lowered 20%; *Curve 6*; constant D_{OH^-} raised 25%; *Curve 7*, constant D_{OH^-} lowered 25%.

• Coming Technical and Scientific Meetings

Optical Society of America, Annual Meeting, October 13–15, Somerset Hotel, Boston

Rapid Processing Symposium, SPSE, October 14–15, Shoreham Hotel, Washington, D.C.

Fifth International High-Speed Congress and Equipment Exhibit, sponsored by the Society of Motion Picture and Television Engineers (SMPTE), October 16–22, Sheraton-Park Hotel, Washington, D.C.

Scientific and Technical Group Conference, RPS, "The Ultimate Sensitivity in Photography—Today and Tomorrow," December 7–9, 1960, London. Contributions should be sent before October 30 to The Secretary, Scientific and Technical Group, The Royal Photographic Society, 16 Princes Gate, London S.W. 7

Optical Society of America, March 2–4, 1961, Pick-Roosevelt Hotel, Pittsburgh, Pa.

89th Semiannual Convention, SMPTE, May 7–12, 1961, King Edward Sheraton, Toronto. Papers Committee Chairman, Rodger J. Ross, Canadian Broadcasting Corp., 354 Jarvis St., Toronto

1961 Annual Conference, SPSE, May 22-26, Binghamton, N.Y. Papers Committee Co-Chairmen, Dr. F. H. Gerhardt and Peter Krause, Ansco, Binghamton, N.Y.

90th Semiannual Convention, SMPTE, October 2–6, 1961, Lake Placid, N.Y.

1962 Annual Conference, SPSE, Boston

91st Semiannual Convention, SMPTE, April 30–May 4, 1962, Ambassador Hotel, Los Angeles

92nd Semiannual Convention, SMPTE, October 22–26, 1962, Drake Hotel, Chicago

PHOTOGRAPHIC SCIENCE AND ENGINEERING
Volume 4, Number 5, September-October 1960

Analysis of Printer Integrating Circuits

ROBERT K. RICKARD, *Apparatus and Optical Division, Eastman Kodak Company, Rochester, N.Y.*

The basic circuit of an automatic exposure control device for a printer consists of a capacitor, a vacuum phototube, and a thyratron. The capacitor integrates the light coming through the negative, and the voltage rise is used to fire the thyratron which, by means of a relay, terminates the exposure. In the ideal case, the printing paper is given an average exposure which is independent of the transmission of the negative and of variations in the output of the printing lamp. It is the purpose of this paper to analyze the effects that practical circuit components have on the accuracy of this circuit in terms of the circuit values used, the leakage resistances that may arise, the background illumination arriving at the phototube, the residual charge remaining in the "discharged" capacitor, and the uncertainty in the firing point of the thyratron. Some recommendations are given for the design of a circuit with an accuracy of 1%.

Automatic photoelectric control of exposure time is used in many types of black-and-white and color printers. This allows the printing to be done during the same period that the correct exposure time is being determined, and also provides the high accuracy needed for color exposures. The basic circuit for such automatic control consists of a capacitor, a vacuum phototube, and a thyratron.

The result of the capacitor integration performed by this circuit is to give an average exposure to the paper that is independent of variations in average transmission of the negatives and in the printing lamp intensity. This, of course, assumes that the circuit is an ideal one, and it is the purpose of this paper to analyze the effects that practical circuit components have on the accuracy of the exposure.

Shown in Fig. 1, which represents an ideal circuit, is a capacitor, called the timing capacitor, C, connected between the control grid of the thyraton and a preset negative voltage, V_s. The capacitor is kept discharged before the exposure starts by a set of relay contacts which open when the exposure begins. The vacuum phototube is illuminated by the average light transmitted by the negative to be printed and produces a photocurrent, i_c, that charges up the timing capacitor in a positive direction. When the voltage across the capacitor matches the preset voltage, the grid voltage is zero. The cathode of the thyratron is biased so that it will fire when the grid voltage reaches zero, operating the finish relay and shutter circuitry to terminate the exposure. The grid voltage is given by Eq. (1) as a function of time.

$$V_g = V_s + \frac{1}{C}\int_0^t i_c dt \qquad (1)$$

Since the photocurrent is proportional to the average transmission, T_n, of the negative and to the intensity, I, of the printing lamp, the time-integrated voltage across the capacitor is proportional to the exposure given to the printing paper. Therefore, the exposure E_0 is governed directly by the preset voltage, V_s, as shown in Eq. (2), since the time-integrated voltage must match this voltage before the grid voltage reaches zero and the exposure ends.

$$-V_s = \frac{1}{C}\int_0^{t_0} i_c dt = \frac{k_1}{C}\int_0^{t_0} T_n I dt = \frac{k_2}{C} E_0 \qquad (2)$$

for $V_g = 0$ at $t = t_0$
where k_1 and k_2 are proportionality constants.

If the photocurrent is low, the exposure time t_0 will be longer to keep the total exposure constant. The preset voltage V_s is referred to as the *exposure voltage*, and is set as required by paper speed, lens aperture, magnification, etc.

The analysis of this circuit is based on the assumption that the printing lamp intensity is constant during the exposure time and that the accuracy of the exposure is determined only by the accuracy of the integration time. This assumption is valid because normal printing times are short compared to most

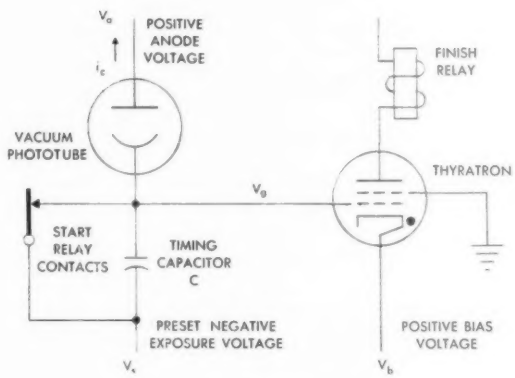

Fig. 1 Ideal circuit.

Presented at the Annual Conference, Santa Monica, California, 11 May 1960. Received 14 April 1960; revised 17 June 1960.

of the time fluctuations of line voltage which would change the lamp intensity. Hence, for a constant photocurrent, the grid voltage in an ideal circuit rises linearly with time and the printing time is given by Eq. (3).

$$t_0 = \frac{-CV_s}{i_c} \text{ for } i_c \text{ constant} \tag{3}$$

An ideal circuit would have the following characteristics:

1. Infinite leakage resistances between the thyratron grid and any other voltage level in the circuit, so that the only current charging the capacitor is the photocurrent.
2. Zero background illumination at the negative gate, to prevent unwanted photocurrent.
3. Absolute stability of the thyratron firing point.
4. Complete discharge of the timing capacitor before each exposure.

Figure 2 shows a circuit which does not meet these specifications because of the practical limitations of components and operating procedures. It has three leakage resistances shown, although these are not the only ones possible. R_1 is the grid cathode leakage resistance of the thyratron before conduction. R_2 is the leakage resistance of the timing capacitor and the open start relay contacts. R_3 is the leakage resistance of the phototube. They are subject to fluctuations with temperature and humidity, so that one must consider the minimum values likely to occur. The phototube current is now composed of two currents, i_c, due to the light from the negative, and i_b, due to the background illumination. The thyratron is assumed to actually fire when the grid reaches a voltage ΔV instead of zero, because of variation in the thyratron firing point, a-c ripple on the exposure voltage V_s, or a wrong bias voltage setting. Lastly, the exposure is assumed to start with a residual positive voltage V_0 across the timing capacitor, due to incomplete discharge following a previous exposure.

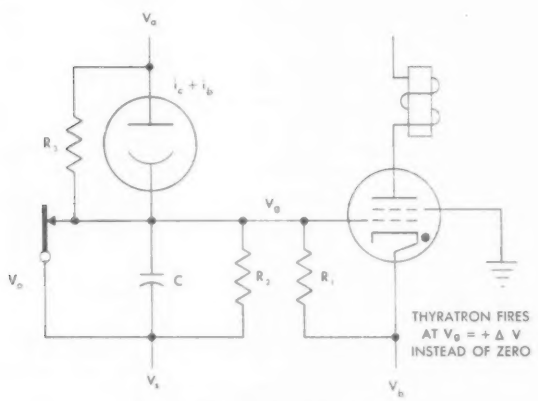

Fig. 2. Nonideal circuit.

The grid voltage V_g is now given in integral form by Eq. (4).

$$V_g = V_s + V_0 + \frac{1}{C}\left[i_c t + i_b t + \int_0^t (V_b - V_g)/R_1 dt + \int_0^t (V_s - V_g)/R_2 dt + \int_0^t (V_a - V_g)/R_3 dt\right] \tag{4}$$

$$V_g = \left[\frac{i_c + i_b + V_b/R_1 + V_s/R_2 + V_a/R_3}{1/R_1 + 1/R_2 + 1/R_3}\right] \times \left[1 - e^{-\frac{(1/R_1 + 1/R_2 + 1/R_3)}{C} t}\right] + (V_s + V_0) e^{-\frac{(1/R_1 + 1/R_2 + 1/R_3)}{C} t} \tag{5}$$

Equation (5) shows the solution. The voltage no longer rises linearly with time, but has exponential variations as well. By setting $V_g = \Delta V$ at $t = t_0$, Eq. (5) leads to an expression for the printing time, t_0, shown as Eq. (6).

$$t_0 = \frac{C}{(1/R_1 + 1/R_2 + 1/R_3)} \times \log_e \left[\frac{i_c + i_b + V_b/R_1 + V_s/R_2 + V_a/R_3 - (V_s + V_0)(1/R_1 + 1/R_2 + 1/R_3)}{i_c + i_b + V_b/R_1 + V_s/R_2 + V_a/R_3 - \Delta V(1/R_1 + 1/R_2 + 1/R_3)}\right] \tag{6}$$

This equation does not allow the printing time to be compared with the ideal time without laborious numerical evaluation.

Considering for the moment the effects of leakage resistance alone, by letting i_b, V_0, and ΔV all be zero, a first order approximation for the printing time can be obtained that is quite accurate for high values of leakage resistance. They must be high enough that the leakage currents are small compared to the phototube current. Equation (7) gives this approximation which is in the form of the ideal printing time reduced by a fractional error term, F, due to the leakage resistances.

$$t_0 \doteq -\frac{CV_s}{i_c}\left[1 - \frac{(V_b - V_s/2)}{R_1 i_c} - \frac{(V_s - V_s/2)}{R_2 i_c} - \frac{(V_a - V_s/2)}{R_3 i_c}\right] = \frac{-CV_s}{i_c}(1 - F) \tag{7}$$

It is apparent from this equation that if R_L is a high leakage resistance between the thyratron grid and any voltage level, V_L, the printing time will be given by Eq. (8).

$$t_0 \doteq -\frac{CV_s}{i_c}\left[1 - \frac{(V_L - V_s/2)}{R_L i_c}\right] \tag{8}$$

The fractional error term shows how much the printing time will be shortened compared to the ideal time. It is worth noting that if V_L is negative, as

in the case of the capacitor leakage, the time can be lengthened instead.

For the case of no leakage, but with the other errors present, the printing time can be shown to be given by Eq. (9).

$$t_0 = \frac{-C(V_s + V_c - \Delta V)}{(i_c + i_b)} \tag{9}$$

From these two expressions, we can draw the following conclusions in regard to reducing errors and improving the accuracy of the circuit. First of all, the photocurrent should be kept as high as possible to reduce both the size of the leakage resistance error term and the effects of i_b. The exposure voltage, V_s, should be made small to further reduce the leakage error. Both of these requirements call for a larger value of capacitor to obtain the same printing time. This is not much of a problem unless capacitor leakage gets worse, but more important, V_s should not become comparable to either V_0 or ΔV.

Referring to Eq. (8) for the time with leakage, it can be seen that the larger the voltage, V_L, to which the leakage resistance connects, the greater the error. Since in a practical circuit the phototube leakage comes from a fairly large positive voltage to insure saturation, the effect of phototube leakage resistance is much greater than that of thyratron grid leakage, which comes from a few volts of bias on the cathode. And since the exposure voltage can also be a large but negative voltage, capacitor leakage might be expected to have as much effect as phototube leakage (and in the opposite direction). However, capacitor resistance is more easily kept high, especially with Teflon and mica capacitors. It is not desirable to attempt to have the capacitor leakage compensate for phototube leakage, since V_s is changed to set the exposure, and humidity and temperature are not likely to change both leakage resistances in the same manner.

One practical way of checking an integrator circuit for leakage is to leave the printing lamp turned off and find the time for the capacitor to charge up only by leakage currents. This is called the "hold-on" time, t_{h_0}, and if it is a hundred times the normal printing time, the magnitude of leakage errors can be expected to be about 1%. However, this is only true under the conditions listed under Eq. (10).

$$t_{h_0} \doteq \frac{-CV_s}{\dfrac{(V_b - V_s/2)}{R_1} + \dfrac{(V_s - V_s/2)}{R_2} + \dfrac{(V_a - V_s/2)}{R_3}} \tag{10}$$

to within 10% if $(V_b/R_1 + V_s/R_2 + V_a/R_3) > -V_s/2\,(1/R_1 + 1/R_2 + 1/R_3) > 0$ for high values of leakage resistance alone. This approximation for the "hold-on" time is good to within 10% only if there is not too much capacitor leakage and the exposure voltage is not too large.

The expression for t_{h_0} can be rewritten in Eq. (11) as the ideal printing time divided by the same fractional error term F that we had in Eq. (7), which held for high values of leakage resistance.

$$t_{h_0} \doteq \frac{-\dfrac{CV_s}{i_c}}{\dfrac{(V_b - V_s/2)}{R_1 i_c} + \dfrac{(V_s - V_s/2)}{R_2 i_c} + \dfrac{(V_a - V_s/2)}{R_3 i_c}} = \frac{-\dfrac{CV_s}{i_c}}{F} \tag{11}$$

For a rough calculation to within 10%, we can assume the normal printing time, t_0, to be the same as the ideal time and arrive at the final Eq. (12) which gives the fractional error as the ratio of the printing time to the "hold-on" time.

$$\mathrm{F} \doteq t_0/t_{h_0} \tag{12}$$

This can be illustrated by the following example: assume a timing capacitor of 0.01 μf, a photocurrent of 0.2 μa, and an exposure voltage of −20 v. Equation (3) will then give an ideal printing time of 1.00 sec. Now assume that the thyratron has a leakage resistance of 10,000 megohms to a bias voltage of +1.6 v, the capacitor has a leakage resistance of 30,000 megohms, and the phototube has a leakage resistance of 15,000 megohms to an anode voltage of +100 v. Equation (7) can be used to calculate the actual printing time of 0.959 sec, which is 4.1% less than the ideal time.

The "hold-on" time is found exactly from Eq. (6) by letting $i_c = i_b = 0$, and it turns out to be 24.1 sec. Then by using Eq. (12), we can calculate the fractional error term F of 0.040, which predicts an error of 4.0% instead of 4.1%. Therefore, the "hold-on" time is a good measure of the effect of the leakage on the accuracy of the circuit.

In conclusion, the use of this circuit calls for careful attention to keeping all leakage resistances, especially that of the phototube, as high as possible when using small photocurrents. As a general rule, if the photocurrent is of the order of 0.1 μa, the leakage resistances should be kept over 100,000 megohms. This will enable voltages as high as several hundred volts to be used with about 1% accuracy. For the same order of accuracy, the background illumination at the negative gate should be kept to less than 1% of the level from the densest negative to be printed. Maintaining this order of accuracy will insure that the exposures have less than 0.01 log E total variation. The contribution of this variation to any final errors in either print density or color balance should be nearly imperceptible.

Bibliography

1. C. M. Tuttle, "Photoelectric Photometry in the Printing of Amateur Negatives," *J. Franklin Inst.*, **224:** 315 (1937).
2. C. M. Tuttle, "Devices for the Photoelectric Control of Exposure in Photographic Printing," *J. Franklin Inst.*, **224:** 615 (1937).
3. H. C. Rentschler, "An Ultra-Violet Light Meter," *Trans. AIEE*, **49:** 576 (1930).

PHOTOGRAPHIC SCIENCE AND ENGINEERING
Volume 4, Number 5, September-October 1960

The Effect of Gamma-Ray Exposure on Camera Films

G. M. CORNEY, *Research Laboratories, Eastman Kodak Company, Rochester, N.Y.*

A gamma-ray fog tends to reduce the effective contrast and speed of a photographic material and to increase the graininess. The consequences of the first two effects can be minimized by proper choice of printing-paper grade and by increasing camera exposure, with the result that the increase of graininess may be the limiting factor. A film for use in the presence of gamma rays should have as low a speed as lens and exposure-time requirements will permit. Additional desirable features are: a high ratio of light to gamma-ray sensitivity, a high contrast, and a long density range over which the useful gradient is maintained.

Recent technical advances in a number of fields (in space research and nuclear power, for example) have caused the problems of photography in the presence of x-rays and gamma rays to be increasingly important.[1] Research on photography in the presence of penetrating radiation has covered investigations of special processing techniques for films which have been exposed to both light and gamma rays,[2] and bleaching processes by which the effect of a prior gamma-ray exposure may be removed, with a greater or lesser loss in effective speed, before a light exposure.[3] The present paper deals with the effects of penetrating radiation on conventional films, conventionally processed, and with the relationships between a number of film properties and the quality of the light record obtained on material which has also been exposed to gamma rays.

The demands made on photographic recording vary widely from application to application; a large variety of photographic materials are used; and the gamma- and x-ray intensities encountered cover a very wide range. For these reasons, it is impossible to anticipate all the combinations of circumstances which may arise. However, consideration of a few general principles will aid in selecting a specific film for a certain application.

In general, films which have a high speed to light also tend to be fast to x-rays and gamma rays. However, the correlation is far from exact, and it is impossible to predict the gamma- or x-ray speed of a film from a knowledge of its light speed alone.

Communication No. 2099 from the Kodak Research Laboratories, presented at the National Conference, Chicago, 27 October 1959. Received 5 July 1960.

1. J. S. Moser, *The Effects of Nuclear Radiation upon Photographic Film*, AD-144586, January 1953, Armed Services Tech. Information Agency, Arlington Hall Station, Arlington 12, Va.
2. D. A. Nepela and H. F. Nitka, *Gamma-Ray Insensitive Emulsions*, AD-154596, September 1957, Armed Services Tech. Information Agency.
3. D. A. Nepela and H. F. Nitka, *Gamma-Ray Insensitive Emulsions*, AD-157582, December 31, 1957; AD-211186, March 1958, Armed Services Tech. Information Agency.

An over-all gamma- or x-ray exposure to a film, added to an image-forming light exposure, has an effect analogous to that of any other over-all, non-image-forming exposure — from safelights, for example. The low densities, in the toe of the characteristic curve, are increased the most, the high densities considerably less, and the maximum density scarcely at all. That this obviously amounts to a decrease in contrast is shown in Fig. 1. Samples of Kodak Super-XX Panchromatic Film were exposed

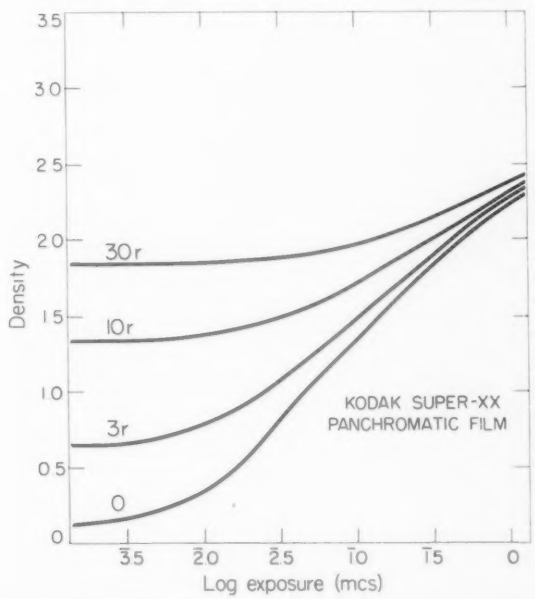

Fig. 1. Characteristic curves of Kodak Super-XX Panchromatic Film (developed 8 min in Kodak Developer DK-50 at 68°F), showing the effect of increasing amounts of hard x-radiation on the effective characteristic curve.

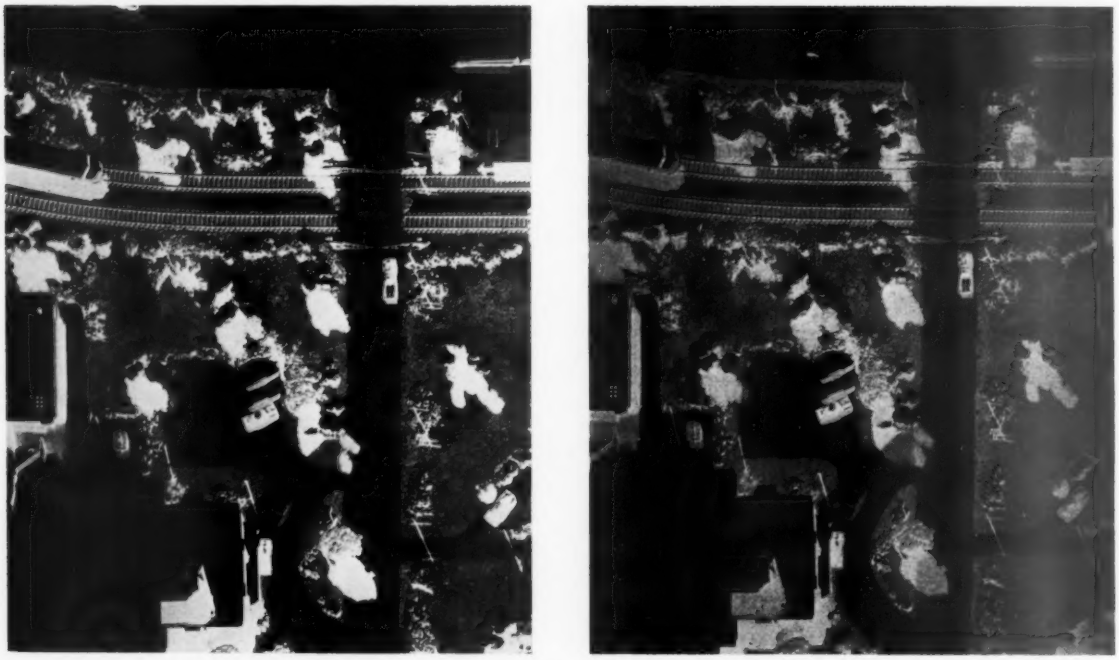

Fig. 2. Simulated aerial photographic negatives (Super-XX Film, developed 8 min in DK-50 at 68°F). A (*left*), Normal negative; B (*right*), Film pre-exposed to 10 roentgens (r) of hard x-rays.

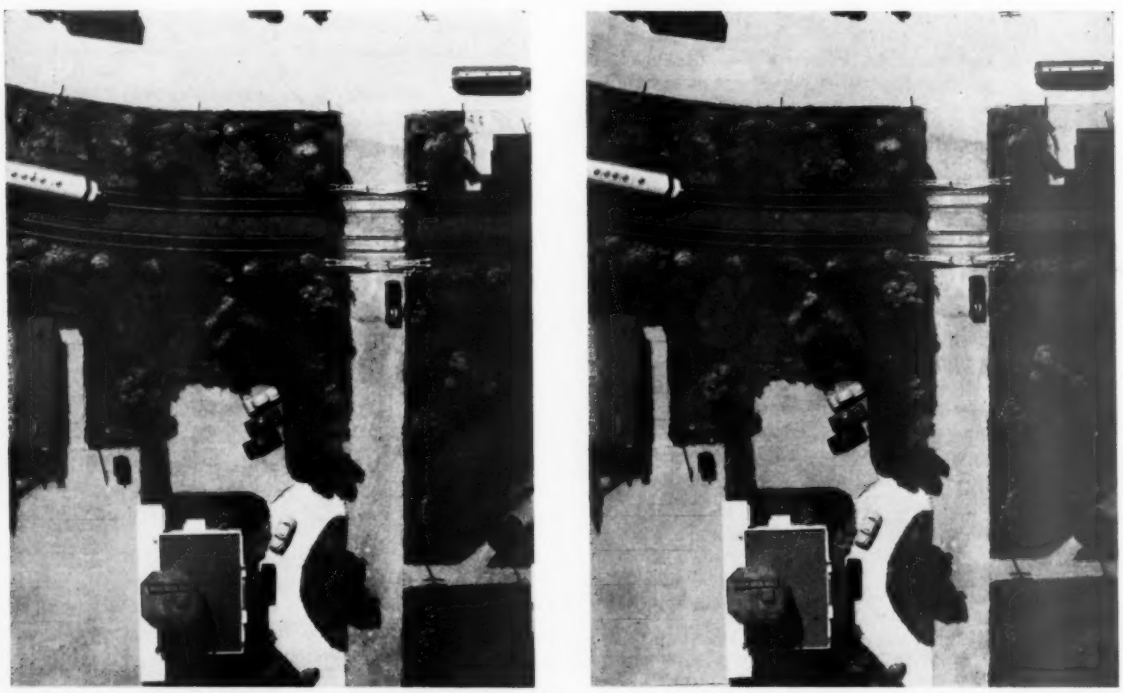

Fig. 3. Prints made from negatives of Fig. 2. A (*left*), Made from negative of Fig. 2A on glossy paper, contrast grade No. 1; B (*right*), Made from negative of Fig. 2B on glossy paper, grade No. 4.

to amounts ranging from 3 to 30 roentgens (r)* of a penetrating x-radiation. (The radiation actually used was 1000-kv x-rays which are representative of all hard radiations, such as cobalt-60 gamma rays or the prompt or residual gamma radiation from an atomic bomb.) After the x-ray exposure, the samples were given conventional light sensitometric exposures, followed by normal processing (8 min in Kodak Developer DK-50, 68°F). The marked change in "effective contrast" of the film is readily seen in the curves of Fig. 1.

That uniform pre-exposure has a great effect on image contrast in the negative can be seen in Fig. 2. Figure 2A is a simulated aerial photographic negative made on unfogged Super-XX Panchromatic Film; Fig. 2B is the same scene photographed with the same camera setting on the film which had received an exposure of 10 roentgens of hard x-rays.

In printing, the differences between these two negatives may be minimized by the choice of paper grade, as in the printing of any fogged negative. Figure 3A is a print of the unfogged negative on contrast grade No. 1, glossy paper; Fig. 3B is a print from the fogged negative on No. 4 glossy paper. An even closer approximation to the appearance of the original (Fig. 3A) may be obtained if the camera exposure for the fogged material is increased by a factor of 2 to 4. This is not illustrated, since the effect of increasing camera exposure on the fogged negative is, in this case, so slight as not to lend itself to halftone reproduction. The improvement is apparent on the prints themselves, however.

Obviously, a level of gamma-ray exposure will eventually be reached at which compensation for the effect of pre-exposure cannot be made by using higher-contrast paper or by increasing the camera exposure. It can also be seen from the foregoing that low-contrast images will suffer more from the effects of gamma-ray exposure of the negative material than will high-contrast images.

The graininess of the silver image resulting from gamma-ray exposures is greater than that resulting from light exposures. Therefore, for most films, graininess will increase appreciably with increasing gamma-ray pre-exposure. In some applications, the increase of graininess will impose a greater restriction on the permissible gamma-ray exposure than will distortion of the characteristic curve. For instance, much higher graininess could be tolerated in photographs of oscilloscope traces or of instrument dials than in an aerial photograph in which very fine detail was desired.

The difference in graininess between Figs. 3A and 3B is difficult to illustrate in a halftone. It shows clearly in the prints, however, particularly in the portions showing the apron in front of the airplane hangar. The effects of graininess are also seen in the deterioration of small detail, such as that in the crossing gates and railroad ties.

* A roentgen (r) is the quantity of x- or gamma radiation such that the associated corpuscular emission per 0.001293 gram of air produces in air ions carrying 1 electrostatic unit of electrical charge of either sign.

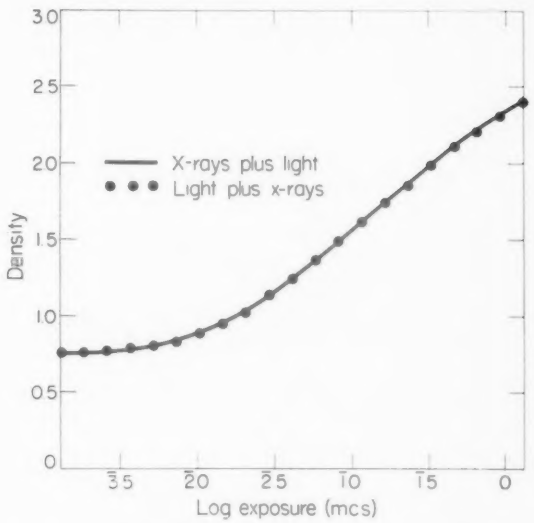

Fig. 4. Effective characteristic curve of Super-XX Film (developed 8 min in DK-50 at 68°F), exposed to 3 roentgens (r) of hard x-rays. The effective characteristic curve of gamma-ray-fogged material does not depend on the order of the exposures.

The effects of x-ray and gamma-ray exposures on conventional photographic film depend only upon the total amount of radiation, i.e., only upon the product of radiation intensity and exposure time. This holds whether or not the film receives a light exposure in addition. So far as the author is aware, no reciprocity-law failure has been reported for gamma- and x-ray exposures on commercially available films.

Further, in combined exposures, it makes no difference whether the gamma-ray exposure comes before, during, or after the light exposure. Figure 4 illustrates this fact. Kodak Super-XX Panchromatic Film was given an exposure of about 3 roentgens of hard x-rays, followed by a conventional light sensitometric exposure. The solid curve represents the effective characteristic curve obtained. The circles show the densities obtained when the x-ray exposure followed rather than preceded light exposure. The coincidence of the circles with the line indicates that the effective characteristic curves are identical.

Before considering the criteria governing the choice of a film for use in a specific application, it is well to discuss a procedure which may be time saving, and which has been used in some of the examples which follow. Although the gamma-ray sensitivity of a film cannot be predicted from a mere knowledge of its light speed, it is not always necessary, in evaluating a film, to perform sensitometric tests on a series of gamma-ray-fogged samples as was done in the preparation of Fig. 1. A reasonable estimate can be made using the characteristic curve to light and a knowledge of the density produced by the gamma-ray

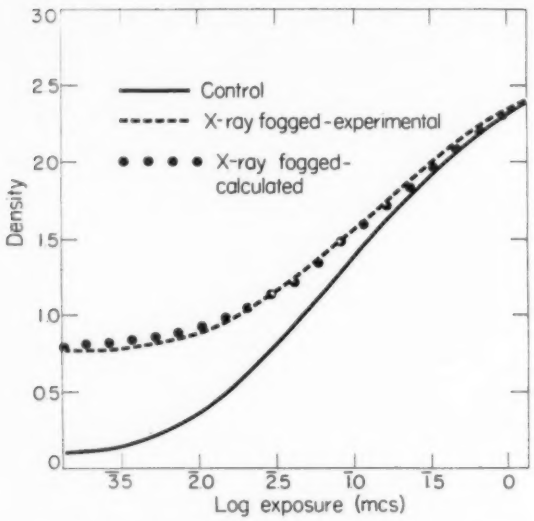

Fig. 5. Experimental and calculated effective characteristic curves of x-ray-fogged Super-XX Film.

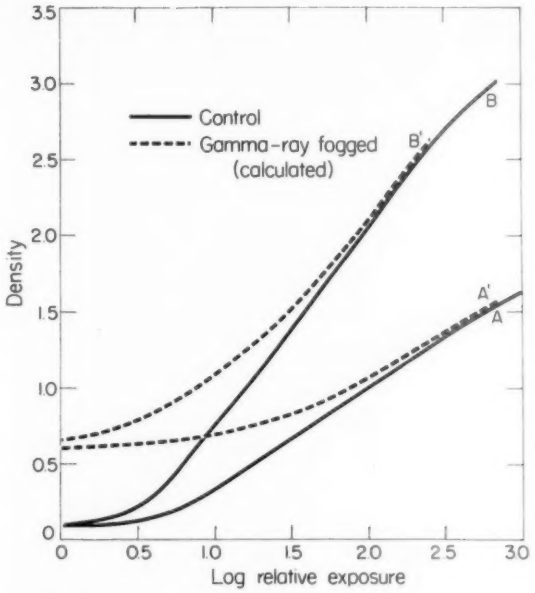

Fig. 6. Characteristic curves of two hypothetical films, having the same fractional-gradient speed and the same speed to gamma rays. Film B would give a more satisfactory record than Film A.

exposure in question.[4,5] The gamma-ray exposure is treated as if it were a light exposure, and its equivalent value (in terms of meter-candle-seconds, for example) is found from the light characteristic curve. This value is added, in succession, to the values of the light exposure given each step of the original sensitometric strip. The densities corresponding to each of these summed exposures are determined, again from the characteristic curve, and are plotted against the logarithm of the light exposure. That this gives a reasonable approximation is shown by Fig. 5. The solid line is the characteristic curve of Super-XX Film. The dotted line is the experimentally determined curve of the same material after an exposure of about 3 roentgens of hard x-rays, and the circled points are the values calculated by the procedure just described. The agreement is not perfect, but it is good enough for a fairly reliable estimate of film performance. As would be expected, the agreement between experiment and this type of calculation becomes less satisfactory as the density produced by the gamma-ray exposure increases.

We shall now turn to the question of choosing a photographic material for use in fields of penetrating radiation and examine a number of the significant film properties. Since gamma-ray sensitivity follows roughly the sensitivity to visible radiation, it is well to choose as slow a film as the limitations of light, lens, and exposure time will allow. There are high-definition aerial films, for example, which can give very acceptable records, even after having been exposed to several hundred roentgens of gamma rays. It is, of course, desirable to have a film whose light sensitivity is high compared to its gamma-ray sensitivity.

That these are not the only criteria, however, is shown by Fig. 6. Curves A and B are characteristic curves of two hypothetical films whose fractional-gradient speeds are identical. The films are also assumed to have equal gamma-ray speeds in terms of the number of roentgens required to produce a density of 0.5 above fog, i.e., the ratios of light sensitivity to gamma-ray sensitivity are the same for both films. The dotted curves are the calculated effective characteristic curves that would be obtained if each film were uniformly exposed with gamma rays so as to produce a density of 0.5 on the area unaffected by light. On the basis of curve shape alone, Film B would give a more satisfactory record on a normal grade of paper than would Film A, despite the fact that the ratios of gamma-ray to light speeds are identical.

Fundamentally, the difference between Films A and B of Fig. 6 is one of contrast, high contrast being desirable when high gamma-ray exposures may be encountered. This leads to the further conclusion that, if the increases in graininess are not prohibitive, full development should be used on films exposed to both gamma rays and light. Figure 7 shows characteristic curves of Super-XX Film developed for a series of times in Kodak Developer DK-50 (solid lines). The effective characteristic curves of the films pre-exposed to 3 roentgens of hard x-rays are dotted. As an example, note that the dotted (x-ray-fogged) curve for 5-min development matches fairly

4. G. M. Corney, *Phot. Sci. and Technique*, (II) **2**: 146 (1955).

5. M. Ehrlich, *Radiology*, **68**: 251 (1957).

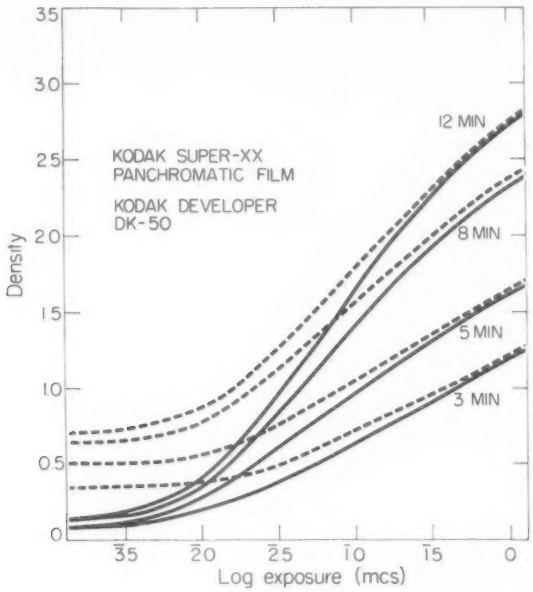

Fig. 7. Development series, Super-XX Film, in Developer DK-50 at 68°F. ——— Control; — — — — gamma-ray fogged.

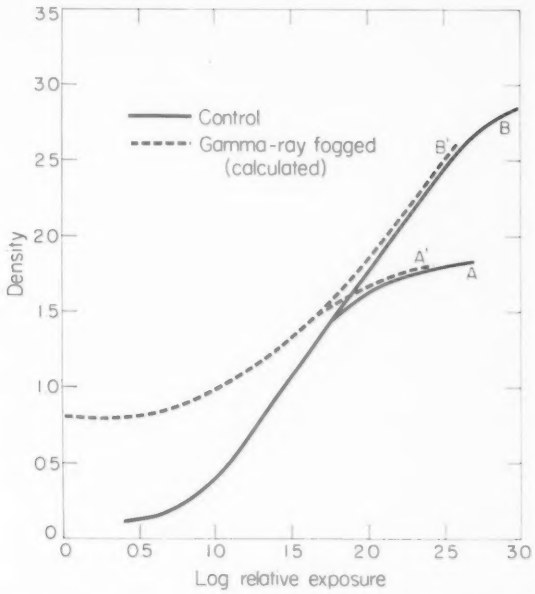

Fig. 8. Characteristic curves of two hypothetical films, differing only in the density range of high useful gradient. Film B will give the more satisfactory records in the presence of gamma or x-rays.

well in shape the solid curve for 3-min development. The 2-min additional development has compensated for an appreciable gamma-ray exposure as far as tone-reproduction quality is concerned. The fogged film developed for 5 min would show increased graininess, because of the effects of both gamma-ray exposure and the longer development time. In many applications, this increase in graininess might not be serious. That the fogged film, developed for 5 min, would take approximately twice the printing exposure as would an unfogged picture developed for 3 min is probably unimportant, considering the usual high technical importance of such records.

The third characteristic to be considered in selection of film is the maintenance of a high useful gradient over a long density range. Figure 8 shows the characteristic curves of two hypothetical films, whose x-ray and light sensitivities are assumed to be the same. Their characteristic curves are the same at the lower end, but differ in the density range of high useful gradient. The dotted line shows the calculated effective characteristic curves of the gamma-ray-fogged materials and demonstrates the advantage of a long range of high useful gradient—an advantage which would increase in importance as the gamma-ray exposure increased.

In all the foregoing, it has been assumed that the unwanted exposure was to very penetrating radiation—the gamma rays of cobalt-60, for example. However, the sensitivity of the film, in terms of the number of roentgens required to produce a given density, is strongly affected by the radiation energy or quality. If radiations less penetrating than heavily-filtered 250-kvp x-rays are encountered, the x-ray spectral sensitivity of the photographic film must be considered. The x-ray spectral sensitivity curves for all black-and-white films[4,6] show a maximum sensitivity to radiation of about 0.04 Mev (effective) and an essentially flat minimum of sensitivity extending upward in energy from 0.2 Mev (effective). Details, among them the ratio of maximum to minimum sensitivity, differ from type to type of film, however. In most cases, the softer radiations present much less of a problem than do the harder, despite the greater film sensitivity, because of the comparative ease with which the film can be shielded from the softer radiations.

Photographic films are sensitive to beta radiation (electrons) as well as to gamma and x-rays, and the photographic effects of all these radiations are quite similar. If beta radiations at least as energetic as those from strontium-90 are considered, 1 rad* of beta radiation will have the same photographic effect as 1 roentgen of energetic gamma radiation.[7] In dealing with the use of photographic materials in the presence of beta rays, it is, in general, necessary to consider only the high-energy beta radiation, since low-energy electrons are easily absorbed and hence shielding against them is easy. However, it should be noted that, wherever high-energy beta radiation is present, there will also be some exposure of the film

6. R. B. Wilsey, *Radiology*, **56:** 229 (1951).

7. E. Tochilin and R. Golden, *Nucleonics*, **11**:26 (1953).

* A rad is 100 ergs of absorbed energy per gram of absorbing material.

PHOTOGRAPHIC SCIENCE AND ENGINEERING
Volume 4, Number 5, September-October 1960

• Short Communications

Cloud Undercast Presentation for Flight Simulator Operation

W. B. KLEMPERER AND J. E. EKSTROMER, *Douglas Aircraft Co., Santa Monica, California*

The acquisition of complex skills and the measurement of these skills are greatly facilitated by simulators which reproduce situations in a realistic manner, with repeatability and precision, but without danger to personnel and equipment. Such simulators have been particularly helpful in flight training.

The Douglas Aircraft Company undertook the development of a particularly complete and sophisticated flight simulator in connection with the introduction of its new jet transport airplane, the DC-8. This flight simulator was designed and constructed to Douglas detailed specifications by Link Aviation Corp., Binghamton, N.Y. The first machine of this type was delivered to Douglas in the summer of 1958.

The simulator facility comprises several rooms and devices:

1. Several classrooms for indoctrination activities. These are equipped with models of power plants, fuel management systems, controls, and instruments.
2. A control cabin which is a faithful replica of the real aircraft cockpit, complete with all instruments and controls, radio appliances, and accessories. This cockpit does not fly; it is quasi-stationary, except for a system of hydraulic actuators which reproduce rudimentary movements in pitch and roll.
3. The computer unit, which is installed in a separate air-conditioned room and which operates on a DC analog principle.
4. The Telorama, especially devised by Douglas to provide vivid realism to the take-off and landing maneuvers where delicate control is particularly critical. An image of the landscape ahead is projected on a large screen in front of the cockpit, 15 ft from the pilot's eyes. It subtends a field of view about 45° wide and fills the windshield in front of him. The image is produced on the screen by a theater-type television projector mounted on top of the cockpit roof.
5. A television camera for providing the picture of the landscape. It is carried on a crane-way over a scale replica of a typical airport and its approach terrain.
6. A radio aids room which includes all the communications equipment required for airline operation as regulated by the FAA.

In real air traffic situations there are usually extended periods during which enough of a cloud undercast horizon or a night horizon is visible to afford visual references for keeping the aircraft on an even keel without constantly having to watch the artificial horizon instrument. In order to simulate this condition, we have developed a cloud undercast projector which makes use of a display of photographically produced panorama in a somewhat unusual manner. It simulates the real appearance of a cloud horizon with a reasonable degree of fidelity and the effect is much appreciated by the pilots when executing simulated flight work on the machine.

The cloud projector system comprises three projector units. The main unit projects the cloud scene forward of the pilot on the same screen as the Telorama. The other two provide a lateral view on separate auxiliary screens visible through the side windows. The projectors are positioned above the cockpit roof, and independently mounted on fixed structures adjacent to the television projectors.

Excerpts from a paper presented at the Annual Conference, Santa Monica, California, 9 May 1960. Received 27 April 1960.

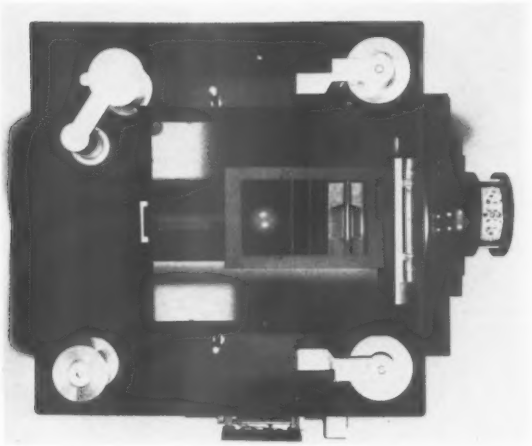

Fig. 1. Optical system.

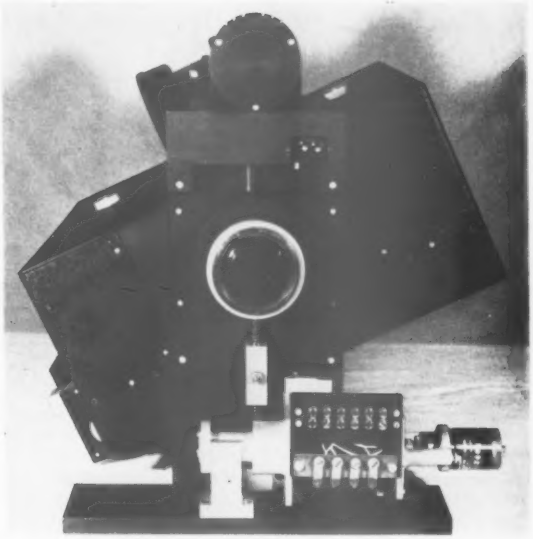

Fig. 2. Banking movement.

The main forward projector reproduces an optical illusion of pitching, banking, and course changing of the aircraft by displacing the horizon image up or down, banking it and allowing it to travel transversely, in the opposite sense whenever the computer determines attitude maneuvers of the aircraft in response to the pilot's control. An actual photograph of a typical cloud undercast scene, taken from an aircraft flying at fairly high altitude, was expanded into an around-the-horizon panorama by means of a montage with carefully blended abutments of alternating right- and left-hand prints of the original picture. This panorama was reproduced on a closed loop strip of 70mm film about 4 ft in length. The film loop is wrapped in a rectangular course around four spools (shown in Fig. 1), with a fifth idler under spring tension to keep it taut. One of the spools is driven by a servomotor at variable speed in either direction in response to the rate of turn of the aircraft as expressed by a signal furnished by the computer. The entire film spool system is mounted on a frame which can be transposed, by means of a screw-jack movement, in the direction normal to the cloud horizon under the control of a servomotor which receives its impulse from the pitch angle output signal of the computer against a potentiometer feedback. Thus the beam of light sent from a strong incandescent lamp and condenser lens system through a fixed frame gate, which does not participate in this pitch movement, remains aligned with the screen, while only the horizon appears transposed. The base structure carrying the spool jack-screw system is itself articulated with respect to the lamp housing so that it can bank laterally about an axis parallel to the optical axis of the projector (Fig. 2). This mechanism is driven by a servomotor governed by the bank angle signal output of the computer and stabilized by another potentiometer feedback. The frame gate, which is 1 by $1^1/_2$ in. in size, does not participate in this banking movement either.

It will be noted that the simulation of the cloud undercast scene is not complete. Of the 6 degrees of freedom only 3 are simulated, but this was considered sufficient for the purpose. The forward motion of the aircraft is not reproduced; in other words, the airplane never gets to the edge of the clouds. Neither is the vertical motion shown during ascent or descent. This is a deliberate omission for the sake of simplification. Lateral transposition of the aircraft with respect to the undercast is normally nonexistent.

The auxiliary lateral cloud projectors are similar in construction to the forward projector except that the up-and-down motion is governed by the bank angle instead of by pitch, and that the tilting movement of the frame, which should be governed by pitch rather than by bank, has been entirely omitted. It was deemed unimportant, since the lateral display is furnished only for the benefit of casual peripheral vision, and not as a primary control clue. The projectors were designed and built by Urban Engineering Co. of Los Angeles to Douglas specifications.

The optics of the projectors are standard 35mm motion-picture projection components. Ample cooling is provided. The electric circuitry and connectors have been designed to conform to the standards of simulator practice, so that reliability, service, and maintenance should be satisfactory.

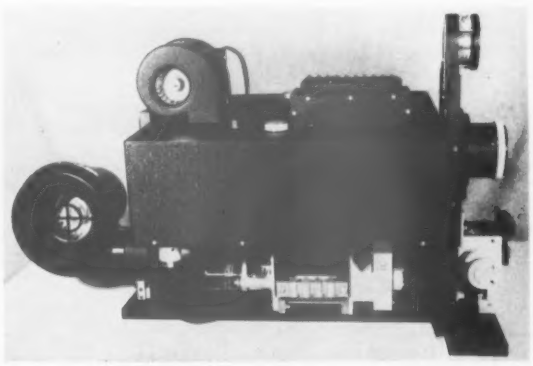

Fig. 3. Assembled projector (side view).

Processing with Saturated Paper

SEYMOUR SCHRECK, *Rapromatic, Inc., Syosset, L. I., N. Y.*

The Rapromatic saturated web processing technique was introduced about four years ago as a means of simplifying the mechanics of processing and particularly to meet the requirements imposed by the unusual conditions peculiar to airborne processing. These conditions are: (a) shock, vibration, and high acceleration forces; (b) extreme ambient temperatures; (c) reduced ambient pressures at high altitudes which cause difficulties in the transfer of solutions; (d) intolerance of solution spillage because of corrosion and electrical conductivity; and (e) limitations of size, weight, and power.

Primarily, the web processing technique utilizes a web of absorbent material containing an aqueous solution of the photographic processing materials. This system has several advantages. The volume of solution used is minimal—approximately the volume of the material to be processed. Each area of emulsion is processed with fresh solution. Undesirable by-products of the reaction are removed with the web upon its separation from the processed film. The web is adaptable to various processing formulations, e.g. monobath, arrested development, standard two-stage processing. Equipment utilizing the saturated web can be operated at any attitude as it is leakproof and independent of gravitational direction. The saturated web requires no pumps, valves, metering devices, or complex machinery.

Presented at the Annual Conference, Santa Monica, California, 11 May 1960. Received 27 April 1960; revised 11 July 1960.

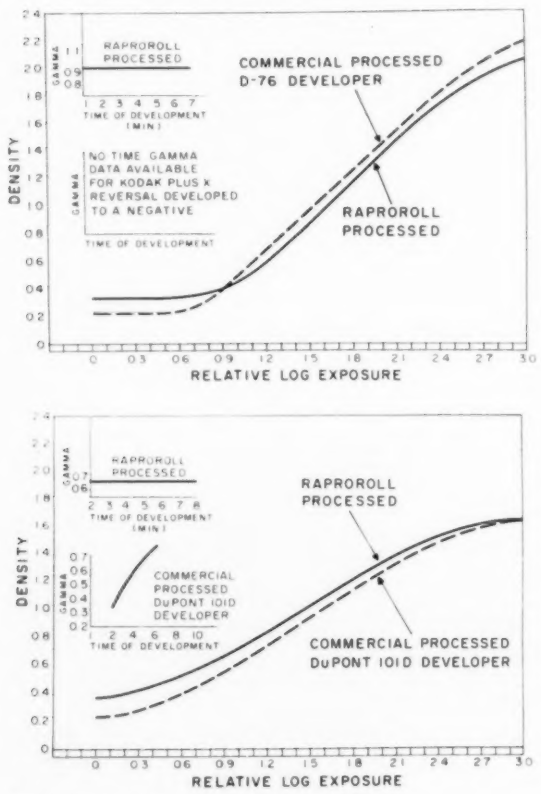

Fig. 1. Standard processing vs Raproroll processing.

Originally, the saturated web was used with relative motion between it and the material being processed, but successful application of this method was limited to recording papers. The present report deals with an investigation of a mechanically simpler and more widely applicable system in which the saturated web is maintained in intimate contact with the emulsion with no relative motion during transport. Virtually all of the work was done with monobaths on Du Pont 931 and Kodak Plus-X Reversal films.

Paper, when viewed under magnification, is seen to be composed of a random collection of fibers. When first used as a chemical carrier in the present "sandwich" technique, these fibers reproduced in the photographic image in outstandingly good detail. The fiber marks varied from dark lines to clear lines in the image, and often both types occurred simultaneously, with dark lines in the low-exposure and light lines in the high-exposure areas of the film. One cause of the fiber markings is physical—the softened gelatin records a relief image of the fiber structure of the paper. A second cause appears to be chemical. The fibers themselves are normally not absorbent, the liquid being held within the interstices. In an area of high-exposure level, the developer at the point of fiber contact would be utilized by the surrounding silver halide grains and the concentration of fixer would be high, resulting in clear lines. In areas of little or no exposure the halide solvents would be depleted and an excess of developer would remain, producing dark lines upon exposure to light. The latter conclusion was confirmed by direct transfer of the processed film to a fix solution without exposure to light. Fiber marks formed in this manner were clear.

Attempts were made to eliminate the fiber marking problem by careful chemical balancing of the processing solution, but the results were not easily controllable and this method placed undesirable limitations on formulation. The use of a thin, smooth, water-absorbing coating on the web showed promise but increased processing time because the processing solution had to diffuse through the coating. The use of thickening agents in the processing solution also showed promise but increased difficulties of handling the processed film and of remov-

Fig. 2. Comparable photographs. *Left*, commercial processing; *Right*, Raproroll processing.

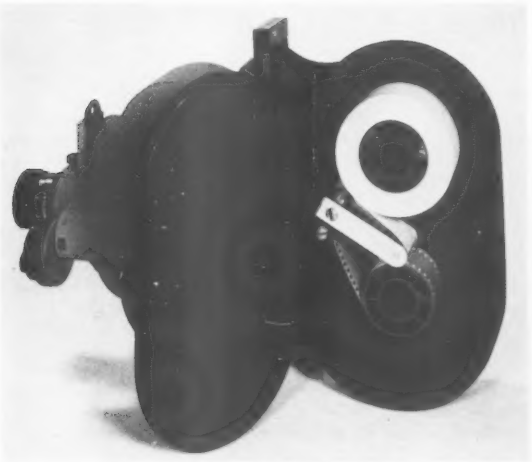

Fig. 3. 35mm Rapromatic magazine processor.

ing the reactants. Finally, a search was conducted for a paper made of fine fibers in a sheet of high porosity permitting uniform compression. A satisfactory paper was found which gave a Raproroll (the trademarked name for the saturated web roll) capable of processing film uniformly and with outstanding quality. This paper had relatively poor wet strength, however, and left fibers behind upon separation from the film. Efforts to increase the strength of the paper resulted in a material with insufficient absorptivity or one that gave mottled images, but several successful approaches to a solution of the problem have been found and others are being evaluated.

To avoid air entrapment which could lead to areas of unprocessed film, it was found necessary to add a pressure roller, thus assuring intimate contact between web and emulsion. This has to be done carefully, since excessive pressure will cause the absorbed fluid to drip.

The use of a nonabsorbent laminate backing on the web has several advantages. The plastic backing gives the Raproroll high tensile strength, decreases the chance of air entrapment, and makes the processing solution available from one side only. It also serves as an evaporation and oxidation barrier.

It is obvious that the sandwiching saturated web technique precludes agitation during processing. This appears to be more an advantage than a hindrance. In use, the fixing action is decreased with a Raproroll, while development remains unaffected, as determined by tray tests. Films processed in the magazine processor are found to have higher speeds, contrasts, and maximum densities than those processed in the identical formula in a tray, even with no agitation. It is also interesting that the fixer concentration often needs to be increased for the saturated web to clear the film completely, as opposed to the results of tray evaluations. Monobaths have the advantage of being rate insensitive as far as the transport speed is concerned. Storage within a magazine needs to go only beyond a minimum time and viewing is possible at any reasonable time thereafter.

Fig. 4. Rapromatic table-top processor.

The photographic quality of material processed with a saturated web can be as good as for material processed in any other manner under like formula limitations. The sensitometric characteristics for the two reversal materials with which we are most familiar are about the same as those given by the manufacturers for their use as negatives (Fig. 1 and Table I). Samples compared to those commercially processed have indicated an over-all subjective quality perhaps a shade better (Fig. 2).

Several pieces of equipment utilizing the Raproroll technique are, or soon will be, available. One is a 16-mm magazine processor, capable of operation at all normal frame rates (8 to 64/sec). A 35 mm magazine processor practically identical to the 16-mm unit which has performed satisfactorily at rates of 80 frames/sec (300 f/min) is also available (Fig. 3). A Rapromatic table-top processor (Fig. 4) consists of a film supply spindle, a Raproroll supply spindle, a take-up spindle, and a pressure roller. Loading and threading requires 10 sec. The unit is motor driven or may be manually operated, and the transport rate is 50 ft/min. A 4-in. CRT recorder-processor-viewer capable of giving a real time display in about 5 sec also has been produced.

Acknowledgment

I wish to thank the management of Rapromatic, Inc., for their patience during the period of this work. I also wish to thank Bell & Howell and the Traid Corp. for cooperation in furnishing us with equipment for our tests, and to express my heartiest appreciation to my co-workers, Gilbert L. Haines, John V. Baccoli, and Alan Miller, for their extensive contributions and cooperation.

TABLE I. Standard Processing vs Raproroll Processing of Du Pont 931-A and Kodak Plus-X Reversal Films

Film	Processing	*D* max	*D* min	Base	Fog	*D*	Gamma	Time, min	Temp, deg F
931-A	Du Pont 101D	1.65	0.22	0.22	0.00	1.43	0.65	5	68
	Raproroll	1.63	0.37	0.22	0.15	1.26	0.65	2	70
Plus X	Kodak D-76	2.20	0.22	0.22	0.00	1.98	0.95	6	70
	Raproroll	2.02	0.33	0.22	0.11	1.69	0.96	1	70

Color Photography at 400,000 Frames per Second

WINSTON O. S. JOHNSON, *Mechanical Development Laboratory, E. I. du Pont de Nemours & Co., Wilmington, Delaware*

For many years, the Du Pont Company has used high-speed photography, both as a trouble-shooting tool to determine the causes of faulty operation in plant equipment and as a research tool to aid in gaining an understanding of rapid processes. A Fastax high-speed camera, capable of framing rates up to 10,000 frames/sec, has been used for this work and has provided much valuable information on mechanical and chemical processes. However, for the study of some phenomena, the Fastax, even at its top speed, is too slow. Critical events occurring during an interval of 100 μsec or less are either seen in a single frame at some indeterminate point in the event cycle or are completely missed by the camera.

Since many such events are of considerable commercial interest to Du Pont, a study was made to determine what commercially available cameras would operate above 10,000 frames/sec. Although several research organizations were found to have such cameras, each camera had been developed as a special-purpose research tool by the persons using it. Since nothing was found that would in any way qualify as a general-purpose ultrahigh-speed camera, we attempted, through consultation with many of these organizations, to establish requirements for such a camera and to develop the arrangement of optical and mechanical elements that would best satisfy our requirements.

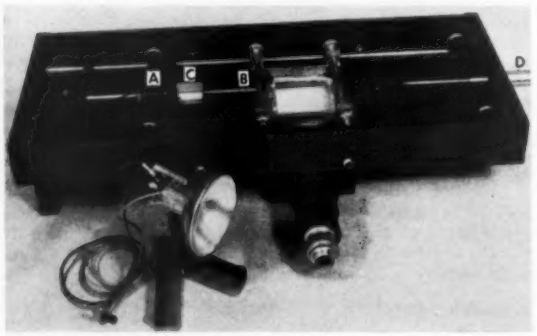

Fig. 1. Lenticular-plate camera. A = spring; B = armature; C = solenoid; D = dash pot.

Du Pont Lenticular-Plate Camera

Optical Arrangement. In our camera, which employs the image dissection lenticular-plate system,[1] the lens, the lens aperture, and the lenticular plates are stationary, and the photographic plate is carried, face down, in a sled traveling on precision rails across the image plane. Figure 1 shows the camera with its lighttight cover removed. A diagram of the optical elements of the camera, Fig. 2, indicates the relative positions of the various components. The scan angle chosen was $5^{3}/_{4}°$, providing a skew ratio of 10 : 1 and was set by rotating the disk carrying the lenticular plates.

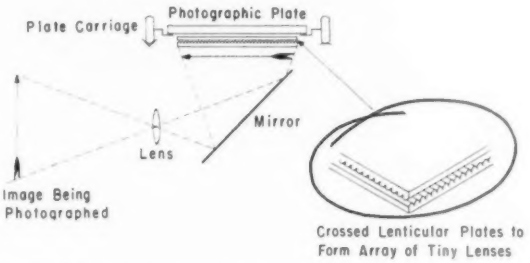

Fig. 2. Schematic diagram of lenticular-plate camera.

Traversing Mechanism. The design of the drive mechanism of the camera was adapted from a Remington Arms Co. line-grid camera. A reaction carriage is mounted on the same rails as the plate-carrying sled and contains the entire acceleration and deceleration apparatus. With the photographic plate in place, the tension spring, A (Fig. 1), is cocked by manually forcing the sled and reaction frame together so that the sled-mounted armature, B, locks home in the solenoid, C, which is part of the reaction frame. This specially modified solenoid holds the 20-lb spring force until released. On release, the sled, carrying its photographic plate, is accelerated to a 100-in./sec velocity by the spring. It travels to a position directly over the lenticular plates, where its passage over a magnetic pickup triggers a special light source or, for self-illuminating subjects, a guillotine-type capping shutter, then continues at no decrease in velocity along its path until it is caught and brought to a stop by the dashpot, D. Since drive spring, dashpot, and solenoid are all integral parts of the 10-lb reaction carriage, all forces applied to accelerate the sled also accelerate the reaction carriage, causing it to move in the opposite direction and to stop moving at the instant the sled is brought to a halt. Thus, no force is transmitted to the body of the camera. The sled weighs 2.5 lb; therefore, it travels four times as fast as and far as the reaction carriage. Its velocity in "free flight" along the rails is remarkably constant. Measurement of a 1000-cps oscilloscope pattern photographed by the camera showed less than 1% velocity variation in 4 in. of travel.

Prevention of Re-Exposure. With the one-in-ten skew angle, re-exposure of the entire photographic plate will occur for each $^{10}/_{64}$ in. (0.156 in.) of travel, which corresponds to an over-all exposure interval of 1.56 msec, during which new, virgin areas of emulsion are exposed in an exact, reproducible sequence. In order to prevent light from fogging the photographic plate or producing doubly exposed areas, some type of capping shutter is

Part of a paper presented at the National Conference, Chicago, 26 October 1959. Received 6 November 1959.

1. Cf. J. S. Courtney-Pratt, "Image Dissection in High-Speed Photography," *Phot. Korr.*, Sonderheft No. 2, Verlag Dr. Othmar Helwich, Darmstadt and Vienna, 1958, for a review (in English) of the image dissection method.

necessary so that light can expose the plate only during this interval. The shuttering, lighting, and control equipment will be described in another part of this paper.

Playback of Motion Sequence. Once a plate has been exposed and developed, it is played back, either for viewing or for transcription onto 16mm film as a normal movie sequence, by placing it again in the translating sled in exact registry and advancing it slowly across the lenticular plates, using an exact duplication of the optical system set up when the sequence was exposed. An intensely illuminated field replaces the subject. The sequential images are viewed from above. A Telechron motor drive translates the plate-carrying sled continuously at 0.01 in./sec for viewing at a time magnification of 10,000×. A stepping relay drive has been developed which moves the plate in discrete 0.0005- and 0.00025-in. steps for photographic transcription at 200,000 and 400,000 frames/sec. An Eastman Kodak Cine-Special camera has been adapted and special circuitry developed so that automatic transcription at several frame rates can be accomplished. Because this camera—like all image-dissector cameras—depends for its image quality on the ability of the eye to construct, from relatively incomplete clues, a better mental image of a moving subject than actually exists in the frames that make up the image, the quality of the directly viewed image is always superior to the picture sequence transcribed on 16mm film.

Associated Lighting and Control Circuitry. As was mentioned earlier, a system is required for illuminating the camera's subject for a period not longer than 1.56 msec, before and after which interval no light can be permitted to reach the photographic plate. We have developed an electronic flash-lamp circuit and pulse-forming energy-storage network that provide intense uniform illumination in the form of a square light pulse lasting 1.3 msec with a rise time of 20 μsec and a quench time only slightly longer.

A 1-msec guillotine shutter has been developed so that the camera can be used in studying continuously luminous subjects such as arcs, lamp filaments, combustion processes, etc. This shutter is driven by a thyratron trigger circuit and opens and closes a $^1/_4$-in.-diameter aperture within 1.2 msec. With this shutter and a $^1/_{16}$-in.-diameter lens, a trapezoidal-exposure-vs-time characteristic can be obtained that has a rise-and-fall time of approximately 50 μsec.

An over-all control and power-supply console has been developed which provides precise microsecond delay and triggering of: (1) the square-pulse light source or the guillotine shutter, and (2) any electronically controllable event. In studying the action of electric blasting caps, it was possible to control the timing of both the event and the lighting so that any portion of the event could be studied.

Color Photography. In many studies, the use of color is of considerable value in adding to our understanding of the observed phenomena. The technique developed for fabricating color plates is relatively simple and consists of applying a suitable, optically clear contact adhesive to a carefully washed glass plate and to the back of a 4- by 5-in. sheet of color film, allowing the adhesive to cure only partially and bonding the two prepared surfaces. A simple registering fixture is used; extreme care must be taken to avoid trapping air between the glass and the film. This entire assembly procedure must be carried on in complete darkness and in a dust-free atmosphere, as any dust speck on either adhesive surface causes air entrapment. These "color plates" are exposed, developed and viewed or played back in normal fashion. The unique optical properties of the lenticular-plate system make it entirely practical to take ultrahigh-speed color sequences of either self-luminous or illuminated subjects.

Applications. The camera has been used in studying a number of extremely rapid phenomena, including the fracture of safety glass and plastic materials under impact, the motions of various components of plasma in an arc stream, the action of blasting caps, and the motion of liquid droplets and solid particles in sonic and subsonic air streams.

PHOTOGRAPHIC SCIENCE AND ENGINEERING
Volume 4, Number 5, September-October 1960

• Discussion and Evaluation

A Reappraisal of Additive Color Photography

LIONEL H. WHEELER, *Colorvision, Inc., Los Angeles, California*

It might, at first, appear that the subject of additive color photography has been so fully investigated that there could be little merit in further attempts to develop a method of applying the principle to motion-picture or still photography. A number of people have tried to use the additive method for motion pictures, and books on the subject by Wall,[1] Friedman,[2] and Cornwell-Clyne[3] closely examine these various systems in great detail. However, these authoritative volumes were published in 1925, 1944, and 1951, respectively. Since then, great technological advances have been made in all branches of science, including optics and photography. Therefore, the subject of additive color photography should be re-examined in the light of comparatively recent technical developments, in order to confirm or disprove the objections which, quite rightly, have been made in the past.

First, a review of the difference between "additive" and "subtractive" color might be advantageous. Subtractive color, as the name implies, involves the "subtracting" or removal from white light of the unwanted part or parts of the spectrum. Cyan, magenta, and yellow dyes, being "minus" colors, will each subtract one of the primary colors of red, green, or blue from the white light source in the projector. If any two of the dyes are superimposed, two of the primary colors are subtracted, leaving only the third primary to be transmitted by the combination. If all three dyes are superimposed, complete opacity results, all three primaries having been subtracted from the single white light source.

In additive projection, separate projection systems of red, green, and blue are added together to form white light. Any two of these primaries projected together will produce one of the complementary colors. Thus red and green will produce yellow, red and blue will produce magenta, green and blue will produce cyan. The addition of all three in the right proportions produces white light. Variation in the relative amounts of each primary contributed by the separate projectors will result in a range of all possible hues (but not necessarily all levels of saturation and brightness) in the visible spectrum.

In the additive system of photography and projection, this variation is provided by the density differences which occur in the black-and-white negative and print if color separations have been recorded. If each separation is projected through a separate lens system with appropriate color filter, the superimposition of all three will provide an accurate color reproduction of the original subject.

Here is a method of color photography which provides excellent color, and furthermore does it on black-and-white film. This would appear to be a very attractive combination: black-and-white negative and print with a cost advantage, simple processing—also with a cost advantage, no storage problems, no fading problems, no color timing problems, ability to vary contrast, and many other advantages.

Just over a hundred years ago, in 1859, Maxwell first demonstrated additive color, and yet no one is using the additive system for motion-picture photography. Apparently the foregoing advantages were offset in the past by other considerations.

Of the many patents granted for beamsplitting color separation optical systems, all but three relied on neutral splitting, supplemented by color filters in each path to absorb the unwanted parts of the spectrum; thus were the required red, green, and blue separations provided. It is worth while to study the efficiency of such a system with regard to the amount of light arriving at the film plane.

Let us imagine a system in which occur no losses of light due to such considerations as high *f*-number, reflection at various glass surfaces, etc. To decide what proportions of the initial light are needed in each path to achieve a balanced exposure on each record, the factors of the color filters to be used must be considered. Taking the Wratten 47B, 58, and 25 color filters as typical, we find that, for tungsten light, the factors are 16, 8, and 6 respectively; the light then must be split in these proportions. The blue path, with its blue filter factor of 16, thus requires approximately 53% of the incoming white light, the remaining 47% being split in the proportions of 20% to the red path, and 27% to the green. If we now divide these percentages by the appropriate filter factors, we find that the maximum percentage of the original energy arriving at each film plane is only 3.3%! This, remember, is ignoring all other losses which must occur. Such a system would demand an increase of exposure over black-and-white photography of at least 30 times. With the present Plus-X or Du Pont Superior 2, approximately 2500 ft-c would be required at *f* 2.0. With the slower film speeds available at the time most of these patents were applied for, at least 5000 ft-c would have been needed for interiors.

It is surprising that many systems of this type were enthusiastically developed at great expense, when five minutes of simple arithmetic show that such a project is not worth pursuing!

Dichroic Mirrors and Additive Color

I have referred to three exceptions to this light-wasting method. One of these was the Technicolor 3-strip beamsplitting camera; another is the more recent development of the Sachtleben optical system, the patents of which were acquired by RCA for use in their color television camera; the third is the Colorvision camera unit.

In each of these systems, the commercial development

Presented at the Annual Conference, Santa Monica, California, 11 May 1960. Received 14 April 1960; revised 29 July 1960.

1. E. J. Wall, *The History of Three-Color Photography*, American Photographic Pub. Co., Boston, Mass., 1925.
2. Joseph S. Friedman, *History of Color Photography*, American Photographic Pub. Co., Boston, Mass., 1944.
3. Adrian Cornwell-Clyne, *Colour Cinematography*, Chapman and Hall, Ltd., London, England, 1951.

of the dichroic coated mirror created the beamsplitting means by which these optical systems were able to escape from the previously inescapable conclusion that a maximum of only 3.3% of the original energy could arrive at each film plane.

Dichroic mirrors consist of glass with a number of evaporated metallic coatings. They have the unique property of being able to reflect selectively a chosen wavelength band of the spectrum while allowing the remaining wavelengths to be transmitted. Furthermore, they do this with an efficiency of approximately 95%.

The Technicolor camera, it may be recalled, used this principle to reflect magenta to the red and blue bi-pack, the green being transmitted for the third separation. This arrangement took partial advantage of the improved efficiency, but by the use of dichroics the red, green, and blue bands of the spectrum may be diverted into separated paths with a theoretical 31% of the total energy arriving at each separation image. In practice, however, a certain amount of trimming of unwanted information must be provided. These trimmers may also be dichroic and in the order of 90% efficient. Thus approximately 28% of the original energy is going to provide the exposure for each image, and approximately $3^1/_2$ times more light is required than if the same film stock were used for normal black-and-white. This, remember, must be compared with the figure of 30 times more required light on a system not using dichroics.

The efficiency of dichroic mirrors should not cause one to expect that, with an efficient beamsplitter, the original black-and-white speed of the negative will be retained. This can never be so. It is apparent that, in an ordinary black-and-white exposure on panchromatic negative, energy from the entire visible spectrum is being used. Even if perfect splitting of red, green, and blue were possible, each band would have only approximately $^1/_3$ of the total energy contained in white light. Each of these thirds is now required to provide a full exposure on the negative. Thus even theoretical perfection would reduce the effective negative speed to $^1/_3$ of its original rated value.

Parallax

Many additive taking systems for motion-picture photography attempted to circumvent the inefficiency of the nondichroic beamsplitter by the deliberate introduction of parallax, either spatial or time. Those systems using an optical system with spatial parallax avoided the splitting of the white light three ways by photographing the red, green, and blue separations from three points of view; thus the speed of the system would be dictated by the highest factored filter. With a blue filter factor of 16, the system still required 16 times the illumination, and a register problem arose that was impossible to solve. Obviously, register could only be achieved in the plane of convergence. Detail behind and in front of this plane could never be made to register.

Those who avoided beamsplitting by introducing time parallax attempted to use a field sequential system which would also have the light requirement of 16 times the illumination. This consisted of a three-bladed shutter in front of the camera, the open segments of which contained the red, green, and blue color filters. The shutter was timed to $^1/_3$ of the frame rate so that red, green, and blue separations were photographed rapidly, one after another, in a three-frame family as the action progressed. A similar device on the projector reproduced each frame through the appropriate filter to reproduce the original color. This proved to be an excellent way of taking still pictures with a motion-picture camera but created an interesting effect if anything, the camera included, ever moved.

Such a system was capable of excellent color, as is indicated by the fact that Technicolor has used this photographic method for animation for many years. They do not, of course, project sequentially, but, by means of skip-frame printing, extract separate matrices for subsequent prints by the imbibition process.

It is obvious then that an operational additive color system must have no parallax; the color separations must be photographed through a single lens at precisely the same time. It would appear at first glance that a single lens, with a dichroic beamsplitter behind it, must provide the solution. On examination, however, this creates a further problem. In order to place these separation images adjacent to each other at a single film plane, it would be necessary to provide some folding, periscope fashion, for each light path. Thus, for the image transmitted by both dichroics, four additional mirrors must be provided if the light-path lengths are to remain identical. We now, therefore, would have to accommodate six mirrors between the lens and the film plane. This situation would demand the use of lenses with a long back focal distance, a minimum of 4 or 5 in. Such a system also places restriction on the f value, as the smaller the f-number the larger the mirrors must be, thus necessitating an even longer focal length to provide sufficient back focal distance.

Yet some systems have been patented and developed regardless of the fact that they could neither provide a wide-angle lens, or even present the opportunity to change focal lengths, and, not using dichroics, were only able to shoot at a daylight level of illumination.

The Relay System

We have defined, to a great extent negatively, what is essential in a beamsplitting optical system for motion-picture use.

First, it must utilize dichroics in order to avoid an excessive light-level requirement.

Second, it must be parallax free, taking the three separation records from the same point of view and at precisely the same time.

Third, it must not rely on the long back focal distance of the objective lens, and must preferably have means of avoiding both lateral color effects and a difference of sharpness in the color separated images due to chromatic aberration.

Fourth, the optical system must have a reasonably low f-number.

Fifth, there must be a means of changing the focal length of the objective lens, thus making the system flexible enough to use commercially.

Strangely enough, the solution to the last three of these problems lay in a device which has been in use for years, and yet the optical principle was never formerly applied to separation photography. The device was the submarine periscope, in which a wide-angle field of view is available at the end of an extremely long tube. This is accomplished by what is known as a "relay" system, and it is interesting to note that, in addition to the Colorvision optical system, the Sachtleben beamsplitter for color television cameras also makes use of this principle.

The Colorvision optical system has provision for separate focussing for each color and adjustment of each light-path length, making it possible to avoid completely the effects of both longitudinal and lateral chromatic aberration and thus to achieve equal sharpness and identical size in the red, green, and blue images. Incidentally, this ideal relationship between size and sharpness, regardless of color, is not possible on a subtractive color negative or reversal color stock.

In addition, with such an optical system each red, green, or blue light path, although separated, is precisely on the true optical axis; thus no spatial parallax can be present.

Not the least of the advantages accruing from the use of a relay system is the ability to change the focal length of the objective lens.

There are three other technical developments which, although not contributed by the additive system itself, make possible the operational efficiency of such a system.

Film Shrinkage

The first is the general change-over in the last decade from a nitrate base as a support for motion picture emulsions to the now universally used low-shrinkage materials such as acetate. The nitrate base had the unfortunate characteristic of being subject to excessive shrinkage, so much so that the printing of an old, long-stored, nitrate negative, perhaps to obtain a duplicate, often required the use of a specially adjusted pull-down mechanism or sprockets which conformed to the greatly reduced pitch of the perforations. For an additive system, this shrinkage in both negative and positive created a hopeless situation with regard to register. Many additive protagonists in the past have claimed that, because the three images are on one frame, all three images shrink at the same rate and that this therefore cancels out any adverse effects. It will be quickly realized, however, that register requires a precise dimensional relationship to be maintained between the *centers* of the images. Any change in these dimensions necessitates a complete reregister. The use of nitrate base would have made a standardized register on cameras, printers, and projectors impossible; the stability of acetate, and its general adoption, solved one of the biggest problems in the additive system.

Additive Projection

Strangely enough, the development of subtractive color processes provided a solution to another additive problem. This problem is concerned with projection and is encountered if it is necessary to use standard commercial projection equipment. If the figures for light losses described earlier in relation to a "taking" system of neutral mirrors and absorption filters are applied to projection, we find that this 3 or 4% efficiency makes it impossible to project additively to any normal-sized screen. Even with typical high-intensity arc projection, if a picture of adequate brightness is to be provided, a screen width of about 6 ft is all that can be achieved. But normal-sized screen projection with standard equipment lies in the ability to make a subtractive color print from the separation negative.

If one is not confined to standard equipment, it is possible to design a dichroic beamsplitting illumination optical system which is not subject to the losses encountered with absorption filters, and which makes a large screen additive display entirely feasible. Colorvision has designed and built such equipment for use by one of the Armed Forces.

It is obvious that in the entertainment field use must be made of projection equipment already installed. How, then, can additive projection, with its superior color from black-and-white film, but with its light losses, be viewed by a large audience. Fortunately, another apparently nonrelated development solves this problem.

During the past few years, color television has been developed to a commercial and fully operational medium. An essential part of the color television equipment is a device which provides the means by which color film may be integrated with the general color programming. Known as a three-vidicon film camera, this piece of equipment is a dichroic beamsplitter (also, incidentally, a relay optical system), which separates the red, green, and blue information from the projected color film, and channels this separated information to three separate vidicon cameras. It requires that an aerial image be formed in a manner very similar in principle to the Colorvision optical system. This aerial image is approximately $3^1/_2$ by $4^1/_2$ in. and the size of the image provides commercially possible additive projection. In spite of the light losses, we are able to project additively into such a system while staying within the normal light range available.

A vital point in favor of additive projection for color television film lies in this operation. The additive projection method delivers information in terms of red, green, and blue, exactly the information required by color television itself. By the use of comparatively narrow band color filters, this information can arrive without contamination at its appropriate vidicon.

Applications

There are certain areas in which subtractive color can offer advantages over additive, including the availability of faster film speeds, larger negative area, and the shooting conveniences of lighter equipment.

There are, however, other fields in which the use of the additive system can solve problems which cannot, at present, be solved by the use of a subtractive process. In these other fields, I suggest that the additive system be considered as an additional tool in the hands of the various industrial photographic departments, and not regarded as a development which attempts to replace all present color techniques.

There is a demand in certain areas of research and display for photographic methods which will deliver a black-and-white result within a few minutes of photography. The Fairchild Camera Corp., for example, has produced excellent equipment by which black-and-white film can be processed and screened almost immediately after photography.

No new invention is required to arrive at an integrated unit consisting of an additive taking system, high-speed reversal processing equipment, and motion-picture projector, capable of almost immediate screening in color.

In such a unit the film would travel continuously through the camera, into the processing, and then into the projector. Furthermore, in an emergency this equipment could work as an independent unit in the field, under fairly rugged conditions, without recourse to a permanently installed, and possibly bomb-damaged, color processing plant.

For instrumentation purposes, the additive system also offers the means of providing simultaneous information in different bands of the spectrum which need not necessarily be red, green, and blue. It would be quite possible, for example, to use infrared film to provide a blue record from the visible spectrum and simultaneously to photograph two different bands of infrared. The information in these spectrally separated bands on each record would, of course, be automatically coincident in time. It would be projected without superimposition, making possible simultaneous observation of phenomena occurring in each record.

I have touched on only two applications in which the additive system would provide a solution to data-obtaining or data-display problems. If there are other color photographic problems in industry which have escaped solution, I sincerely hope that this reappraisal of the additive system may in some cases provide the key.

• Book and Journal Reviews

The Study of Elementary Particles by the Photographic Method

An Account of the Principal Techniques and Discoveries Illustrated by an Atlas of Photomicrographs

C. F. Powell, P. H. Fowler, and D. H. Perkins, Pergamon Press, New York, 1959, *xvi* + 669 pp., 8¼ by 11½ in., $40.00

The history of the action of high-energy radiation and elementary particles on the photographic plate might have started in 1867. In that year, Niépce de St. Victor observed the fogging action of uranium salts on the photographic layer, but he attributed the effect to the luminescence of the uranium salt and thereby missed the discovery of radioactivity which Becquerel made in 1896 as a result of a similar observation. In 1910, Kinoshita showed that alpha-particles fogged photographic emulsions, and in the following year Reinganum recognized tracks produced by the individual alpha-particles. The emulsions of that day, however, were designed to record the action of light and, although various investigators used them as a means of recording nuclear particles, their usefulness for this purpose was limited. In 1935, partially successful attempts were made to produce emulsions with improved properties which were specially adapted to the recording of tracks, but Taylor, after a careful examination of the precision which could be obtained, concluded that "it is impossible to deduce with any accuracy the energy of individual protons from a measure of the range in the emulsion." Although further improvements were made in the photographic method by 1945, it had not gained very wide acceptance by physicists engaged in nuclear research, and the ionization chamber, the Geiger-Mueller counter, and the Wilson cloud chamber techniques were used almost exclusively for quantitative measurements.

The introduction of the concentrated emulsion in 1945 brought about a rapid change in the attitude of nuclear physicists towards the usefulness of the photographic method of recording ionizing particles, and the discovery of the π-meson in 1947 from an examination of plates which had been exposed at high altitudes led to a general recognition of the value of the method. Professor C. F. Powell and his associates at the University of Bristol played an important role in the development of the nuclear-emulsion technique as a quantitative tool for the study of nuclear processes—a role recognized by the award to him of a Nobel Prize in physics. His rich store of experience, extending over the whole of the period from the introduction of the nuclear track emulsions to the present time, is amply evident in *The Study of Elementary Particles by the Photographic Method*. The book gives a highly interesting account of the photographic technique and its influence on an exciting period in the history of physics.

The book opens with a section on the history of the method and the theory of the formation of the latent image. The preparation and processing of the concentrated emulsions are described briefly. There follows a section on the basic technical features of nuclear emulsions, in which the physical characteristics and chemical composition are given, the mechanism of track formation is discussed, and methods of examination of the plates, "loading" the emulsions, preparation of sandwich emulsions, and use of stripped emulsions are described. The care needed in the handling of the plates and the various pitfalls that may be encountered in their use are pointed out. About half the book deals with the discovery and properties of specific elementary particles and their action on nuclear emulsions. The final sections deal with track production by elementary particles of high energies and by heavy nuclei of cosmic origin. Useful summary tables on the properties of the elementary particles are included.

Both the student and the research worker should find this volume useful. The price may discourage many potential purchasers, but it does not seem unreasonable for a book of this size and excellence of production. The book is lavishly illustrated with well-prepared graphs and numerous photomicrographs, some of the latter published for the first time. As noted in the preface, the book does not cover all phenomena that have been studied with nuclear emulsions. In particular, track radiography, with its medical and geological applications, is not included, and much of the earlier work in nuclear physics, already treated adequately in the literature, has been omitted. Some minor flaws may be noted. The treatment of latent-image formation is sketchy and lacking somewhat in clarity, and the choice of literature references to this subject could be improved. Apart from references to Mitchell's papers, the most recent paper referred to on latent-image formation was published in 1947, and even the reference to Mees, *The Theory of the Photographic Process*, is to the first (1942) rather than the revised (1954) edition. (On pages 42–43, the date is given as 1946). A few inconsistencies and inaccuracies in other journal and book references were noted, but the literature coverage is extensive for most of the subjects. The flaws are minor, and do not detract seriously from the general excellence of the book. — *T. H. James*

Zhurnal Nauchnoĭ i Prikladnoĭ Fotografii i Kinematografii

Vol. 5, No. 1, January-February 1960 (in Russian)

Résumés by S. C. Goddard

A Study of the Influence of Photographic Intensifiers on Detail Rendering

E. U. Braĭchevskaya, pp. 7–9

Photographic plates were exposed in a Hurter and Driffield sensitometer, turned through 90°, and re-exposed in the same sensitometer with a grid of lines superimposed, the second exposure being one tenth of the first. From the negative so obtained, a curve was constructed showing the just-visible detail plotted against log exposure. A similar curve was obtained for a print made from the same negative. The negative was intensified and curves showing detail against log exposure were once more plotted. This was carried out for a number of intensifying agents. It was concluded that detail

rendering is not improved by intensification of normal negatives, but only gives an improvement for negatives which have been considerably underexposed.

Studies in the Processes of Aging and Stabilization of Photographic Material. III. Physicochemical Mechanism of Anomalous Aging

V. I. SHEBERSTOV, pp. 10–14

Two mechanisms are considered in explanation of the anomalous aging of photographic materials described in two earlier publications (V. I. Sheberstov: *Zhur. Nauch. i Priklad. Fotografii i Kinematografii*, 4:100, 241 (1959)). The first mechanism, the adsorption of bromide ions onto sensitivity centers, thereby reducing their activity, is not excluded but is thought to be comparatively unimportant compared with the oxidation of the centers, which are assumed to be of silver, by atmospheric oxygen, possibly with the intervention of heavy-metal ions as catalysts or of peroxides of sensitizing dyes. Evidence for the oxidation theory is collected from the literature.

Studies on the Ability of Photographic Materials to Reproduce Small Elements of an Optical Image. III. The Influence of the Conditions of Positive Printing on Reproduction of Two-Dimensional Objects

YU. K. VIFANSKIĬ, YU. N. GOROKHOVSKIĬ, AND N. D. KHRUL'KOVA, pp. 15–19

The correctness of the photographic reproduction of small two-dimensional elements of an optical image as a result of a two-stage photographic process is characterized as satisfactorily by the magnitude of the resolving power in the positive image as it is when only the negative stage of the process is carried out, the resolving power of the negative material then serving the same purpose. (*Translation of author's abstract*)

Influence of the Concentration of Developing Agents on Rapid Development. I. Properties of Metol Developer

P. I. LEVINA AND V. A. VEĬNDENBAKH, pp. 20–27

Earlier workers have found a straight-line relation between the optical density of a developed negative and the log concentration of the developing agent. This relation has now been studied in the case of a highly alkaline (sodium hydroxide) Metol developer used for high-speed black-and-white development. All the work was carried out with a fine-grain positive film, developed in the developer at 20°C, the pH being kept constant at 13.6 to 13.7, determined by a lithium glass electrode.

The plot of density against log concentration was not a straight line in this case, but was broken into three straight-line portions. The first part shows a slow rise of density, the next a more rapid rise, and the final portion is horizontal. Fog is independent of concentration up to a certain concentration, which depends on the length of the development, and then increases.

Potassium bromide has no influence on the density over a wide range of concentration. Its only effect is observed in some cases of prolonged development (80 and 120 sec) and with large concentrations of bromide (0.04 to 0.08 *M*). Fog, however, is affected by the bromide concentration, decreasing as the bromide is increased.

The reasons why the electrochemical theory of development is inadequate to explain all the details of high-speed development in highly alkaline developers are discussed.

A New Criterion for the Quality of Photographic Papers

M. I. SHOR, B. G. VOL, AND G. A. ZARANKINA, pp. 28–33

The criterion used as a measure of the latitude of photographic papers is obtained by printing step-wedges onto the sample of paper, developing them for different times in a standard developer, and plotting the sensitometric curves. Over a certain range, the curves will not differ in form but will be only laterally displaced: the two extreme curves of this form are taken and the difference between their log speeds ($\Delta \log S$) forms the criterion.

The values of $\Delta \log S$ have been obtained for a number of Soviet-produced papers. Several factors studied had no influence on $\Delta \log S$, including the content of stabilizers in the emulsion, the concentration of silver per unit area, and the original silver iodide content of the emulsion. The type of gelatin, however, showed a marked effect on $\Delta \log S$, apparently associated with the rate at which maximum sensitivity is reached during digestion in the given gelatin; $\Delta \log S$ is also influenced by the pBr of the emulsion and the conditions existing during ripening and digestion. When the pBr is lowered, $\Delta \log S$ also decreases. The more intense the conditions of ripening and digestion, due either to raised temperature or increased duration of the process, the larger will be the $\Delta \log S$. Hardening of the emulsion lowers $\Delta \log S$.

As far as development is concerned, $\Delta \log S$ is apparently not influenced by the nature of the developing agent but is significantly affected by the temperature of development, increasing as the temperature is increased.

Action of Slow Electrons on Photographic Emulsion. I. Quantitative Rules of Formation of the Latent-Image by the Action of Electrons with Energies of Less than 40 Electron Volts

V. V. KRYACHKO, pp. 34–38

It was found that 2X, Agfa Laue, and Agfa Texo x-ray films were sensitive to electrons with energies of 2 to 40 ev. The most sensitive of these films to electrons with energies of 2 to 20 ev was Agfa Laue.

For these films, the relationship between the density and the energy of electrons in the range 2 to 40 ev is shown. It is shown that the density has a minimum at 12 to 20 ev. On development in a "subsurface" developer, the relation between density and time of radiation, when the energy of electrons is constant and equal to 4 ev, shows a minimum or point of inflection, while with development in a "surface" developer, the density changes according to an exponential law.

The theoretical interpretation of the results obtained needs further experimental work which will be carried out.

The Problem of the Effect of Volatile Products of Tissue Disintegration on the Photographic Emulsion

M. B. RAZUMOVICH, pp. 39–43

Animal tissues give off volatile products capable of reducing the silver bromide of a photographic emulsion. A similar reducing effect is shown by extracts of these substances. The substances liberated appear to have a protistocidal action and are probably a defense mechanism of the wounded tissue.

The Accuracy of Measurements Carried Out by the Methods of High-Speed Cinematography

E. A. TARANTOV, pp. 44–47

A mathematical analysis is made of the accuracy of measurement of the speed of a moving body by two methods of high-speed cinematography: by scanning and by framewise exposure.

Some Methods of Synchronization in High-Speed Cinematography (from Experimental Work with the FP-22 Camera)

S. R. ZHUKOVSKIĬ, pp. 48–53

The Soviet-made FP-22 high-speed motion-picture camera is provided with a synchronizing device, but cases arise which require a supplementary device. Three such cases are described. The first was the impact of a loaded rod on a glass block. The second was a study of the deformation of drops of molten metal striking a glass surface in a metallization process. The third case was a study of cavitation erosion of solid bodies in an ultrasonic field.

Influence of Dye Adsorption on the Photoelectric Sensitivity of a Photographic Layer

L. G. GROSS (Letter to the Editors), pp. 54–55

Studies of a number of sensitizing dyes (cyanines) adsorbed to silver bromide have shown a spectral sensitization of the photoconductivity. A supersensitizer (a styryl base) gave a sharp increase in photoconductivity in the region of sensitization corresponding to the region in which the supersensitizer particularly affected photographic sensitivity.

A Study of the Sensitivity of 'R'-Type Emulsion Under Different Conditions of Processing

D. M. SAMOĬLOVICH, E. S. BARINOVA, A. A. VLASOV, AND O. P. YUKHNOVSKAYA (Letter to the Editors), pp. 56–57

Experiments are described to show that the fall in sensitivity of emulsion layers containing electron tracks after they have been stuck to glass is due to regression of the latent image during drying.

Fatty Impurities in Photographic Gelatin

E. A. ZIMKIN AND A. F. SHIMORINA (Letter to the Editors), pp. 57–58

Analyses of the fatty content of some gelatins have been made and figures are quoted for the fat, fatty acids, cholesterin, and phospholipids. Figures are also given for the extent to which they are removed from gelatins by treatment with magnesium oxide and hydrated aluminum oxide.

Effect of Low-Intensity Reciprocity Failure for Nuclear Emulsions Sensitized with Triethanolamine

A. L. KARTUZHANSKIĬ and L. I. SHUR (Letter to the Editors), pp. 58–60

The low-intensity reciprocity failure of two nuclear emulsions sensitized with triethanolamine has been studied. By the application of a formula due to Meiklyar, it is deduced from the slope of the curves that the triethanolamine sensitizes by forming subcenters consisting of 3 silver atoms.

A Study of Reciprocity Failure at Exposure Times of 10^{-5} to 10^{-8} Seconds

YU. A. ZATSEPIN (Letter to the Editors), pp. 60–61

Reciprocity-failure measurements have been obtained on Pankhrom film exposed to an electronic flashlamp in a high-speed camera, making possible exposure times of $10^{-5} - 3 \times 10^{-8}$ sec. It is concluded that any reciprocity failure in the region of sensitized sensitivity is insignificant and falls within the limits of experimental error.

On "Normal" and "Anomalous" Aging of Photographic Materials

M. I. SHOR, pp. 62–63

A paper by V. I. Sheberstov (*Zhur. Nauch. i Priklad. Fotografii i Kinematografii*, 4:100 (1959)) on anomalous aging is criticized. There is no essential difference between normal and anomalous aging, all aging being a complex of several kinds of processes. (See next abstract.)

Answer to M. I. Shor on the Problem of "Anomalous" and "Normal" Aging of Photographic Materials

V. I. SHEBERSTOV, pp. 63–64

Shor (see preceding abstract) attributes to Sheberstov views which are not in the paper cited or in others by Sheberstov. Shor's criticisms are therefore misplaced. His assertion that there is no distinction between the two kinds of aging is presented without evidence and is refuted by facts quoted from earlier papers.

Chemical Sensitization in the Ripening of Photographic Emulsions

K. V. CHIBISOV, pp. 65–74

A review is given of modern ideas on the processes occurring during the ripening and digestion of photographic emulsions. Emphasis is placed on the part played by lattice imperfections and impurity centers, and it is considered that the primary centers are silver molecules (Ag_2), and that subcenters and development centers are larger aggregates of silver. (An English language review by Chibisov was published in *J. Phot. Sci.*, **7**:14 (1959).)

The Work of the All-Union Scientific Research Institute on Chemical Reagents Used in the Field of Developing Agents, Optical Sensitizers, Desensitizers, and Intermediates for Their Syntheses

G. I. MIKHAĬLOV, pp. 74–76

A brief review of 31 published papers is given.

Zhurnal Nauchnoĭ i Prikladnoĭ Fotografii i Kinematografii

Vol. 5, No. 2, March-April 1960 (in Russian)

Résumés by S. C. Goddard

On the Topography of the Primary Photographic Process in the Emulsion Grain

K. ONDREĬCHIK, pp. 81–83

Earlier Soviet workers have tended to concentrate on the effect of the conditions of ripening on sensitivity, while workers in the West have been more interested in

the effect of exposure conditions on the distribution of the latent image. The present work attempts to study the effect of the distribution of the sensitivity centers on the formation of the latent image. For this purpose, emulsions with "layered" grains have been prepared by taking a monodisperse emulsion of moderate coarseness and adding to it a known amount of fine-grain (Lippmann-type) emulsion. Physical ripening then caused recrystallization of the fine grains onto the large grains, thus covering the surface sensitivity centers of the latter with a known amount of silver halide. A subsequent chemical digestion then established further sensitivity centers on the surface of the layered grain. By varying the duration of the first and second center-forming digestions and by varying the thickness of the added layer it was possible to study the effect of the internal centers on surface sensitivity and of the surface centers on the internal properties of the grain. The results show that the presence of internal centers has a much greater influence on surface sensitivity than the presence of surface centers has on internal sensitivity. An explanation of this phenomenon is given in terms of electron trapping.

A Study of the Kinetics of Development of Color-Positive Film at Different Temperatures

N. I. KIRILLOV AND L. P. LYSENKO, pp. 84–89

Although manufacturers give directions for processing their film, batch-to-batch variations are sufficiently large to require modifications of the processing conditions in order to obtain standard sensitometric properties. The effect of such modifications has been studied for Agfa Type 5 color-positive film. In addition to the processing temperatures, the concentration of the developing agent and the time of development were varied and their effect on the gamma and speed of the layers was studied. The effect of a preliminary hardening of the film for development was also studied. The data obtained form a basis for the modification of the color processing in order to obtain a constant speed and gamma.

The Kinetics of the Chemical Photographic Processing of Photographic Materials

I. B. BLYUMBERG, pp. 90–97

The kinetics of any of the stages of photographic processing, development, fixing, etc., depend on the diffusion processes taking place in the layer and on the kinetics of the purely chemical reaction. According to circumstances, either diffusion or chemical reaction may be the predominating factors and mixed types are possible. The thickness of the emulsion layer and the presence of a stagnant layer of solution at the surface determine the extent to which diffusion processes play a part. The idea of "buffer capacity" should be extended from acid-alkali buffering and oxidation-reduction buffering to the remaining components of the developer. The concept of "photographic capacity of the layer" is developed. It is a measure of the ratio of the quantity of a component of the solution within a swollen layer to the quantity of the same com ponent necessary to carry out the process to the end. From a study of the general buffer capacity of a processing solution and the photographic capacity of the layer, it is possible to evaluate the type of kinetics relevant to a given set of processing conditions.

A Comparison of Artificial-Sunlight Filters Used for Sensitometric Testing

S. S. GILEV AND E. M. SHIPILOVA, pp. 98–100

The filters compared are made from thicknesses of colored glasses. [*Abstractor's note:* The glasses are designated by letter symbols. In the absence of a key, it is difficult to draw conclusions from the data.]

Nonlinear Color Separation Correction with Two-Stage Negative Masks. II. The Calculation of the Optimal Parameters of the Process

L. F. ARTYUSHIN, pp. 101–107

In the absence of a linear relationship between the effective densities and the surface concentrations of the dye, it is convenient to use nonlinear intensifying negative masks to obtain the most complete color separation correction. It is recommended that the construction of characteristic curves for the masking images ensuring optimal color separation be carried out for two saturated chromatic colors and for one of the achromatic colors of the subject being photographed. Formulae necessary for calculating the sensitometric parameters of the optimal characteristic curves are set out in the article. (*Translation of author's abstract*)

The Relation Between the Influence of Silver Halide Concentration in the Emulsion Layer on its Resolving Power and the Nature of the Developing Agent

I. M. KILINSKII AND A. N. IORDANSKII, pp. 108–113

Three emulsions with different silver/gelatin ratios were digested to approximately the same speed and coated to the same thickness (approx. 30μ). After exposure to a test object the plates were developed in either a developer containing diethyl-*p*-phenylenediamine sulfate or Metol-hydroquinone. In order to obtain a fairly constant contrast in spite of differences in development time, a color coupler giving a cyan image on development was introduced into all the emulsions.

The results show clearly that the effect of changes in the silver/gelatin ratio varies according to the composition of the developer. In the Metol-hydroquinone developer, the curve showing the relation between the resolving power and concentration of the silver halide passes through a maximum at a relatively small concentration of silver halide. With development in the diethyl-*p*-phenylenediamine developer, the resolving power continues to improve as the silver/gelatin ratio is increased, and at the same time the resolving power for any given silver/gelatin ratio is greater than for development in the Metol-hydroquinone developer.

A Study of the Principles of Automation of Stereophotogrammetric Work on Aerial Photographs

N. F. ORELKIN, pp. 114–122, 1 plate

Methods of simultaneous photoelectric scanning of a stereoscopic pair of aerial photographs, in such a way that the combined signal represents the parallax, are described. The most promising appears to be a compensation method in which a negative of one picture is combined with a positive of the other, both on transparent base, a single scanning beam passing through both. With no displacement of the images, a uniform grey background is observed. Any displacements due to parallax are shown up as a difference in density. By a relative motion be-

tween the negative and the positive, it is possible to pick out the required contours.

The Use of the Photographic Method in Light-Model Studies of Radiant Heat Exchange

V. N. ADRIANOV AND G. L. POLYAK, pp. 123–132, 1 plate

In the light-model method of studying radiant heat transfer, light sources are used instead of heat sources and the distribution of intensity in the light field is studied either photoelectrically or photographically. An analysis is made of the accuracy of determining light intensities from photographic density measurements. In light-model studies, it is essential to know the variation of sensitivity of the receiving surface with direction of incidence of the light. This has been measured for the Soviet MZ film and for a selenium photocell. An experiment with a simple arrangement of light sources has shown that the photographic method can be used in light-model studies, provided that the necessary precautions are taken to obtain accuracy.

The Use of High-Speed Cinematography for the Study of Processes Occurring in Liquids under the Action of Ultrasonics

S. R. ZHUKOVSKIĬ, V. F. KAZANTSEV, AND L. O. MAKAROV, pp. 133–140, 2 plates

Descriptions are given of the experimental arrangements used in making high-speed motion-picture films of ultrasonic phenomena studied at the Acoustics Institute of the Academy of Sciences USSR. They included the destruction of a film of dirt on a glass surface and ultrasonic drilling, with their related phenomena of cavitation, erosion, and bubble formation. A wide range of frame frequencies (750-50,000 frames/sec) was used, enabling the processes to be studied both as a whole and in detail. Frame-by-frame analysis allowed a quantitative study of the processes to be made and curves to be drawn.

The Relation Between the Form of the Spectral Sensitivity Curve of Photographic Material and Emulsion Factors

P. V. MEĬKLYAR (Letter to the Editors), pp. 141–142

A series of emulsions was made with gelatins of different types, mixing being carried out for periods ranging from 10 sec to 1 hr, the combined period of mixing and ripening always being made equal to 1 hr. The spectral sensitivity of these emulsions was studied over the range 400- $>$ 500 mμ. Curves of the ratio of the spectral sensitivity for 10 sec mixing to that for 1 hr mixing showed peaks at λ_{max} = 410–420 mμ and 440–450 mμ. These were shown particularly clearly by emulsions, made from fast gelatins with thiosulfate, which had not undergone digestion. Similar peaks were found when the emulsions were given 1 hr digestion. The curves are similar in form to that of the spectral photoconductivity of silver bromide crystals. The results are explained on the hypothesis that donor sensitivity centers—silver atoms or F-centers—are formed in emulsion grains.

Increasing the Sensitivity and Equalizing the Development of Stuck-Down Type-R Emulsion

D. M. SAMOĬLOVICH, E. S. BARINOVA, A. A. VLASOV, AND O. P. YUKHNOVSKAYA (Letter to the Editors), pp. 142–143

Nuclear track emulsions stuck on glass develop less evenly and with a lower emulsion speed than the stripped layers. Adding alkali to the emulsion before coating so as to bring the pH up to 6.5–6.7 improves both the evenness of development and the emulsion speed.

Greater Accuracy in the Methods of Determining the Elementary Composition of Nuclear Emulsions

M. F. RODICHEVA (Letter to the Editors), p. 144

The elementary analysis of NIKFI R emulsion at 58% relative humidity has been carried out with greater accuracy, especially for the lighter elements, than in an earlier determination (M. F. Rodicheva, *Zhur. Nauch. i Priklad. Fotografii i Kinematografii*, **3**: 286 (1958)). The new results are tabulated, together with estimates of the accuracy of the determinations.

Nuclear Emulsions from Lead-Silver Salts

N. R. NOVIKOVA (Letter to the Editors), pp. 145–146

In obtaining nuclear emulsions containing lead salts, it is preferable to introduce the latter at the time of mixing the emulsion. An electron microscope study has shown that in an emulsion with 30% silver bromide replaced by lead sulfate, the grains are mainly 0.08μ in size with an insignificant distribution of coarser grains. Emulsions containing more than 30% lead sulfate have a fraction of coarser grains up to 1μ. A silver bromide emulsion partly substituted with lead sulfate will detect protons up to 60–70 mev, α-particles and fission products. By increasing the time of digestion and hypersensitizing with 6% triethanolamine, they may be made sufficiently sensitive to record 50 grains per 100μ.

The Contrast Function of an Aberration-Free Objective and Properties of the System: Real Objective—Light Sensitive Material

G. A. ISTOMIN (Letter to the Editors), pp. 146–147

An equation representing the reproduction of an absolute black band on a light field is modified to represent the conditions in a real system and is compared with experimental data.

The Application of the Fourier Integral to the Study of the Properties of the Optical and Photographic Image. II. The Photographic Image

A. T. ASHCHEULOV, pp. 148–157

The review begun in *Zhur. Nauch. i Priklad. Fotografii i Kinematografii*, **4**: 465 (1959) is completed.

The Problem of International Standardization in Sensitometry

I. A. CHERNYĬ, pp. 158–159

The modifications suggested by an American Sub-Committee to the draft ISO Standard, which is to be discussed this year, are outlined, and their implications are discussed. It is concluded that the suggestions deserve serious attention and could form the basis of international agreement.

PHOTOGRAPHIC SCIENCE AND ENGINEERING
Volume 4, Number 5, September-October 1960

• New Products and Developments

FRANK SMITH

Electrophotography in Color

An ingenious system of producing images by electrophotography in natural color directly in a single step without the use of separation images is disclosed in a recent invention by Edward K. Kaprelian, now Deputy Director of Research, U.S. Army Signal Research and Development Laboratory, Fort Monmouth, N.J.

Although color images can be obtained by indirect means in other electrophotographic systems, in this invention, the color image is produced by the selective migration of charged color particles in an electrical field according to the color or wavelength of the light. In the use of any of these particles, the essential action is that, in a layer of mixed color particles, those particles of a given color migrate or, if desirable, remain unmoved when subjected to light of the given color. The system, by using suitable particles, can be adapted to produce either an additive color image or a subtractive color image.

The color particles are composed of one or more bits of a suitable photoconductor, surrounded by a layer or coating of dyed gelatin or similar material. Typical photoconductive materials that can be used include selenium, zinc oxide, cadmium sulfide, cadmium telluride, anthracene, and sulfur, and it is preferred that the particle sizes fall in the range of 2 to 30 μ. The dyed layer may consist of any suitable dye in gelatin, wax, vinyl or silcone resin, cellulose ester or similar material in a thickness of from 4 to 25 μ.

Full details of Kaprelian's invention are contained in U.S. Patent No. 2,940,847, dated June 14, 1960.

• Cameras and Accessories

Photomechanisms Camera-Processors

The Rapidata Photo-Processor Model 414, recently announced by Photomechanisms, Inc., Huntington Station, L.I., N.Y., is a camera-processor which provides photographic recording of an event, rapid processing of the recorded image, and viewing of the film record with a minimum delay of approximately 20 sec.

The unit is designed to expose and process 70mm Kodak SO-264 and SO-265 films and Ansco Hyscan Film. These films have blue-sensitive emulsions of medium speed.

The Model 521 70mm Rapidata Camera-Processor provides automatic processing of several available special emulsions at elevated temperatures and very short times. Conventional emulsions can be processed at normal temperatures with correspondingly longer times required. The processing system has only one moving part with a processing rate of 10 in./min. The unit is loaded with a 100-ft cassette, and chemicals are supplied in sealed containers or dry for mixing.

Although the information contained in this section is compiled from sources believed to be reliable, the author cannot assume responsibility for its accuracy. Publication of the information here is not to be construed as an endorsement or recommendation of the product or equipment described.

Pinhole Cylinder Wall Camera

A camera, based on the principles of the simple pinhole camera, has been developed by General Motors' Detroit Diesel Engine Division for taking pictures inside an engine cylinder. The camera, referred to as a liner camera, provides distortion-free pictures of a cylinder in its true condition.

The liner camera, which has good depth of field, is simple to operate. After the camera is inserted into the liner, a bulb shutter is opened. A No. 5 flash bulb is then fired above the liner and its duration of approximately $^1/_{50}$ sec controls the exposure time. The shutter is then closed, the camera removed, and the film changed; the camera is then ready for the next exposure. The camera has a 0.012-in. diameter pinhole made in 0.0015-in. stock instead of a lens. The pinhole admits a ray of light from any given point on an object in front of the camera. These light rays enter the pinhole from all points and form an image on the film plane of the camera. The diameter of the pinhole provides an angle of coverage of 165° and covers 192° of the liner bore. An illustrated article covering details of the camera is contained in the April-May-June 1960 issue of *General Motors Engineering Journal*, from which the above information was extracted.

Williamson "Miss Distance" Camera

Williamson Manufacturing Co. Ltd., Litchfield Gardens, Willesden Green, London N.W. 10, England, has developed a camera for mounting directly on a missile for "miss distance" assessment.

The camera, which is annular in shape, consists of 8 small cameras covering a 360° circle, each containing single-exposure film with individual shutters simultaneously triggered.

Explosive motors, electrically detonated, are used to trigger the shutters and the camera is said to be sufficiently rugged to withstand loadings of 100 G without derangement.

• Optics

NBS Inverting Interferometer for Stellar Studies

The National Bureau of Standards, Washington D.C., has developed an interferometer for astronomical research which consists of a double-image prism and a telescope objective. With this combination, the separation, the diameters, and the time of meridional transit of stars can be accurately measured. In addition, the instrument provides a means of checking on aberrations in astronomical objectives, both reflectors and refractors.

The instrument is a wavefront-inverting interferometer. This optical property is introduced by the nature of the prism used—a modified Koesters prism consisting of two identical prisms cemented together with a partially reflecting film on the inner face. The fringes produced by this device can be viewed from either side of the prism. From either side, a segment of the objective

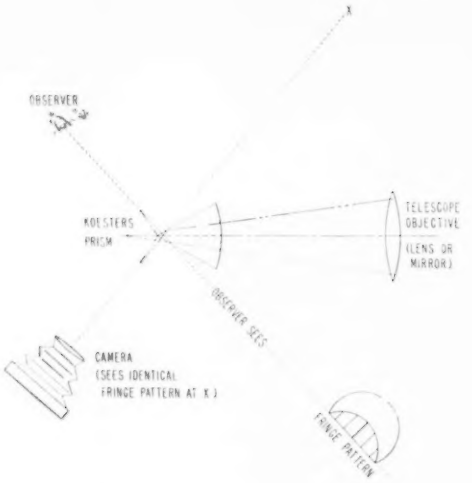

appears to be folded over onto the remaining part. If the objective is bisected by the dividing plane of the prism, fringes occupy exactly half of the lens area. If it is bisected off center, only the overlapping area contains fringes and the remaining portion is interference free. The fringes are pivoted to the dividing plane so that any motion due to atmospheric effects does not affect the position of fringes along one margin of the field. This property provides a degree of stability that almost suppresses vibration effects. Another advantage is the permanent position of the bound end of the zero order or darkest fringe. This fringe is "frozen" in the center of the prism during construction, so that the searching usually required in interferometric observations is eliminated.

This prism is mounted together with a specially designed eyepiece and a camera to form a compact astronomical instrument. When it is attached to a telescope in place of the regular eyepiece, this arrangement permits fringes to be observed and photographed simultaneously.

Kodak Wratten Filters for Scientific and Technical Use

A revised 1960 edition of *Kodak Wratten Filters for Scientific and Technical Use*, has been announced by Eastman Kodak Co., Rochester 4, N.Y. The 81-page illustrated manual is written primarily for the technical and scientific laboratory worker whose use of filters requires spectrophotometric data, but some information of a more general photographic nature is also included.

• Reproduction and Copying

Kecofax Electrophotographic Projector-Printer

An electrophotographic projector-printer capable of reproducing engineering drawings up to 34 by 48 in. is available from Keuffel and Esser Co., Hoboken, N. J. Film to be printed is loaded manually into a holder, and the exposure time is set. Projection size is varied by moving the projector head on an overhead track to print any dimension ranging from $8^1/_2$ by 11 to 34 by 48 in.

A turret film holder on the projector keeps several negatives ready for exposure and allows the film holder to be loaded while exposures are being made. Forty seconds are required to produce a finished print. A preset regulator permits the equipment to make up to 19 prints automatically from a single negative. The use of a high-intensity point source light which provides shorter exposure times is a major factor in both the high speed of the printing cycle and the sharpness of the black-line print. The unit operates on the electrostatic principle, using paper coated with a semiconductor. The paper is electrostatically charged by means of a corona bar (charging wand) that travels back and forth across the paper.

The charge is dissipated in exposed areas and the latent electrostatic image is formed when the paper is exposed to light passed through the negative. The paper then enters a toning chamber where the toners are attracted to the image areas.

Finally, controlled heat is applied and the image is fused onto the paper. The finished print is delivered at the front of the machine where it is automatically cut off the paper roll. The projector-printer is 5 ft wide, 14 ft long, and $7^1/_2$ ft high, and weighs 2100 lb. It operates on 115 v and 50 amps ac.

Litton Industries "Printapix" Electronic Printing Tube

A special cathode-ray tube has been developed by Litton Industries, San Carlos, Calif., for direct electronic printing at high speed on nonsensitized dielectric material. The tube employs a metallic element mosaic target or printing head in place of the phosphor screen usually found in cathode-ray tubes. Present tubes provide a 2.75-in. wide writing capability. The metallic elements have a diameter of 0.001 in. on approximately 0.004-in. centers, providing an element density of 62,500 conductors/sq.in. Additional tube types are being developed with writing head widths of 5, $8^1/_2$, and $12^1/_2$ in. and metallic element diameters of 0.0005 in., at spacings of approximately 0.001 in., with a resultant density of one million elements/sq. in.

In operation, deflection of the electron beam along the printing-head width provides one dimension of motion. The dielectric material, positioned immediately adjacent to the writing head, is moved past the tube face to provide the orthogonal displacement.

For image development, a powder with two components, a toner and a carrier, is released as a cloud or fog in close proximity to the charged dielectric surface. The resultant image can be erased for reuse of the base material and powder, or can be permanently fixed by a rapid heat cycle, pressure, or other means. Ordinary paper can be used as the base material for image rendition.

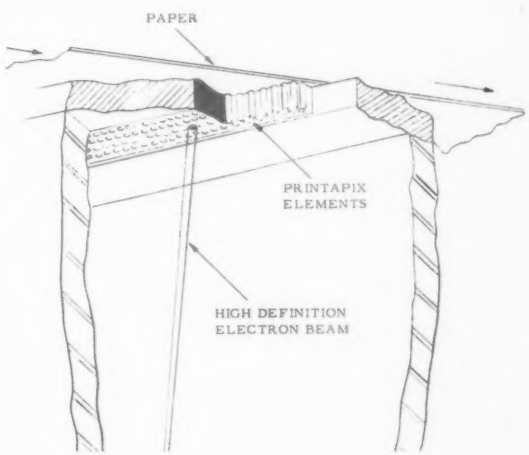

• Miscellaneous

Spectrometric Measurements of Missile Exhaust

IR spectrometric studies of missile flights are being made at the Air Force Missile Test Center's ROTI missile tracking installation at Melbourne Beach, Fla. An 8-in. aperture Rapid Scan system, operating in conjunction with the 24-in. aperture ROTI optical missile tracking system, covers the power flight portions of missiles launched from Cape Canaveral. ROTI (Recording Optical Tracking Instrument), with its long focal length, provides photographic information of missile performance at great distances.

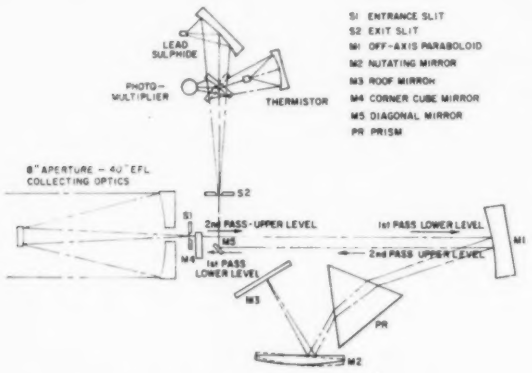

The classified infrared studies of missile exhaust plume characteristics are being made by the Perkin-Elmer Corporation, Norwalk, Conn., under contract from the Air Force Cambridge Research Center. They are part of the Interservice Radiation Measurement Program (IRPM 59/60) which is sponsored by the Advanced Research Projects Agency.

X-Ray Photograph of the Sun

Scientists of the Naval Research Laboratory have succeeded in obtaining the first x-ray photograph of the sun, using an Aerobee-Hi rocket to carry the camera above the atmosphere. The sun's x-rays do not penetrate the air below a height of 60 miles. The photograph shows the sun rimmed by a bright x-ray halo and several intense spots of bright X-ray emission distributed over the disk.

The visible disk of the sun is characterized by a surface temperature of 6000° K. Extending high above the disk is the thin outer atmosphere of the sun—its corona. Because its brightness is only one millionth that of the disk—roughly equal to the full moon—the corona can be seen only during a total eclipse, at which time it appears to stretch millions of miles into space. The coronal gas is very tenuous but very hot, the average temperature being about a million degrees with local hot spots reaching perhaps ten million degrees. At this very high temperature, the gas is completely ionized and the electrons move at such high speeds that their collisions with heavy nuclei generate x-rays. The x-ray intensity has been measured from rockets and has been found to play an important role in the formation of the ionosphere, which in turn controls long-range radio communication.

A simple pinhole camera was used which was flown in the rocket from White Sands Missile Range on April 19, 1960, at a height of 130 miles. To recover the camera,

the instrumentation section was separated from the rocket before impact and parachuted to the ground. For the x-ray camera, the pinhole was 0.005 in. in diameter and the camera was 6 in. long. The pinhole was covered by a thin plastic film supporting an opaque coating of aluminum. In this way, visible light was blocked but x-rays were passed. The wavelengths effectively transmitted were in the range 20 to 60A.

Fifty-Million Lumen Rocket-Borne Light Flasher

A rocket-borne beacon with a precisely timed flash that can be photographed from a distance of up to 400 miles was demonstrated at the 1960 Design Engineering Show in New York City's Coliseum on May 23, 1960.

Developed by Battelle Memorial Institute research engineers for the Grimes Manufacturing Co., the beacon has been designed to be carried in missiles. When used in conjunction with ground-based photographic equipment, the beacon will permit more precise study of missiles launched at night. The controlled high-intensity flashes will be photographed as a series of dots on a photographic plate which will provide a record of the missile's trajectory. A radio signal will be used to control the beacon. The first production model weighs 33 lb and is 27 in. long and about 8 in. square. When placed in a missile, the beacon's lens will become an integral part of the missile's surface. Inside the beacon unit is transistorized circuitry which steps up a nominal 28 vdc supplied by a battery to 4000 v. The battery consists of a series of silver cells 7 in. long by about 3 in. square. The voltage build-up is necessary to set off the specially designed quartz flash-tube twice each second. At its peak, the tube gives off a light rated at 50,000,000 lumens.

The unit has been designed so that each flash does not exceed 0.0001-sec duration and the timing between flashes, 0.001 sec, and it must continue flashing for a minimum of 25 sec.

The beacon is capable of withstanding environmental conditions from about −80 to +160°F at 100% RH. The unit must also withstand thermal radiation from the missile's walls which may be at 700°F for 3 min. The unit has been designed to meet extreme shock, vibration, and noise conditions.

The Society of Photographic Scientists and Engineers

Box 1609 • Main Post Office • Washington, D.C.

OFFICERS

President	GEORGE T. EATON, Building 59, Kodak Park, Rochester 4, New York
Executive Vice President	STEVEN LEVINOS, Ansco, Binghamton, New York
Engineering Vice President	JOHN A. MAURER, 116–118 West 29th Street, New York 1, New York
Editorial Vice President	R. CLARK JONES, Polaroid Corporation, 730 Main Street, Cambridge 39, Mass.
Financial Vice President	HERBERT MEYER, 325 Sequoia Drive, Pasadena 2, California
Secretary-Treasurer	FRANCIS J. HEYDEN, S.J., Georgetown College Observatory, Washington 7, D.C.
Managing Secretary	EDWARD S. COBB, Box 1609, Main Post Office, Washington, D.C.

CHAPTERS *and* CHAPTER OFFICERS

Binghamton, New York	*President*	HARRY G. MORSE, 326 Riverside Drive, Binghamton, New York
	Secretary	E. SCUDDER MACKEY, Stone Road, MR-98, Binghamton, New York
Boston, Massachusetts	*President*	JOHN B. TAYLOR, 290 Davis Road, Bedford, Massachusetts
	Secretary	MISS SHEILA A. BARRY, 35 South Street, Waltham 54, Massachusetts
Chicago, Illinois	*President*	ROBERT W. MAZOR, Standard Studios, Inc., 540 North Michigan Avenue, Chicago 11, Illinois
	Secretary	NELSON W. RODELIUS, 2749 Reese Avenue, Evanston, Illinois
Cleveland, Ohio	*President*	HARRY L. FICHTER, JR., 1256 Overlook Road, Lakewood 7, Ohio
	Secretary	JOHN N. PIKE, 1480 Belle Avenue, Lakewood 7, Ohio
Monmouth, New Jersey	*President*	D. L. CASTELLINI, 98 Leland Terrace, New Shrewsbury, New Jersey
	Secretary	MISS MARILYN LEVY, 100 McLaren Street, Red Bank, New Jersey
New York, New York	*President*	HENRY CROIX, Industrial Photo Products, Inc., 86 Worth Street, New York 13, New York
	Secretary	JAMES W. HOWARD, Interchemical Corporation, 432 West 45th Street, New York 36, New York
Northern California	*President*	PHILIP B. CARNAHAN, Building 47, University of California, Berkeley 4, California
	Secretary	PETER L. CICCARELLO, Ansco Division, General Aniline & Film Corporation, 640 Second Street, San Francisco 8, California
Rochester, New York	*President*	JOHN F. ENGLERT, JR., Sales Service Division, Eastman Kodak Company, Rochester 4, New York
	Secretary	WOODLIEF THOMAS, JR., Color Technology Division, Eastman Kodak Company, Rochester 4, New York
Southern California	*President*	L. L. BUNNING, 9045 Fairview Avenue, San Gabriel, California
	Secretary	JOHN N. HARMAN, JR., 550 West Colorado Street, Glendale 4, California
Washington, D.C.	*President*	JOSEPH A. SCHANTZ, 5409 24th Avenue, S.E., Washington 21, D.C.
	Secretary	LOUIS WERNER, 3610 North Powhatan Street, Arlington 13, Virginia

Sustaining Members / Society of Photographic Scientists and Engineers

Abrams Instrument Corporation
Lansing 1, Michigan

Aero Service Corporation
Philadelphia 20, Pennsylvania

Ansco Division, General Aniline & Film Corporation
Binghamton, New York

Atkinson Laboratory, Incorporated
Hollywood 38, California

Atlantic Gelatin Div., General Foods Corporation
Woburn, Massachusetts

Bar-Ray Products, Incorporated
Brooklyn 32, New York

Bausch & Lomb Incorporated
Rochester 2, New York

Bell & Howell Company
Chicago 45, Illinois

Charles Beseler Company
East Orange, New Jersey

Bulova Watch Company, Inc., Photographic Division
Woodside 77, New York

Burke & James, Incorporated
Chicago 4, Illinois

Byron Motion Pictures, Incorporated
Washington 7, D.C.

Chicago Aerial Industries, Incorporated
Melrose Park, Illinois

Consolidated Film Industries
Hollywood 38, California

De Jur-Amsco Corporation
Long Island City 1, New York

E. I. du Pont de Nemours & Company
Parlin, New Jersey

Eastman Kodak Company
Rochester 4, New York

Edgerton, Germeshausen & Grier, Incorporated
Boston 15, Massachusetts

Elgeet Optical Company, Incorporated
Rochester 6, New York

Fairchild Camera & Instrument Corporation
Syosset, Long Island, New York

Farrand Optical Company, Incorporated
New York 70, New York

Oscar Fisher Company, Incorporated
MD-27, Newburgh, New York

The F-R Corporation
New York 56, New York

General Electric Company
Schenectady, New York

General Film Laboratories Corporation
Hollywood 28, California

W. & L. E. Gurley Company
Troy, New York

Haloid Xerox Incorporated
Rochester 3, New York

Hardale Associates
New York 22, New York

Hi-Speed Equipment, Incorporated
Waltham 54, Massachusetts

Houston Fearless Corporation
Los Angeles 64, California

Charles A. Hulcher Company, Incorporated
Hampton, Virginia

Philip A. Hunt Company
Palisades Park, New Jersey

Hycon Manufacturing Company
Pasadena, California

Itek Corporation
Waltham 54, Massachusetts

The Kalart Company, Incorporated
Plainville, Connecticut

Kollmorgen Optical Corporation
Northampton, Massachusetts

LogEtronics Incorporated
Alexandria, Virginia

L-W Photo Products Company
Northridge, California

J. A. Maurer, Incorporated
Long Island City 1, New York

The Morse Instrument Company
Hudson, Ohio

National Research and Chemical Company
Hawthorne, California

North American Aviation, Incorporated
Los Angeles 45, California

Pako Corporation
Minneapolis 11, Minnesota

Photogrammetry, Incorporated
Silver Spring, Maryland

Polaroid Corporation
Cambridge 39, Massachusetts

Rolor Industrial Corporation
New York 17, New York

Simmon Brothers, Incorporated
Long Island City 1, New York

Technicolor New York Corporation
New York 19, New York

Viewlex, Incorporated
Long Island City 1, New York

Wollensak Optical Company
Rochester 21, New York

Zoomar, Incorporated
Glen Cove, New York